A MODEL TO PREDICT FUEL CHANNEL FAILURE

A MECHANISTIC MODEL TO PREDICT FUEL CHANNEL FAILURE IN THE EVENT OF PRESSURE TUBE OVERHEATING

By ALEXANDER DION, B.Sc.

A Thesis Submitted to the School of Graduate Studies in Partial Fulfillment of the

Requirements for the Degree Master of Applied Science

McMaster University MASTER OF APPLIED SCIENCE (2016) Hamilton, Ontario

(Engineering Physics)

TITLE: A Mechanistic Model to Predict Fuel Channel Failure in the Event of Pressure Tube Overheat

AUTHOR: Alexander Dion, B.Sc. (University of Guelph)

SUPERVISOR: Dr. John Luxat

NUMBER OF PAGES: xx, 135

Abstract

Under normal operating conditions a CANDU reactor pressure tube (PT) is insulated from its outer calandria tube (CT) by a CO_2 gas annulus. If the primary loop coolant flow is compromised the PT can overheat and, if still pressurized, balloon into contact with the CT. At this point the moderator acts as an emergency heat sink. If the heat transferred from the CT to the moderator exceeds the critical heat flux (CHF) the CT can overheat, begin to strain due to the contact pressure, and eventually fail. A mechanistic model is presented that describes ballooning contact of the PT and CT, the resulting thermal contact conductance, heat flux to the moderator, and, if CHF is exceeded, the development of film boiling and potential CT strain. The goal is to create a software package that predicts fuel channel failure during a pressure tube overheat event.

Acknowledgements

I would like to take the time to acknowledge the help I received from Dr. John Luxat to complete this project. He allowed me to approach this project with my own vision while still providing guidance when I needed it. I am truly grateful for the opportunities I've been given because he chose to accept me as a graduate student.

I would also like to thank my partner Kathryn Montgomery. I really don't think I would be submitting this thesis if it wasn't for her love and support. I met her at a turning point in my life and the completion of this thesis symbolizes everything I set out to do when I met her.

Table of Contents

List of Tables

List of Figures

List of Symbols and Abbreviations

Roman Letters

A_c, A_{ct}	Gas molecule collision and outer calandria tube wall area
c_p, c_v	Heat capacity at constant pressure and volume
C_{sf}	Surface fluid constant
d	Maximum tube defect depth
D, D_b	General and bubble (b) diameter
f	Frequency of bubble departure
g	Acceleration due to gravity
G_b, G_c	Vapor bubble and column mass flow
h_{cont}, h_s, h_g	Total contact, solid and gas conductance
h_{conv}, h_{fb}	Convective and film boiling heat transfer coefficient
h_{fg}	Latent heat of vaporization
$h'_{rad}, h'_{eff}, h'_{conv}$	Linear radiation, effective and convective heat transfer coefficient
H, H_M	Microhardness and Meyer's harness (M) index
k	Thermal conductivity
l_s	Tube segment length
L, L_a	Characteristic and axial (a) length
m	Asperity slope

m_λ	Wave number
m_s	Tube segment mass
m'	Mass per unit length
n	Number of nucleation sites
n_v	Number of molecules per unit volume.
$N_{Re,b}, N_{Nu,b}$	Bubble Reynolds and Nusselt number
N, N_{av}	Local and average heat and mass flux between a spherical bubble and surrounding liquid
Nu	Nusselt number
N_A	Avogadro's number
P, P_o, P_c, P_b	Internal PT, reference (o), contact (c), and bulk fluid (b) pressure
P_{cr}, P_R	Critical and reduced pressure
Pr	Prandtl number
q'	Linear power
q'_{loss}	Axial pressure tube heat loss
$q''_{chfsat}, q''_{chfsc}$	Saturated and subcooled critical heat flux
q''_{nb}	Nucleate boiling heat flux
q''_{cond}, q''_{rad}	Conduction and radiation heat flux
$q''_{sh}, q''_{evap}, q''_{v-l}$	Superheat, evaporation and vapor/film heat flux
r	Component radius
R	General radius

Ra	Rayleigh number
t	Time
T	Temperature
u	Velocity
U, U_r, U_θ	Total, radial (r) and θ vapor/film interface velocity
U_{sub}, U_{br}	Density induced and bubble rise velocity
V, V_v, V_b	Gas, film and bubble volume
Y	Mean plane separation

Greek Letters

α	Accommodation parameter
α_d	Thermal diffusivity
β	Fluid parameter
β_{th}	Thermal expansion coefficient
β_θ	Bubble contact angle
γ	Specific heat ratio
γ'	Heat loss fraction from heater to pressure tube
δ_t, δ_f	Thermal boundary layer and film thickness
ϵ	Emissivity
$\dot{\epsilon}, \epsilon_f$	Strain rate and failure strain limit
λ	Critical wavelength
Λ	Gas mean free path
μ	Kinematic viscosity
ν	Dynamic viscosity
ρ	Density
σ	Surface tension
$\sigma_{pt}, \sigma_{ct}, \sigma_i$	Azimuthal and internal stress
σ_{rms}	Root means square roughness
$\tau_s, \tau_{pt}, \tau_{ct}$	Segment and tube thickness

Subscripts

ct	Calandria tube
f	Film
g	Gas
h	Heater
l	Liquid
mfb	Minimum film boiling
o	Reference
pt	Pressure tube
s	Solid
sat	Saturation
v	Vapor
w	Wall

Abbreviations

CANDU	Canadian deuterium uranium
CHF	Critical heat flux
CT	Calandria tube
HTC	Heat transfer coefficient
HTS	Heat transport system
LZC	Liquid zone controller
PT	Pressure tube
RMS	Root mean square
SDS	Shutdown system

CHAPTER 1 - Introduction

1.1 Reactor Description

Coolant passes through the Canada deuterium uranium (CANDU) reactor core via the primary coolant loop which splits into 380, or 480 depending on the reactor, zirconium 2.5% niobium pressure tubes (PT). The 4 mm thick, 10.34 cm inner diameter, PTs each house 12 natural uranium fuel bundles which, through the process of nuclear fission, heat the coolant to temperatures in excess of 300^{o}C. In order to reduce in-channel boiling the primary loop is pressurized to ~10 MPa. Since natural uranium only contains 0.71% fissile uranium 235 (U-235), by weight, extra care is used when selecting materials for in reactor components. The goal is to ensure high enough neutron population to sustain criticality. To this end zirconium was selected as the primary PT material due its low neutron absorption cross section. Additionally, criticality in a natural uranium reactor cannot be sustained in the presence of light water due to the neutron absorption cross section of protium, the most common (99.985%) isotope of naturally occurring hydrogen.

This necessitates the use of heavy water, deuterium oxide (D_2O) as both primary loop coolant and moderator.

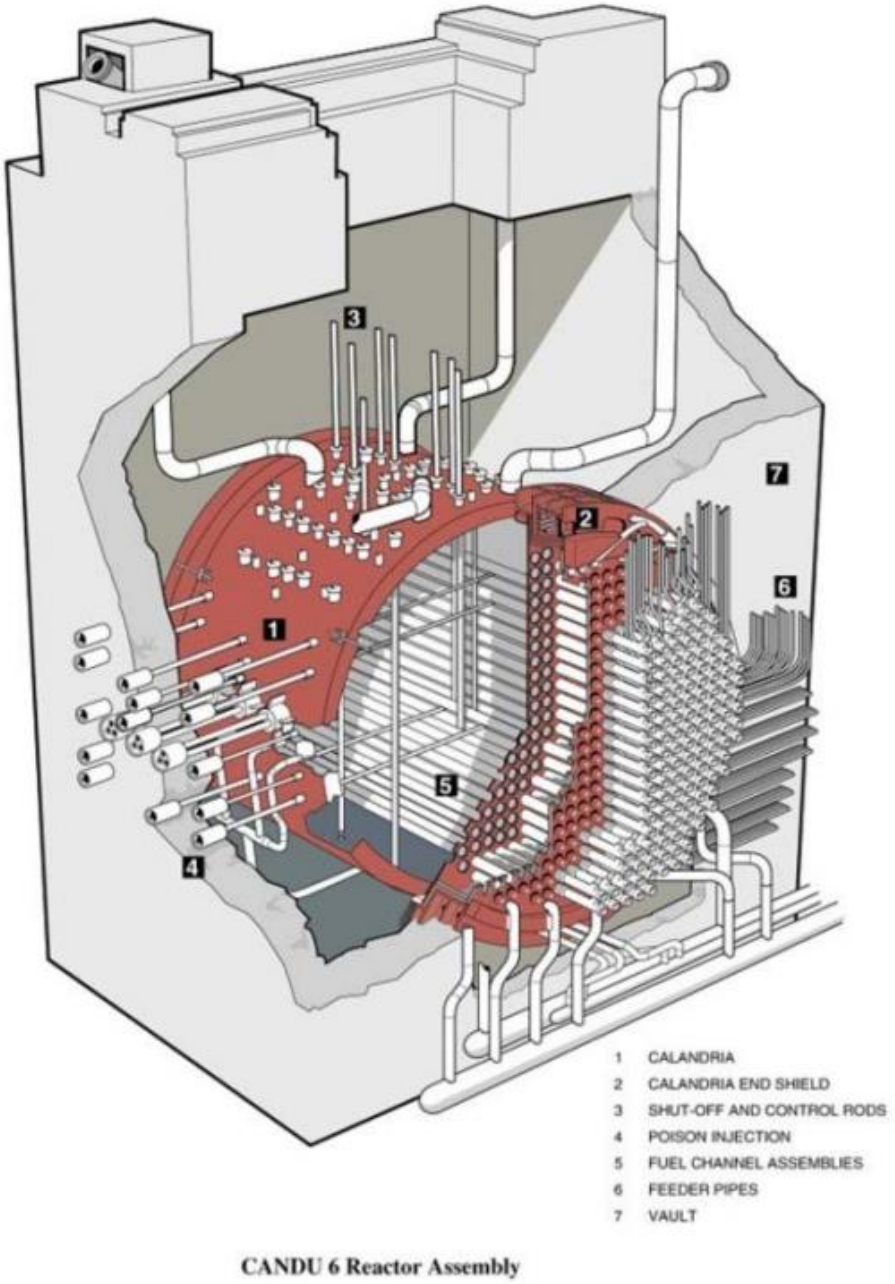

Figure 1.1 General layout of a CANDU reactor [1]

To further increase neutron economy CANDU fuel channels are spaced further apart than fuel assemblies in light water reactors (LWRs). This ensures fission neutrons are sufficiently thermalized below the uranium 238 (U-238) resonance absorption energy. The moderator is contained within the reactor's calandria vault and the primary loop PTs pass through the vault via the 1.4 mm thick, 12.92 cm inner diameter, calandria tubes (CT). The annulus of space formed between the PT and CT is filled with CO_2 as insulation, reducing the exchange of heat between the primary loop and the moderator.

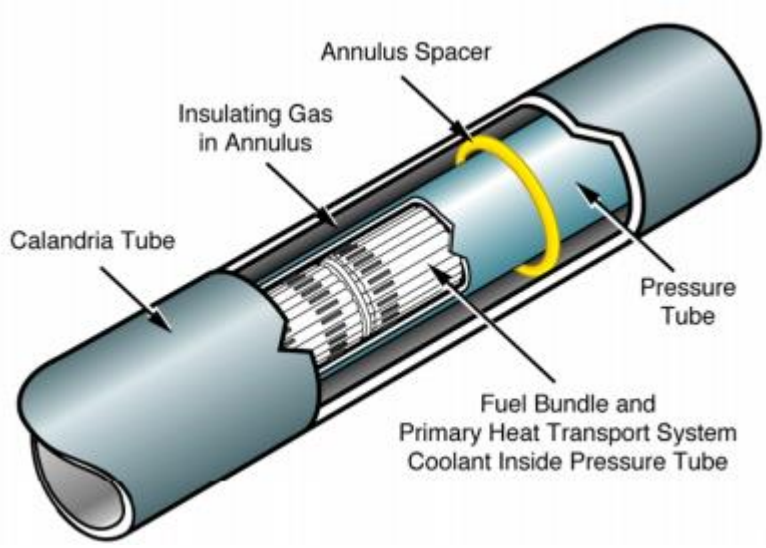

Figure 1.2 A CANDU fuel channel [2]

1.2 Reactivity Control and Shutdown Systems

The CANDU reactor control and safety systems consist of a set of redundant design features that shape the power distribution of the reactor core and prevent severe power excursions. During normal operation the neutron flux profile of the reactor is controlled through the use of 14 liquid zone controllers (LZC). As previously described, heavy water is used as a moderator in the CANDU and the presence of even a small

amount of light water is enough to reduce the neutron flux. With that in mind reactivity is controlled in a particular zone by passing light water through the LZC tubes. The water leaves the LZC at a constant rate and the level of light water in the zone is increased, or decreased, based on the flow rate into the LZC. Since the amount of reactivity that can be removed/added by the LZCs is limited (~7 mk) a separate control system is used for larger reactivity changes. 21 stainless steel adjuster rods (~15 mk) are placed within the core during normal operation in order to flatten the neutron flux profile of the reactor. This allows more fuel bundles to operate close to the maximum allowable power, resulting in higher average fuel burnup. These rods can be withdrawn from the reactor in cases where additional reactivity desirable; if refueling has been delayed for example. The rods enter from the top of the reactor, with gravity, rather than from bottom (as is the case for LWRs) reducing the chance that they could be ejected during potential accident situations. 4 more control rods made of cadmium and stainless steel are kept outside of the reactor and can be inserted for a 10 mk reactivity reduction.

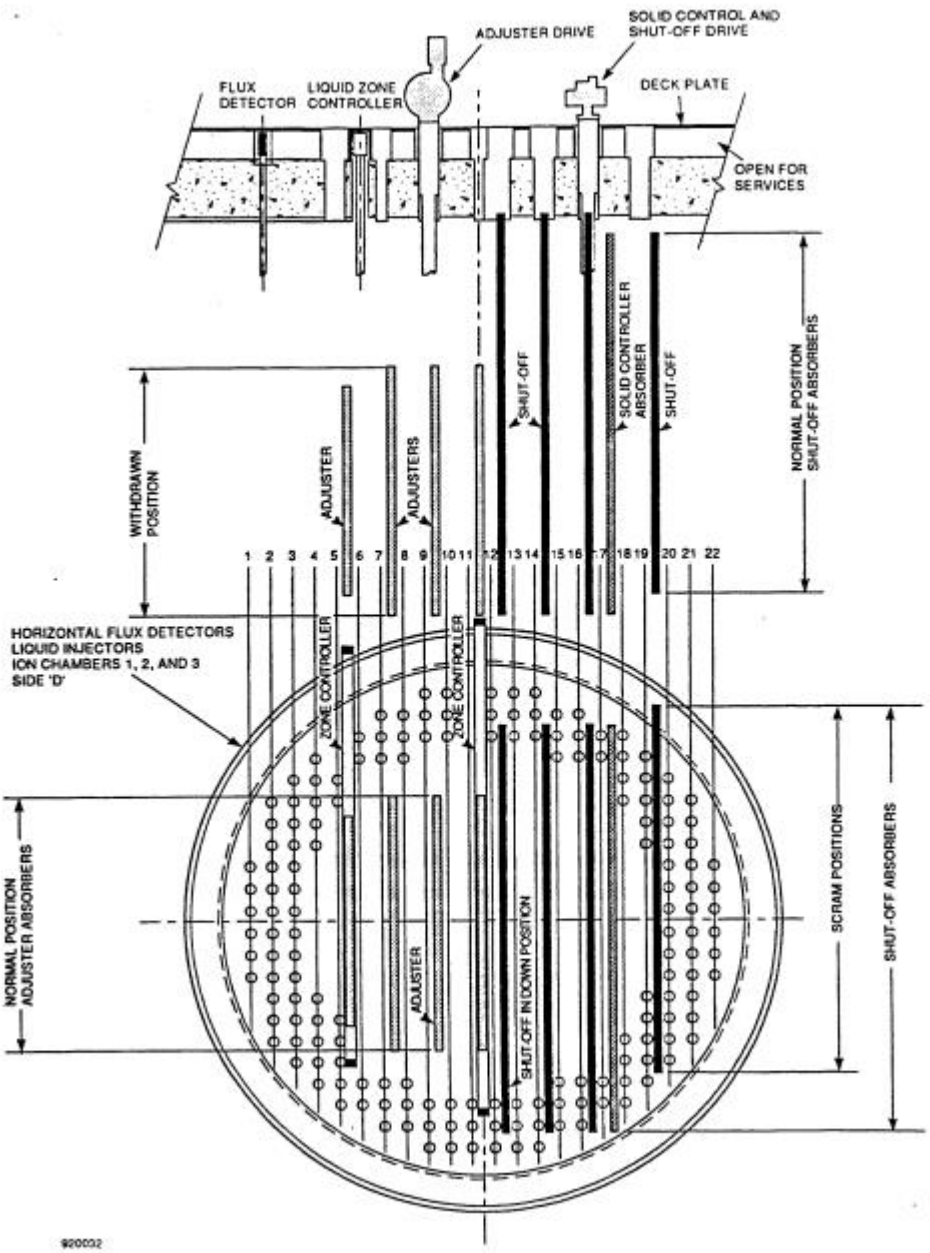

Figure 1.3 A cross section of the CANDU reaction and the positon of LZC, adjuster rods and shut-off rods [1]

In addition to reactivity control there exist two independent shutdown systems (SDS) poised to prevent severe reactivity excursions. SDS1 consists of 28 cadmium/stainless steel shutoff rods that can be rapidly inserted into the reactor. These rods have the ability to reduce reactivity by roughly 80 mk and can be fully inserted into the core in 2 seconds using spring assisted gravity drop. The rods can be removed once the signal initiating reactor trip has been addressed allowing the reactor to return to operation. SDS2 is a, ~300 mk worth, solution of gadolinium nitrate that will rapidly poison the reactor, bringing the nuclear chain reaction in the core to a halt. Within about 3 minutes of shutdown the thermal power of the reactor will drop to about 3% full thermal power. The main contributor to reactor heat at this point will be the decay of fission products. In the event of an emergency reactor shutdown the progression from the initiating event, such as complete loss of power, to severe accident status will be entirely dependent on the reactor's ability to offset the decay heat generated in the fuel channels.

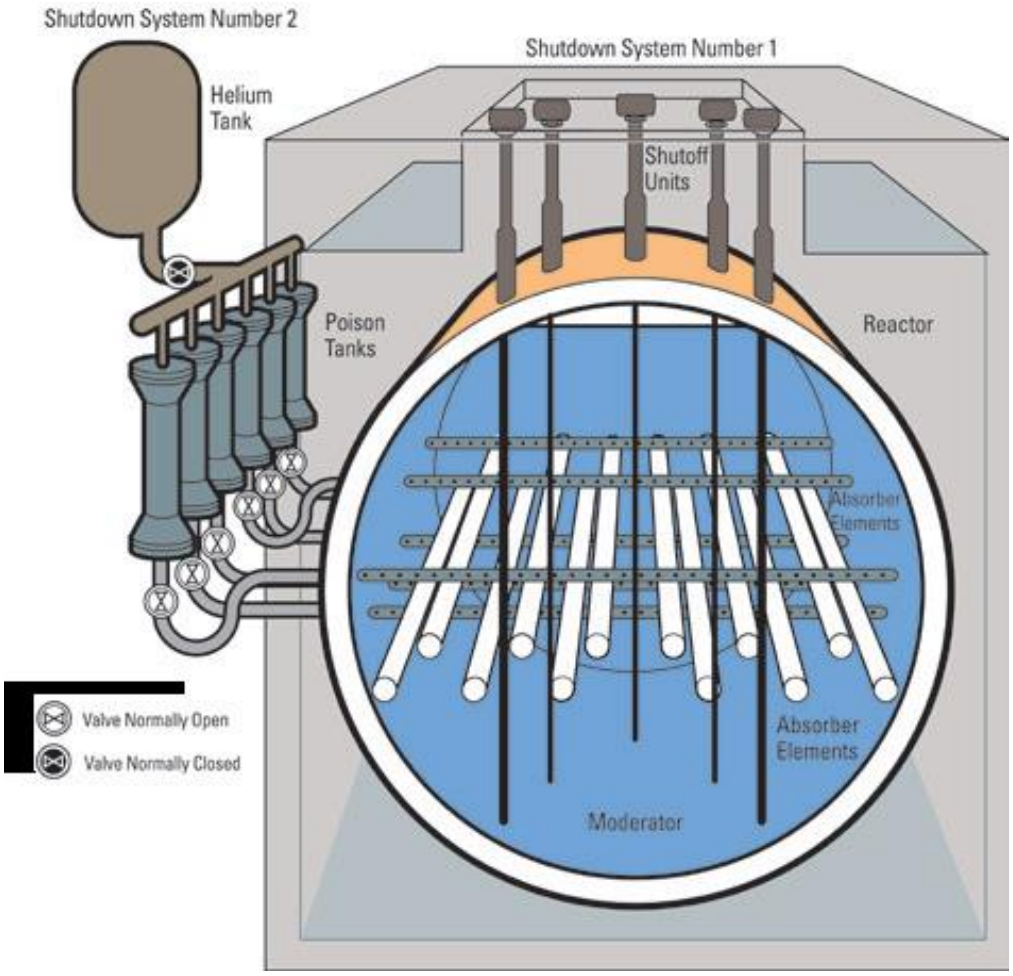

Figure 1.4 CANDU shut down systems 1 (shut-off rods) and 2 (gadolinium poison) [3]

1.3 Total Loss of Power Accident Progression

A complete station blackout would require a loss of off-site (grid) power, a loss of on-site power and the loss of both the standby and emergency backup generators. The effect each loss has on the heat transport system's (HTS) ability to mitigate decay heat is increasingly severe. Nuclear generating stations in Canada typically consist of more than one on site reactor. In the event of loss of grid power the energy produced by a single reactor is sufficient to keep the station operational. In this case the reactor will not trip

and will continue to operate as normal. If both the connection to on-site and grid power is lost then the reactor will shut down automatically. At this point the pumps for the HTS have lost power and heat will be removed from the reactor core through natural circulation. The core will be sufficiently cooled provided that cool water is pumped into the steam generators and the steam produced is able to be vented. Pumps supplying water to the steam generators are powered by backup generators; if all backup and emergency generators fail the station will enter total blackout conditions.

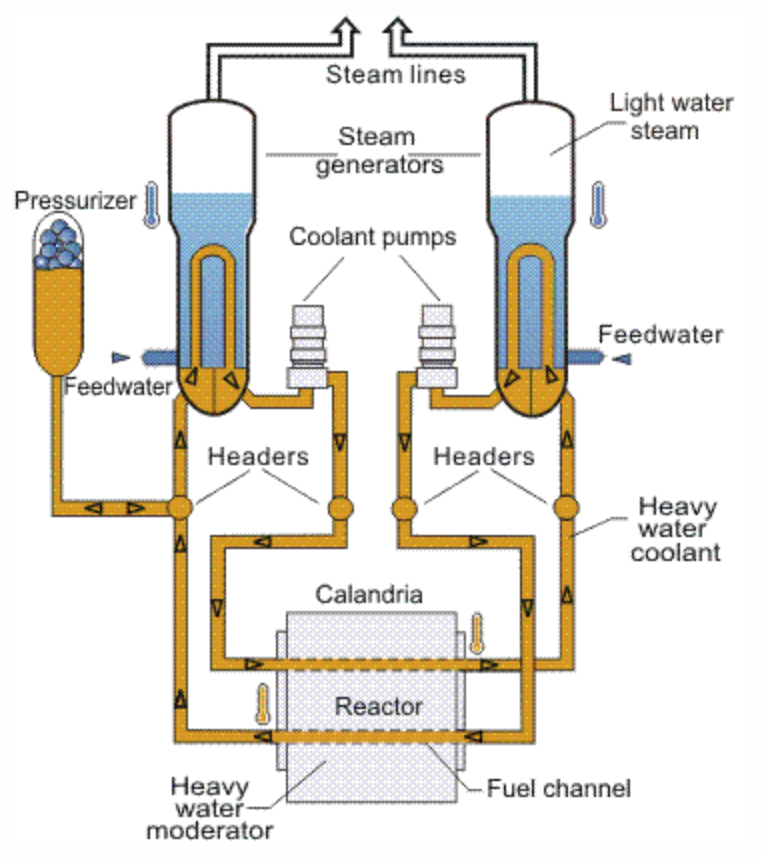

Figure 1.5 The primary coolant loop of the CANDU reactor [4]

Natural circulation can be temporarily sustained by gravity assisted flow from a reserve water storage tank above the reactor allowing enough time for additional pumps and portable generators to be transported to the generating station. If the supply of water is not restored the coolant in the primary loop will begin to boil, the steam produced will be vented to the reactor building, and the fuel channels will eventually void. With no way to remove heat from the fuel channels PT temperatures will begin to increase and, if temperatures exceed 600^{o}C, become malleable. If the channel is still pressurized the PT will balloon into contact with the CT at which point the moderator acts as an emergency heat sink. Subsequent heat rejection from the PT, through the CT to the moderator, will then be wholly dependent on the thermal contact conductance between the PT and CT and the heat transfer coefficient between the CT and moderator. Fuel channel failure will result if heat rejection to the moderator is insufficient to limit CT temperature increase.

1.4 Heat Rejection to Moderator

Heat transfer from the PT to the CT will depend on the thermal contact conductance between the two tubes. Contact conductance between two solids is dependent on the thermal conductivity and surface microstructure of both materials as well as the contact pressure. The surface of any solid is, of course, rough to some degree; a macroscopically smooth surface can have a non-uniform topology at a scale of micrometers. These surface asperities will be the location of initial contact resulting in a total contact area less than the total surface area. Gaps formed between the contact points will also trap any fluid present prior to contact and contribute to the total conductance. Heat transferred to the CT will then be rejected to the moderator where the magnitude of

heat flux will depend on the phase of the surrounding fluid. As the CT temperature increases from bulk fluid to saturation temperature so too will the liquid in the immediate vicinity of the CT. The increasing liquid temperature results in a decreasing density with respect to the bulk fluid and buoyancy forces transport the warm liquid away from the CT surface. The surrounding cool liquid will take the warm liquid's place and begin to heat up, repeating the process. This type of density induced flow is known as natural convection. If the heat transfer provided by natural convection is unable to stop the CT temperature from increasing it will eventually exceed saturation temperature and begin to boil the surrounding fluid. Water vapor will begin to form in microscopic cavities around the CT called nucleation sites. These bubbles grow and then depart from the surface due buoyancy forces. The main mechanism of heat transfer here comes from the energy needed to effect a phase change in the surrounding liquid. While the CT is in nucleate boiling the heat transfer coefficient will be in the range of 10-50 $kW/m^2/K$ depending on the number of active nucleation sites. At the moment of contact the temperature difference between the hot ($>600^oC$) PT and the cool, bulk fluid temperature, CT will be at its largest. This large temperature difference, coupled with high enough contact conductance, can result in a heat flux from the CT to the moderator exceeding critical heat flux (CHF). Exceeding CHF will result in the initiation of a phenomenon known as film boiling, where a film of vapor begins to develop between the CT and moderator. This vapor film will severely reduce CT's ability to transfer heat to the moderator and can cause the CT temperature to rise rapidly. Similar to the PT, if the CT temperature rises

above 600^{o}C it will begin to strain under internal pressure. If the CT becomes thin enough in the region of a defect it can rupture resulting in fuel channel failure.

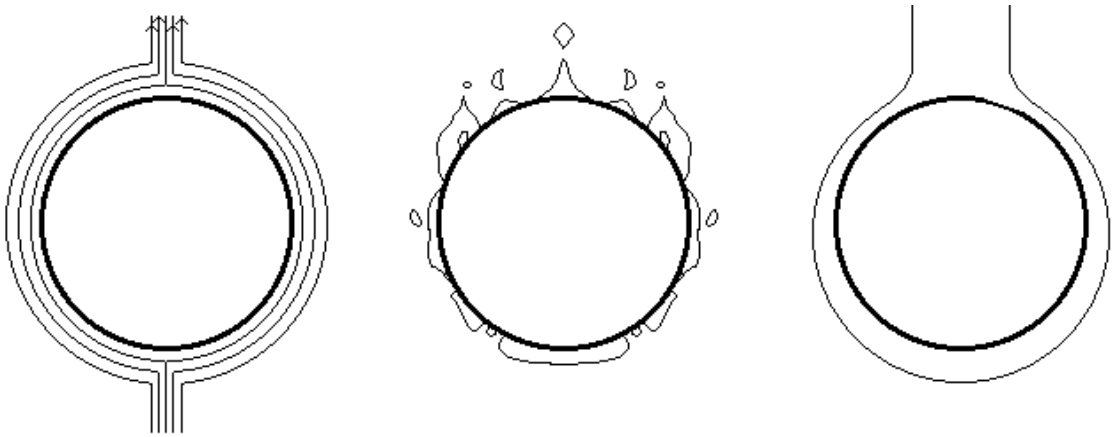

Figure 1.6 A sketch of the three boiling regimes considered in this thesis: natural convection (left), nucleate boiling (middle), and film boiling (right)

1.5 Objective

The objective of this thesis is to develop a mechanistic model that describes the real time thermal and mechanical behaviour of a voided fuel channel subject to varying decay heats, internal pressures and degree of moderator subcooling. The model is also expected to accurately predict fuel channel failure based on the severity of creep deformation. Three distinct phases of heat transfer were observed in experimental high pressure contact boiling tests:

Pressure Tube Heatup and Deformation

The PT is initially insulated from the CT heat transfer between the two is negligible. As PT temperature rises due to lack of heat primary coolant liquid it begins to strain based on material properties of Zr 2.5% Nb and internal channel pressure.

Initial Pressure Tube / Calandria Tube Contact

Once PT/CT contact occurs heat is transferred through the CT out to the moderator. The heat flux from the PT to the CT is limited by the thermal contact conductance between the two tubes. Thermal contact conductance is dependent on contact pressure, material properties and the microstructure of the two contacting tubes. The PT/CT temperature difference will be largest at the moment of contact. If the difference is severe enough the heat flux to the moderator may cause the development of film boiling at the CT surface.

Heat Rejection to Moderator

Heat is rejection from the CT to the moderator will depend on the boiling regime of the surrounding moderator. If the heat flux to the moderator exceeds CHF film boiling will develop reducing the heat transfer from the CT. If internal channel power is unable to sustain film boiling the CT will quench and return to nucleate boiling conditions. If quench does not occur and the CT temperature rises above $600^{o}C$ it will begin to strain and possibly fail.

CHAPTER 2 - Literature Review

The development of the model required the description of several complicated processes that are dependent on temperature, internal PT pressure, material properties of the PT/CT and thermophysical properties of water. Included were the PT/CT strain rate calculations, thermal contact conduction, interfacial contact pressure, boiling heat transfer from the CT to the moderator and finally criteria for PT or CT rupture. The following will describe the reference material used to create the model.

2.1 Pressure Tube & Calandria Tube Strain

Shewfelt et al. [5] performed a series of experiments on Zr 2.5% Nb (PT) test sections to determine the dependence of PT strain on thermal and mechanical stresses. Test sections were cut in both the longitudinal and transverse direction, straightened, and subjected to varying stresses using resistive heating and a hydraulic testing machine. It must be noted that the microstructure of PT material is known to be temperature dependent. Below 610^{o}C the crystal structure will be in the so called alpha phase and take the shape of a hexagonal close packed lattice. As the temperature increases and exceeds

925°C the crystal structure will be transformed into body centered cubic lattice referred to as the beta phase.

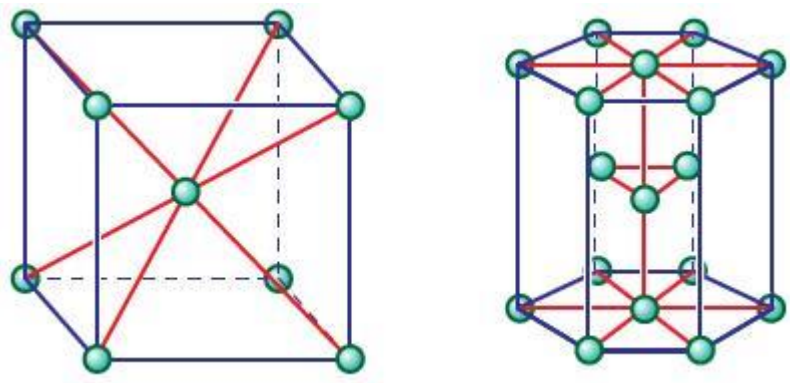

Figure 2.1 Representation of body centered cubic (left) and hexagonal close packed (right) crystal structures [6]

Between these two limits (610-925°C) the crystal structure of the solid will be a combination of both phases. Shewfelt [5] acknowledged this behaviour and chose a set of experimental conditions that would allow him to account for this lattice change. Strain data was obtained for temperatures ranging from 450-1200°C and internal stresses between 1-100 MPa. The experiments concluded that the two main components of Zr 2.5% Nb transverse creep, for temperatures between 450°C and 850°C, were the power-law creep in the α-phase ($\dot{\epsilon}_{\alpha}$) and the grain boundary sliding ($\dot{\epsilon}_{gb}$). Total strain rate was evaluated as the simple addition of the two components such that:

$$\dot{\epsilon}_{pt} = \dot{\epsilon}_{\alpha} + \dot{\epsilon}_{gb} \quad (2.1)$$

$$\dot{\epsilon}_{pt} = 1.3 \times 10^{-5}\sigma_{pt}^{9}\, exp\left(-\frac{36600}{T_{pt}}\right) + \frac{5.7 \times 10^{7}\sigma_{pt}^{1.8}\, exp\left(-\frac{29200}{T_{pt}}\right)}{\left[1 + 2 \times 10^{10}\int_{t_1}^{t} exp\left(-\frac{29200}{T_{pt}}\right) dt\right]^{0.42}} \quad (2.2)$$

Here σ_{pt} is the stress applied to the specimen and t_1 is the time at which the temperature of the PT (T_{pt}) reaches 700°C. For temperatures between 850 to 1200°C the main contributors to transverse creep were the grain boundary sliding and the β-phase power-law creep ($\dot{\epsilon}_{\beta}$) yielding:

$$\dot{\epsilon}_{pt} = \dot{\epsilon}_{gb} + \dot{\epsilon}_{\beta} \quad (2.3)$$

$$\dot{\epsilon}_{pt} = 10.4\sigma_{pt}^{3.3}\, exp\left(-\frac{19600}{T_{pt}}\right) + \frac{3.5 \times 10^{4}\sigma_{pt}^{1.4}\, exp\left(-\frac{19600}{T_{pt}}\right)}{1 + 274\int_{t_2}^{t} exp\left(-\frac{19600}{T_{pt}}\right)\left(T_{pt} - 1105\right)^{3.72} dt} \quad (2.4)$$

In this case t_2 is the time at which the temperature reaches 850°C.

Further experiments conducted by Shewfelt et al. [7] included Zircaloy-2 (CT) test sections, subject to the same temperature dependent crystal structure behaviour as Zr 2.5% Nb. The total transverse creep of the sample, for temperatures below 850°C, was shown to be the sum of the dislocation creep ($\dot{\epsilon}_{d}$) and grain boundary sliding:

$$\dot{\epsilon}_{ct} = \dot{\epsilon}_{d} + \dot{\epsilon}_{gb} \quad (2.5)$$

$$\dot{\epsilon}_{ct} = 22000(\sigma_{ct} - \sigma_{i})^{5.1}\, exp\left(-\frac{34500}{T_{ct}}\right) + 140\sigma_{ct}^{1.3}\, exp\left(-\frac{19000}{T_{ct}}\right) \quad (2.6)$$

σ_i is the internal stress in the α-phase defined by:

$$\sigma_i(t) = 1.4 + \int_0^t \left[110\dot{\epsilon}_d - 3.5 \times 10^{10}\sigma_i^{1.8}\, exp\left(-\frac{34500}{T_{ct}}\right)\right] dt \quad (2.7)$$

2.2 Thermal Contact Conductance

Yovanovich [8] presented a model describing the thermal contact conductance between two solids sandwiching some interstitial fluid. This study provided correlations for both the conduction of heat through points of solid contact (h_s) and the conduction through the fluid trapped between asperities (h_g). The total conductance is then the simple addition of the two mechanisms:

$$h_{cont} = h_s + h_g \quad (2.8)$$

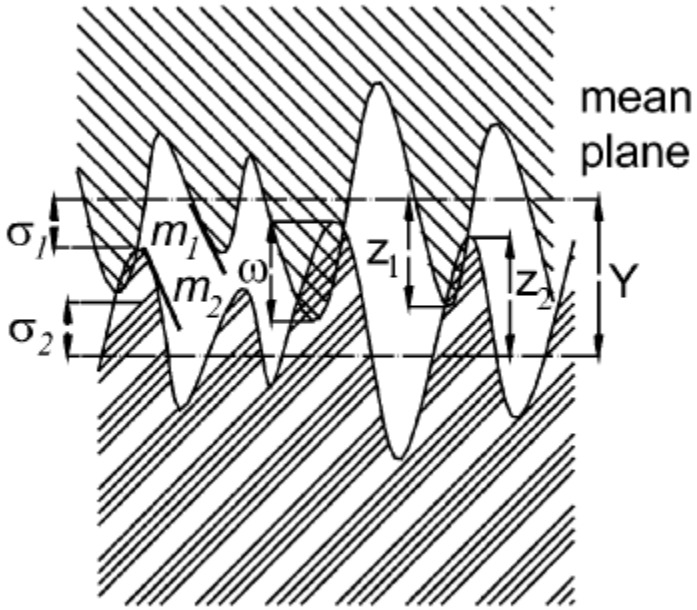

Figure 2.2 Two solid surfaces coming into contact. The average plane separation (Y) is determined by the roughness (σ) and average slope of asperities (m) of the two surfaces [9]

The solid contact conductance will depend largely on the total contacting surface area. Since all engineered surface will be rough on a scale of micrometers a technique was devised to estimate the total contact area. Yovanovich assumed that any surface asperities would follow a Gaussian distribution over the surface of a solid. The average roughness for both surfaces could then be estimated as the root mean square (RMS) of each individual surface roughness (σ_{rms}) and this same principal could be applied to the average asperity slope (m). Any plastic deformation experienced by these contact asperities would serve to increase total contacting area and Yovanovich accounted for this deformation by including the ratio of contact pressure (P) to microhardness (H) of the solids. Finally, the contact conductance logically depends on the thermal conductivity of the two solids and to that end the harmonic mean of both conductivities (k_s) was used in the evaluation of contact conductance.

$$h_s = \frac{1.25mk_s}{\sigma_{rms}}\left(\frac{P}{H}\right)^{0.95} \quad (2.9)$$

The harmonic average of two conductivities, RMS asperity slope and RMS roughness were evaluated as:

$$k_s = \frac{2k_1k_2}{k_1 + k_2} \quad (2.10)$$

$$m = \sqrt{m_1^2 + m_2^2} \quad (2.11)$$

$$\sigma_{rms} = \sqrt{\sigma_1^2 + \sigma_2^2} \quad (2.12)$$

The hardness of the configuration is based on the softer of the two contacting materials' Meyer hardness values (in Pa) [10].

$$H_M = exp(26.034 - 2.639 \times 10^{-2}T + 4.3504 \times 10^{-5}T^2 - 2.5621 \times 10^{-8}T^3) \quad (2.13)$$

Using H_M the ratio of contact pressure to microhardness was related to the Vickers correlation coefficient (c_1) and size index (c_2) by:

$$\frac{P}{H} = \left[\frac{P}{1.62\, c_1(\sigma \times 10^6)^{c_2}}\right]^{\frac{1}{1+0.071c_2}} \quad (2.14)$$

$$c_1 = \frac{0.442H_M}{c_2 + 0.370} \quad (2.15)$$

Conduction through the gas pockets formed between the solids was determined to be dependent not only on the conductivity of the gas (k_g) but also on the average gap size between the solids. This average gap size is related to the average plane separation (Y), the mean free path of the gas (Λ), fluid (β) and accommodation (α) parameters.

$$h_g = \frac{k_g}{Y + \alpha\beta\Lambda} \quad (2.16)$$

Similar to the number of solid contact areas the average plane separation will depend on the RMS roughness of the two solids and the degree of asperity deformation. Yovanovich [8] accounted for this by including the ratio of contact pressure to microhardness in the estimate of average plane separation.

$$Y = 1.184\sigma_{rms}\left(-ln\left(\frac{3.132P}{H}\right)\right)^{0.547} \quad (2.17)$$

The molecular mean free path, in this system, is an estimate of the average distance a gas molecule will travel before colliding with another molecule. In this case the collisions impede the transfer of heat between the two solids and will reduce the overall gas conductance. The mean free path is a function of the number of molecules per unit volume (n_v) and the effective collision area (A_c).

$$\Lambda = \frac{1}{\sqrt{2}A_c n_v} = \frac{1}{\sqrt{2}\pi d^2 n_v} \quad (2.18)$$

d is the diameter of the gas molecules. The number of particles per unit volume can be determined using Avogadro's number and the ideal gas law relating Λ to gas pressure and temperature.

$$n_v = \frac{nN_A}{V} \quad (2.19)$$

$$V = \frac{nRT}{P} \quad (2.20)$$

$$\Lambda = \frac{RT}{\sqrt{2}\pi d^2 N_A P} \quad (2.21)$$

Yovanovich assumed the interstitial gas behaved as an ideal gas and related the influence of temperature, and pressure, change on mean free using a reference mean free path (Λ_o), temperature (T_o) and pressure (P_o).

$$\Lambda = \Lambda_o \left(\frac{T_g}{T_o}\right)\left(\frac{P_o}{P}\right) \quad (2.22)$$

The fluid parameter is dependent on the heat capacity ratio ($\gamma = c_p/c_v$) and the Prandtl number (Pr) for the interstitial gas:

$$\beta = \frac{2\gamma}{\gamma + 1}\frac{1}{Pr} \quad (2.23)$$

The accommodation parameter is a measure of how readily the gas molecules will impart their kinetic energy to a solid surface upon collision. It is affected by properties including surface microgeometry, gas/solid molecular mass and surface contaminants on the solid. Song and Yovanovich [11] correlated the parameter as a function of temperature and molecular mass.

$$\alpha = \frac{2 - \alpha_1}{\alpha_1} + \frac{2 - \alpha_2}{\alpha_2} \quad (2.24)$$

$$\alpha_n = exp\left[-0.57\left(\frac{T_n - T_o}{T_o}\right)\right] M_g^{**} + \frac{2.4\mu}{1 + \mu^2}\left\{1 - exp\left[-0.57\left(\frac{T_n - T_0}{T_o}\right)\right]\right\} \quad (2.25)$$

$$M_g^{**} = \left(\frac{M_g^*}{6.8 + M_g^*}\right) \quad (2.26)$$

Where α_n is the accommodation coefficient between the gas/solid1 interface ($n = 1$) or the gas/solid2 interface ($n = 2$) and T_n is the temperature of solid1 or solid2. μ is the ratio of gas molecular weight to solid molecular weight and, for polyatomic gases, M_g^* is equal to 1.4 times the molecular weight of the interstitial gas. In the evaluation of the accommodation parameter Song and Yonvanovich used a reference temperature (T_o) of 273K.

2.3 Contact Pressure

As can be seen in section 2.2 both the solid and gas conductance depend on the contact pressure between the two solids. Once the PT and CT make contact part of the internal PT pressure will be exerted onto the inner CT wall. It is assumed the tubes do no separate after contact meaning that if the CT begins to strain the strain rate of the two tubes will be equal:

$$\dot{\epsilon}_{pt} = \dot{\epsilon}_{ct} \quad (2.27)$$

Both strain rates are dependent on their respective temperatures and the azimuthal stress exerted on the tube walls. The degree of contact pressure will limit the strain experience by the PT and increase that of the CT.

$$\sigma_{pt} = \frac{(P_{pt} - P_{contact})r_{pt}}{\tau_{pt}} \quad (2.28)$$

$$\sigma_{ct} = \frac{(P_{contact} - P_{ext})r_{ct}}{\tau_{ct}} \quad (2.29)$$

r and τ are the radius and thickness, respectively, of the particular tube in question. Using equation (2.27) and the creep strain equations (2.2) & (2.6) it is possible to iteratively solve for the contact pressure. This method will be described in chapter 3.

2.4 Boiling Water Heat Transfer

The heat transfer coefficient between the calandria tube and the moderator (h_{conv}) will depend on the boiling regime. The three main regimes considered in this model are

natural convection, nucleate boiling and film boiling. The following section will review various correlations that predict h_{conv} in each boiling regime.

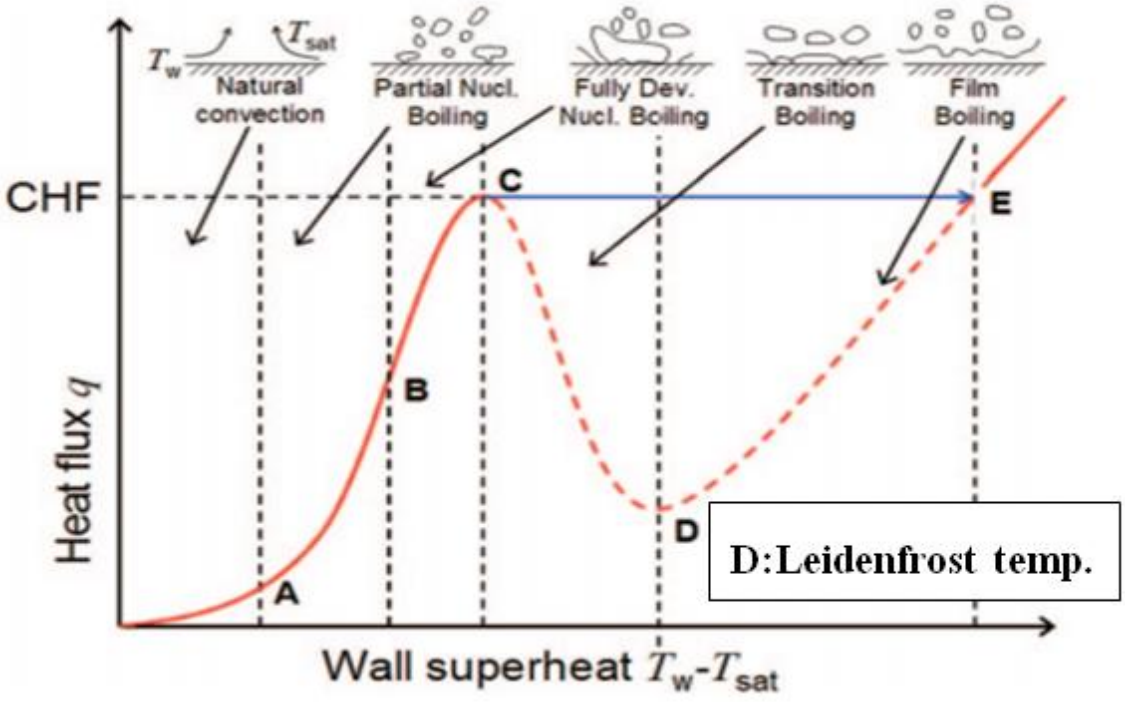

Figure 2.3 Boiling curve relating the heat flux to the wall superheat [12]

2.4.1 Natural convection

As described in section 1.4 at the moment of PT/CT contact the CT will be initially at bulk fluid temperature. As the CT temperature rises the surrounding fluid temperature also begins to increase inducing a density driven flow known as natural convection. This will be the sole contributor to CT heat removal until the CT temperature rises above saturation temperature. Churchill and Usagi [13] developed an empirical correlation for the ratio of convective to conductive heat transfer (known as the Nusselt

number Nu), in terms of the buoyancy driven flow, related to the Rayleigh number (Ra), and the ratio of momentum to thermal diffusivity (the Prandtl number Pr).

$$Nu = \frac{h_{conv}L}{k} \quad (2.30)$$

$$Ra = \frac{g\beta_{th}}{\nu\alpha_d}(T_{ct} - T_b)L^3 \quad (2.31)$$

$$Pr = \frac{c_p\mu}{k} \quad (2.32)$$

$$Nu = 0.36 + \frac{0.518Ra_D^{\frac{1}{4}}}{\left[1 + \left(\frac{0.559}{Pr}\right)^{\frac{9}{16}}\right]^{\frac{4}{9}}} \quad (2.33)$$

Values for the conductivity (k), kinematic viscosity (ν), dynamic viscosity (μ), thermal diffusivity (α), specific heat (c_p), and thermal expansion coefficient (β_{th}) of the fluid are all evaluated at film temperature which is the average of CT surface and bulk fluid temperatures. L in this case is the characteristic length of a horizontal cylinder ($\pi D_{ct}/2$). However, the above correlation was only relevant for laminar boundary conditions ($10^{-6} < Ra_D \leq 10^9$).

Churchill and Chu [14] shifted their focus to the development of a correlation applicable for all Rayleigh numbers. Experimental data shows that, for a vertical plate, as Ra approaches infinity Nu can be expressed as:

$$Nu \to C\ Ra^{\frac{1}{3}} f\{Pr\} \quad (2.34)$$

Where C is a constant and $f\{Pr\}$ is related to the Prandtl number such that:

$$Pr \to \infty \quad f\{Pr\} \to 1 \quad (2.35)$$

$$Pr \to 0 \quad f\{Pr\} \propto Pr^{\frac{1}{3}} \quad (2.36)$$

Combining equation (2.33) with the behaviour of the Prandtl number above, they arrived at the following test expression.

$$Nu^n = 0.36^n + \left(C\, Ra^{\frac{1}{3}} f\{Pr\}\right)^n \quad (2.37)$$

The value of n was chosen to be 1/2 which was used by Bosworth [15] to describe natural convection in air but deemed appropriate for all fluids. I order to maintain the same Pr dependence observed in equation (2.33) $f\{Pr\}$ was set to:

$$f\{Pr\} = \left[1 + \left(\frac{0.559}{Pr}\right)^{\frac{19}{6}}\right]^{\left(\frac{16}{9}\right)\left(-\frac{1}{3}\right)} \quad (2.38)$$

The correlation for the Nusselt at all Rayleigh numbers is then estimated as:

$$Nu = \left\{0.60 + \frac{0.387 Ra_D^{\frac{1}{6}}}{\left[1 + \left(\frac{0.559}{Pr}\right)^{\frac{9}{16}}\right]^{\frac{8}{27}}}\right\}^2 \quad (2.39)$$

Based on the experimental data used in the study this correlation accurately predicts Nu between $10^{-5} < Ra < 10^{13}$.

2.4.2 Nucleate Boiling

Once the CT temperature has risen above saturation temperature water vapor bubbles will begin forming at nucleation sites on the surface of the CT. The nucleate boiling heat transfer coefficient will be affected by properties such as the surface tension of the fluid, the number of nucleation sites and the frequency of bubble departure. Several nucleate boiling correlations exist for a variety of application. The following are some of the more general relationships.

2.4.2.1 Rohsenow

$$h_{conv} = \mu_l h_{fg} \left(\frac{c_{pl}}{C_{sf} h_{fg} Pr^n} \right)^3 \sqrt{\frac{g(\rho_l - \rho_v)}{\sigma}} (T_w - T_{sat})^2 \quad (2.40)$$

Rohsenow [16] developed a nucleate boiling HTC correlation by estimating the number, and size of bubbles, generated on the heated surface and accounting for the local agitation of the surrounding fluid induced by the bubble departure. The heat flux to the fluid was approximated by the number (n) and frequency (f) at which bubbles, of diameter D_b and density ρ_v, formed on the heated surface based on the latent heat of vaporisation (h_{fg}) of the liquid.

$$q''_{nb} = h_{fg} \rho_v n \frac{\pi}{6} D_b^3 f \quad (2.41)$$

A bubble rise Reynolds number ($N_{Re,b}$) was introduced to account for the agitation induced by bubbles once they leave the surface. $N_{Re,b}$ was described as function of bubble diameter (D_b), mass velocity (G_b), and viscosity of the surrounding liquid (μ_l).

$$N_{Re,b} \equiv \frac{G_b D_b}{\mu_l} \quad (2.42)$$

Using work done by Frity [17] the bubble diameter was based on the bubble contact angle (β), liquid and vapor densities, surface tension (σ) and the acceleration due to gravity (g).

$$D_b = C\beta_\theta \sqrt{\frac{2\sigma}{g(\rho_l - \rho_v)}} \quad (2.43)$$

By writing the bubble mass velocity as:

$$G_b = \frac{\pi}{6} D_b^3 f \rho_v n \quad (2.44)$$

and substituting it into equation (2.41):

$$G_b = \frac{q''_{nb}}{h_{fg}} \quad (2.45)$$

the bubble rise Reynolds number takes the form:

$$N_{Re,b} = C\beta \frac{q''_{nb}}{\mu_l h_{fg}} \sqrt{\frac{2\sigma}{g(\rho_l - \rho_v)}} \quad (2.46)$$

From this point Roshenow [16] introduced a relationship for the bubble Nusselt number based on bubble diameter.

$$N_{Nu,b} = \frac{h_{conv} D_b}{k_l} \quad (2.47)$$

Postulating that the method of heat transfer was directly from wall to liquid, the Prandtl number was included in the heat transfer correlation. The final relationship between all three parameters was:

$$N_{Nu,b} = \frac{1}{C_{sf}} N_{Re,b}^{\frac{2}{3}} Pr^{n} \quad (2.48)$$

where $1/C_{sf} = \sqrt{2}C$. The value of C_{sf}, called the surface fluid combination, and the exponent n are dependent on the solid and liquid involved in the heat exchange.

2.4.2.2 Sarma

$$h_{conv} = \left[\frac{3.36 \times 10^{-5} l^{*0.586} P^{-0.174} \mu_l^{0.594} h_{fg}^{0.797}}{(T_w - T_{sat}) k_l^{1.18}}\right]^{-\frac{1}{0.18}} \quad (2.49)$$

$$l^{*} = \sqrt{\frac{\sigma}{(\rho_l - \rho_v) g}} \quad (2.50)$$

The presence of a surface fluid combination factor (C_{sf}) and variable exponent n is a limitation of the Rohsenow correlation. These values, dependent on factors such as bubble contact angle and the roughness of the heated surface, will determine the success of the correlation and need to be determined experimentally. This limitation, shared with other correlations such as Mikic [18] and Pioro [19], was the motivation for the work done by Sarma et al. [20]. Seven separate nucleate boiling HTC correlations were compared to the data consolidated by Borishansky from a collection of articles. Sarma et al. then developed a correlation based on what they deemed the most relevant

dimensionless parameters in each correlation. Parameters included Rohsenow's modified Reynolds number (equation (2.46)), Mostinski and Borishansky's reduced pressure consideration (P_b/P_{cr}) and the consideration of Tien et al. regarding boiling heat transfer as inverted stagnation flow perpendicular to the heater wall. The initial correlation took the form:

$$\frac{q''_{nb}}{\mu_l h_{fg}}\sqrt{\frac{\sigma}{(\rho_l-\rho_v)g}} = 0.0312\left(\frac{D}{\delta_t}\right)^{1.15}\left(\sqrt{\frac{\sigma}{(\rho_l-\rho_v)gD^2}}\right)^{-1.99}\left(\frac{P_b}{P_{cr}}\right)^{0.208} \quad (2.51)$$

Where δ_t is the thermal boundary layer given by:

$$\delta_t = \frac{(T_w - T_{sat})k_l}{q''_{nb}} \quad (2.52)$$

Average deviation between the above correlation and Borishansky's [21] data was ± 37%. This deviation was reduced by introducing another dimensionless parameter.

$$\frac{P_b D}{\mu_l h_{fg}^{0.5}} \quad (2.53)$$

The final correlation was then:

$$\frac{q''_{nb}l^*}{\mu_l h_{fg}} = 3.8\times10^{-6}\left(\frac{D}{\delta_t}\right)^{1.22}\left(\frac{P_b}{P_{cr}}\right)^{-0.72}\left(\frac{P_b D}{\mu_l\sqrt{h_{fg}}}\right)^{0.55}\left(\frac{l^*}{D}\right)^{1.65} \quad (2.54)$$

with an average deviation to about ± 16 %. In future work by Sarma et al. [22] it was revealed that the above equation is valid for cylinder diameters between 4.9 mm and 6.94

mm. A new correlation, independent of diameter, was suggested taking the form of equation (2.49).

2.4.2.3 Borishansky

$$h_{conv} = \left(0.1011 P_{cr}^{0.69} f(P_R)\right)^{\frac{10}{3}} (T_w - T_{sat})^{\frac{7}{3}} \quad (2.55)$$

$$f(p_R) = 1.8 P_R^{0.17} + 4 P_R^{1.2} + 10 P_R^{10} \quad (2.56)$$

As previously mentioned the work performed by Sarma et al. [20] was heavily reliant on data obtained from Borishansky [21]. Borishansky had developed a nucleate boiling HTC correlation based on experimentally collected data and reliably predicted the HTC when water was the heat transfer medium. However, it consistently under predicted the nucleate boiling HTC for ethyl alcohol. This was another contributing factor to Sarma et al.'s desire for a more generally accurate HTC correlation. Borishansky's correlation was based on the law of corresponding states and was dependent on the reduced pressure ($P_R = P_b/P_{cr}$) and the wall superheat ($T_w - T_{sat}$).

2.4.2.4 Correlation Selection

Pioro provides values for C_{sf} and n in equation (2.40) for a variety of liquid solid interfaces. As observed in Figure 2.4 and Figure 2.5 the predicted value of h_{conv} can vary widely and cannot be attributed to the type of materials alone.

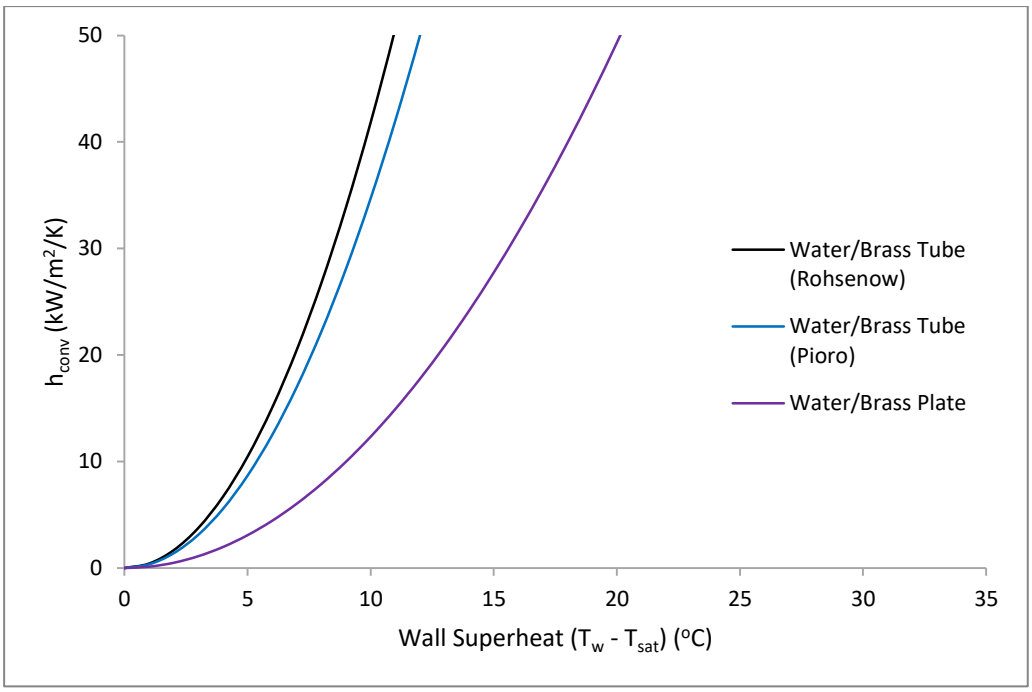

Figure 2.4 Variation in correlations for the nucleate boiling HTC of a heated brass surface in water

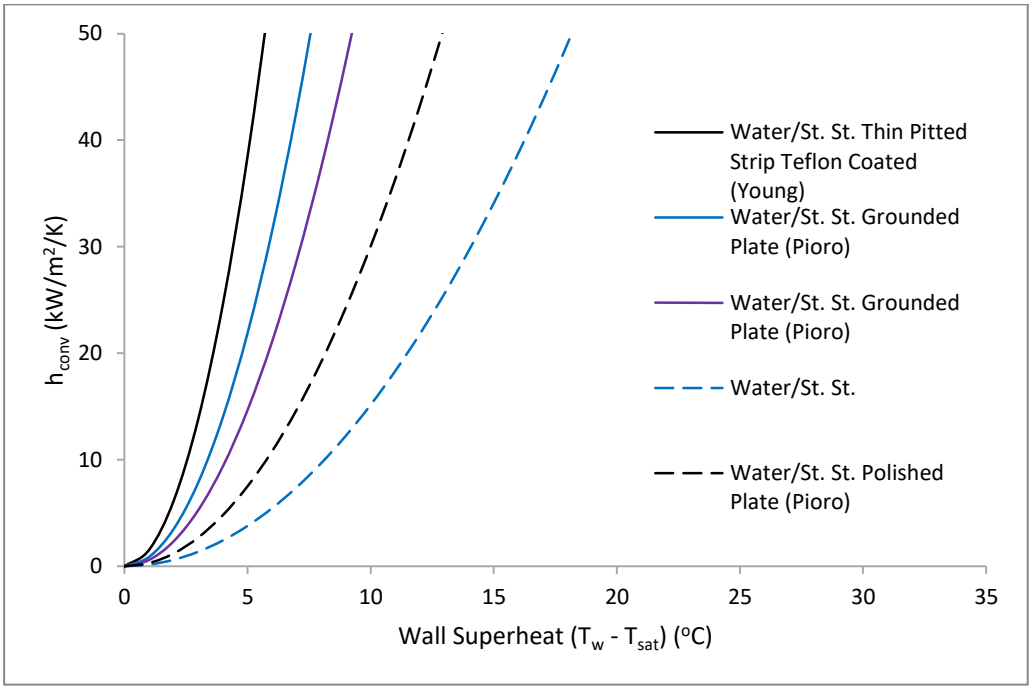

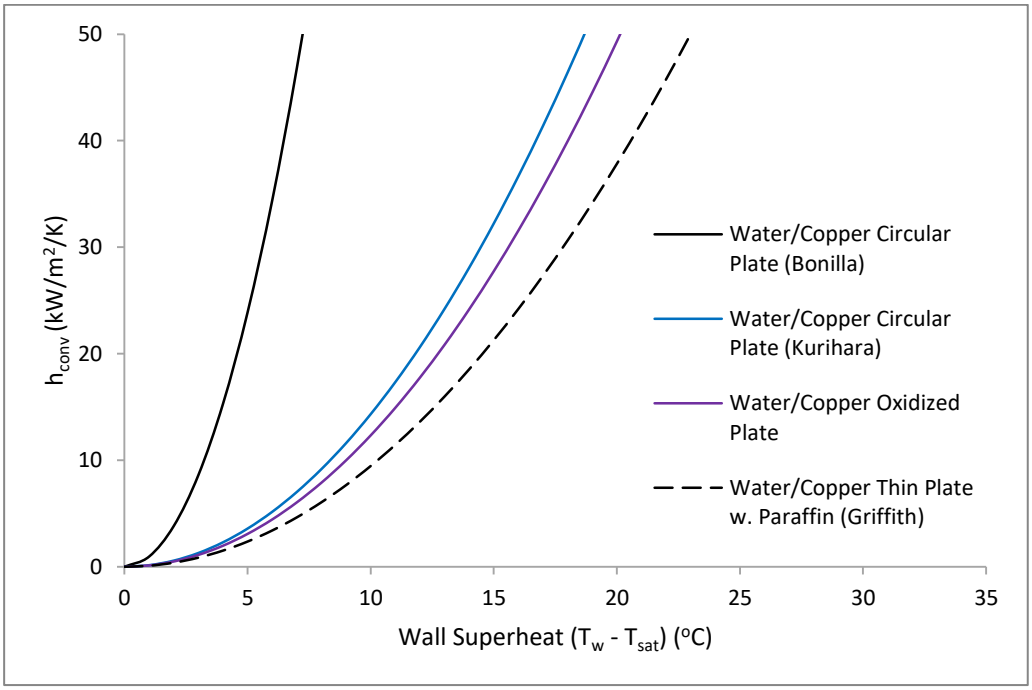

Figure 2.5 Correlations obtained for the nucleate boiling HTC of heated stainless steel (top) & copper (bottom) surfaces, of varying geometries, in water

We can see that for the specific case of a circular copper plate (Kurihara and Bonilla) h_{conv} can exhibit widely different behaviours that are likely attributed to surface finish. Since values of C_{sf} and n could not be found for a water/zirconium interface Rohsenow's correlation was not used for this project.

The diameter independent correlation provided by Sarma et al. was a promising candidate. However, based on Figure 2.6 we see that the values predicted for h_{conv} are quite low compared to any other water/solid interface studied by Pioro. The nucleate boiling HTC remains below 10 kW/m^2/K until the surface temperature increases to 20^{o}C above saturation.

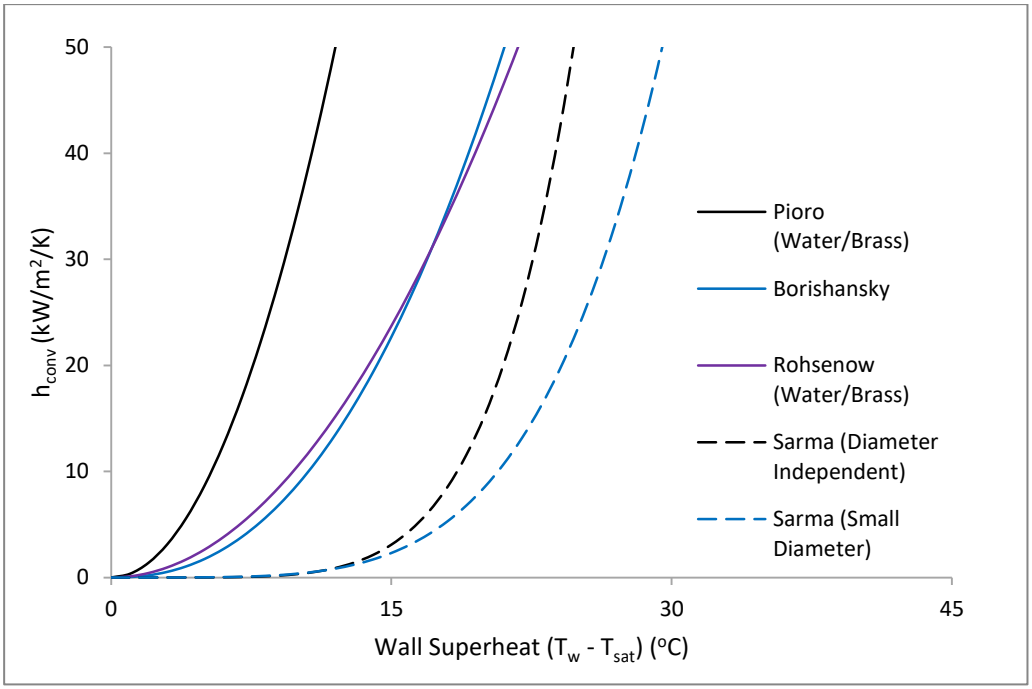

Figure 2.6 Various general nucleate boiling HTC correlations

That isn't to say the prediction is incorrect but, based on the amount of available data, the behaviour of h_{conv} for water/zirconium is expected to fall at least somewhat more in line with other water/solid combinations.

This leaves Borsishansky's correlation which, as shown in Figure 2.6, falls somewhere in the middle of the previous correlations. The material interface that comes closest to the Borishansky correlation is the water/brass combination reported by Pioro. For Rohsenow's original work the value of n was locked at 1.7 which would put the value of C_{sf} at about 0.0095 if we wanted to force Roshenow's [16] correlation to match the Borishansky correlation.

2.4.3 Film Boiling

Although the nucleate pool boiling HTC correlations suggest a continuing increase with increasing wall temperature this is not the case. Instead, if the heat flux to the surface fluid is large enough a blanket of evaporated liquid can begin to form. This vapor film creates a barrier between the wall and the surrounding fluid, severely reducing the heat flux to the surrounding fluid. The wall temperature will rise at the location of film boiling and can cause the film to spread; eventually covering the entire heating surface. This boiling regime is known as film boiling and the heat flux required to induce film boiling is referred to as the critical heat flux (CHF).

Zuber [23] described the development of film boiling in an attempt to predict the critical heat flux for a flat heating surface. It was suggested that as the heat flux increased vapor jets would begin to form at nucleation sites rather than bubbles.

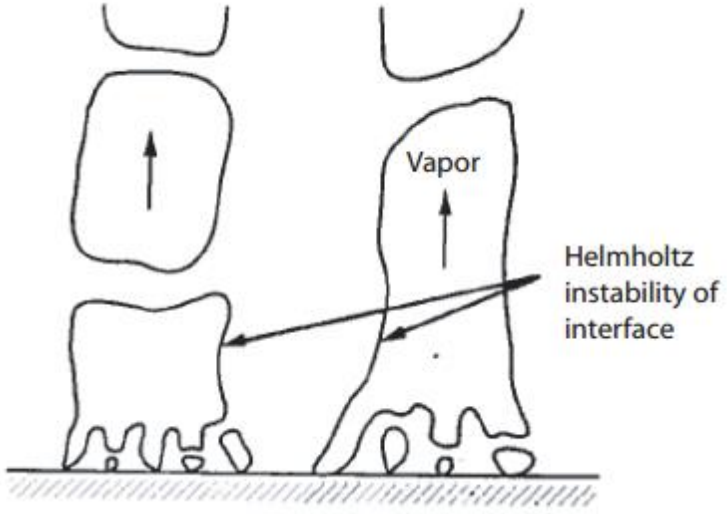

Figure 2.7 The development of vapor jets at the nucleation sites of a heated surface [24]

These vapour jets, flowing away from the heater surface due to buoyancy forces, would then interfere with the ability of the surrounding subcooled water to wet the heater surface. Referring to work performed by Lamb [25] and Milne-Thomson [26] the propagation equation for small disturbances is:

$$c^2 = \frac{\sigma m_\lambda}{(\rho_l + \rho_v)} - \frac{\rho_l \rho_v}{(\rho_l + \rho_v)^2}(u_l + u_v)^2 \quad (2.57)$$

Where c is some real constant, m is the wave number, and u is the velocity of the fluid identified by the subscripts. Zuber [23] postulated that critical heat flux would be the flux at which the vapor mass velocity was equal to that of the subcooled fluid.

$$\rho_v u_v = \rho_l u_l \quad (2.58)$$

Substituting the above relationship into equation (2.57) and setting c to zero Zuber arrived at the critical velocity:

$$u_v = \left(\frac{\sigma m_\lambda}{\rho_v}\right)^{\frac{1}{2}} \left(\frac{\rho_l}{\rho_l + \rho_v}\right)^{\frac{1}{2}} \quad (2.59)$$

Since the focus of this project uses water as the pool liquid the following simplification can be made.

$$\left(\frac{\rho_l}{\rho_l + \rho_v}\right)^{\frac{1}{2}} \approx 1 \quad (2.60)$$

The value of the wave number was handled by referring to Rayleigh's work on the stability of circular gas jets in liquid. It was found that instability will only occur in the event of a disturbance with wavelength (λ) larger than the jet circumference ($2\pi R$).

$$\lambda = 2\pi R \quad (2.61)$$

The wave number is then:

$$m_\lambda = \frac{1}{R} \quad (2.62)$$

Zuber assumed the vapor column radius was equal to $\lambda/4$ resulting in a single column mass flow rate of:

$$G_c = \rho_v \pi \left(\frac{\lambda}{4}\right)^2 u_v \quad (2.63)$$

The mass flow rate per unit area λ^2 is then:

$$\frac{G_c}{\lambda^2} = \rho_v \frac{\pi}{16}\left(\frac{\sigma 4}{\rho_v \lambda}\right)^{\frac{1}{2}} \quad (2.64)$$

Re-inserting the wave number

$$\frac{G_c}{\lambda^2} = \rho_v \frac{\pi}{8}\frac{1}{\sqrt{2\pi}}\left(\frac{\sigma \mathrm{m}_\lambda}{\rho_v}\right)^{\frac{1}{2}} \quad (2.65)$$

For a pool of saturated liquid we do not need to provide energy to raise the surrounding fluid temperature and the energy necessary to initiate film boiling would be the fluid's latent heat of vaporisation.

$$q''_{chfsat} = \frac{1}{8}\sqrt{\frac{\pi}{2}}\, h_{fg}(\sigma \rho_v m_\lambda)^{\frac{1}{2}} \quad (2.66)$$

Experimental data suggests that the value of m is between

$$\left(\frac{g(\rho_l - \rho_v)}{\sigma}\right)^{\frac{1}{2}} \geq m_\lambda \geq \left(\frac{g(\rho_l - \rho_v)}{3\sigma}\right)^{\frac{1}{2}} \quad (2.67)$$

Resulting in a CHF range of

$$0.1566\, h_{fg}(\sigma g \rho_v^2(\rho_l - \rho_v))^{\frac{1}{4}} \geq q''_{chfsat} \geq 0.119 h_{fg}\left(\sigma g \rho_v^2(\rho_l - \rho_v)\right)^{\frac{1}{4}} \quad (2.68)$$

The lower limit of saturated CHF was chosen as a conservative estimate for this project. Ivey and Morris [27] provided a correction factor for the subcooled critical heat flux.

$$\frac{q''_{chfsc}}{q''_{chfsat}} = 1 + 0.1 * \left(\frac{c_{p,f}(\Delta T_{sub})}{h_{fg}}\right)\left(\frac{\rho_l}{\rho_v}\right)^{0.75} \quad (2.69)$$

As previously mentioned once CHF has been exceeded the heat flux decreases rapidly. Gillespie and Moyer [28] performed experiments to determine the pool film boiling heat transfer coefficient (h_{fb}) for large diameter cylinders. Their findings indicated that h_{fb} was related to the degree of pool subcooling by:

$$h_{fb} = h_{fbo}(1 + 0.031\Delta T_{sub}) \quad (2.70)$$

$$h_{fbo} = 0.2 \text{ kW/m}^2\text{/K} \quad (2.71)$$

2.4.4 Quench

At this point it should be noted that only at the time of initial PT/CT contact is there a risk of film boiling. This is the moment where the temperature difference between the two tubes will be at its largest. However, there exists the possibility that film boiling is initiated at contact but the internal channel power is insufficient to sustain film boiling conditions. This will result in CT rewet and return to nucleate boiling conditions. There exist several empirical correlations that predict the minimum wall temperature required for film boiling based on the degree of subcooling. As can be seen in Table 2.1 the two consistently highest predictions of minimum film boiling temperature are the Bradfield [29] and the Onishi [30] correlation. Experimental observation of high pressure PT/CT contact boiling suggest that, for 20^{o}C pool subcooling, quenching will occur below 500^{o}C which eliminates the Ohnishi correlation. Since the Bradfield correlation predicts the highest minimum film boiling temperature below 500^{o}C it was selected as a conservative estimate for this model.

Table 2.1 A collection of minimum film boiling temperature correlations

T_{mfb} Correlation	Author
$T_{mfb} = 7.00\Delta T_{sub} + 275$	Adler [31]
$T_{mfb} = 6.15\Delta T_{sub} + 300$	Bradfield [29]
$T_{mfb} = 6.30\Delta T_{sub} + 290$	Groeneveld & Stewart [32]
$T_{mfb} = 7.50\Delta T_{sub} + 240$	Mori [33]
$T_{mfb} = 5.10\Delta T_{sub} + 450$	Ohnishi [30]

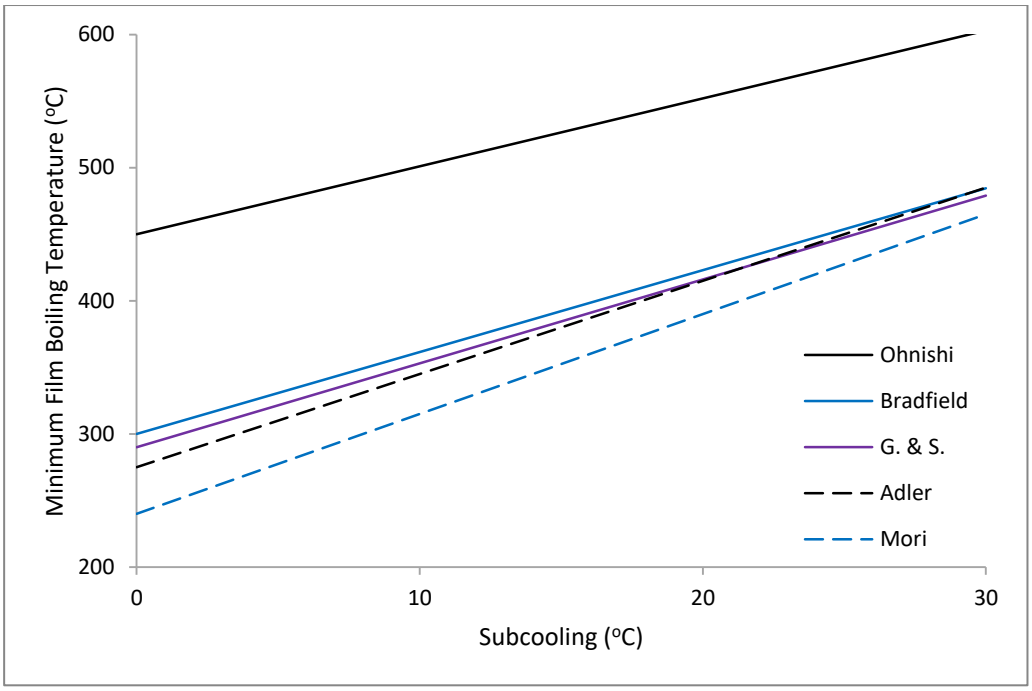

Figure 2.8 Graphical representation of the correlations provided in Table 2.1

2.5 Criteria for Failure

A continuation of Shewfelt's work [34] focused on determining the limiting creep that resulted in PT sample failure. In this work both lower and upper bound failure estimates were provided. For the upper limit Shewfelt's model considered the deformation that would result from above average local temperatures. To this end the PT circumference was broken up into segments, small enough that the temperature could be considered uniform, and strain was evaluated for each finite element. It was assumed that the PT would retain its circular geometry; the increase in radius was determined by summing all segment lengths and dividing by 2π. Each segment should have a finite mass (m_s) based on the segment volume, where the cross sectional area of the segment is given by the wall thickness (τ_s) and segment length (l_s).

$$m_s = \rho_s \tau_s l_s L_a \quad (2.72)$$

L_a is the axial length of the pressure tube. Shewfelt postulated that the failure would occur if the PT wall thinned to zero thickness as a result of local strain. As seen in Figure 2.9 the assumption is that once the segment has strained to the critical length (l_c) failure occurs at the center of the segment. Assuming that the segment's mass is conserved the volume of the two chisel edges will be:

$$\left(\frac{\tau_1 l_c}{4} + \frac{\tau_2 l_c}{4}\right) L\rho = \tau_o l_o L_a \rho_s \quad (2.73)$$

Solving for the critical length

$$l_c = \frac{4\tau_o l_o}{\tau_1 + \tau_2} \quad (2.74)$$

where τ_1 and τ_2 represent the thicknesses of the adjacent segments. If the length of any segment exceed the critical length l_c the PT was considered failed.

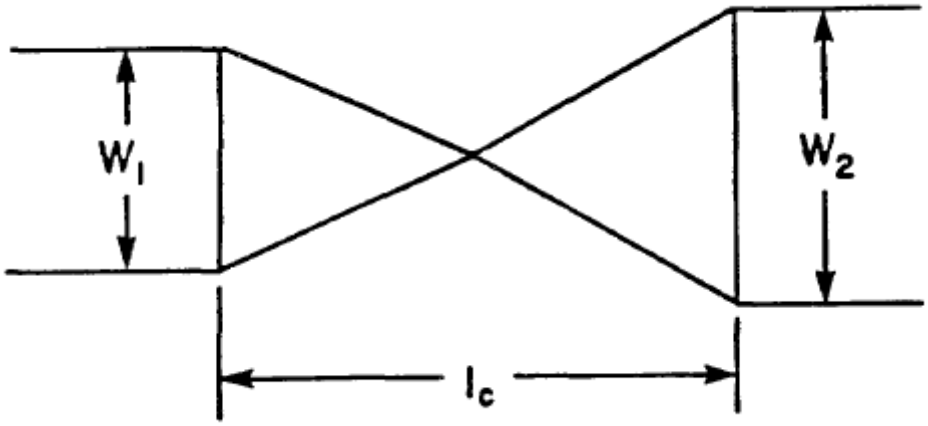

Figure 2.9 The formation of a chisel for a material undergoing severe strain [34]

The lower bound failure limit developed by Shewfelt considered the average strain that would result in PT rupture. This average strain limit (ϵ_f) prediction was based on the degree of thinning required to reach zero wall thickness in the presence of a manufacturing defect (d).

$$\epsilon_f = -\frac{1}{n_f} ln\left(1 - \left(\frac{\tau_0 - d}{\tau_0}\right)^{n_f}\right) \quad (2.75)$$

Here n_f is the stress exponent of the temperature dependent strain mode.

$$n_f = \left(\frac{\partial \ln \dot{\epsilon}}{\partial \ln \sigma}\right)_T = 1.8 \quad (2.76)$$

Shewfelt selected a defect depth of 13 μm based on the maximum allowable defect depth in PT manufacturing. The failure strain is approximately:

$$\epsilon_f \approx 2.7 \quad (2.77)$$

The model described in this thesis is one dimensional so all thermal and mechanical properties are constant over the circumferences of both the PT and CT. For this reason the average strain failure limit ϵ_f was used as the criteria for failure. Although Shewfelt's work focused on PT material neither equation is dependent on material properties and both failure modes are applicable to the CT.

2.6 Experimental Results

The data used to verify the model accuracy was obtained from a study done by Luxat [35] in association with Ontario Power Generation. Experimental results consist of temperature transients for single PT, high pressure ballooning, CT contact experiments. A test section, shown in Figure 2.10, consisted of a 0.95 m long, 19 mm radius (r_h), graphite heater positioned off center within a 1.7 m long 4 mm thick (τ_{pt}) section of Zr-2.5% Nb pressure tube. The heater was positioned off center to promote a circumferentially uniform temperature distribution around the PT circumference. The PT was placed inside a 1.75 m long 1.4 mm thick (τ_{ct}) CT and the entire apparatus was submerged in a pool of subcooled water. Six tests were performed at various internal pressures, channel powers, and pool temperatures. Temperature recordings for both the PT and CT were obtained

through the used thermocouples placed at various locations around the circumference of both tubes. The experimental conditions are outlined in Table 2.2 and the resulting thermocouple data is shown in Figure 2.11 to Figure 2.14.

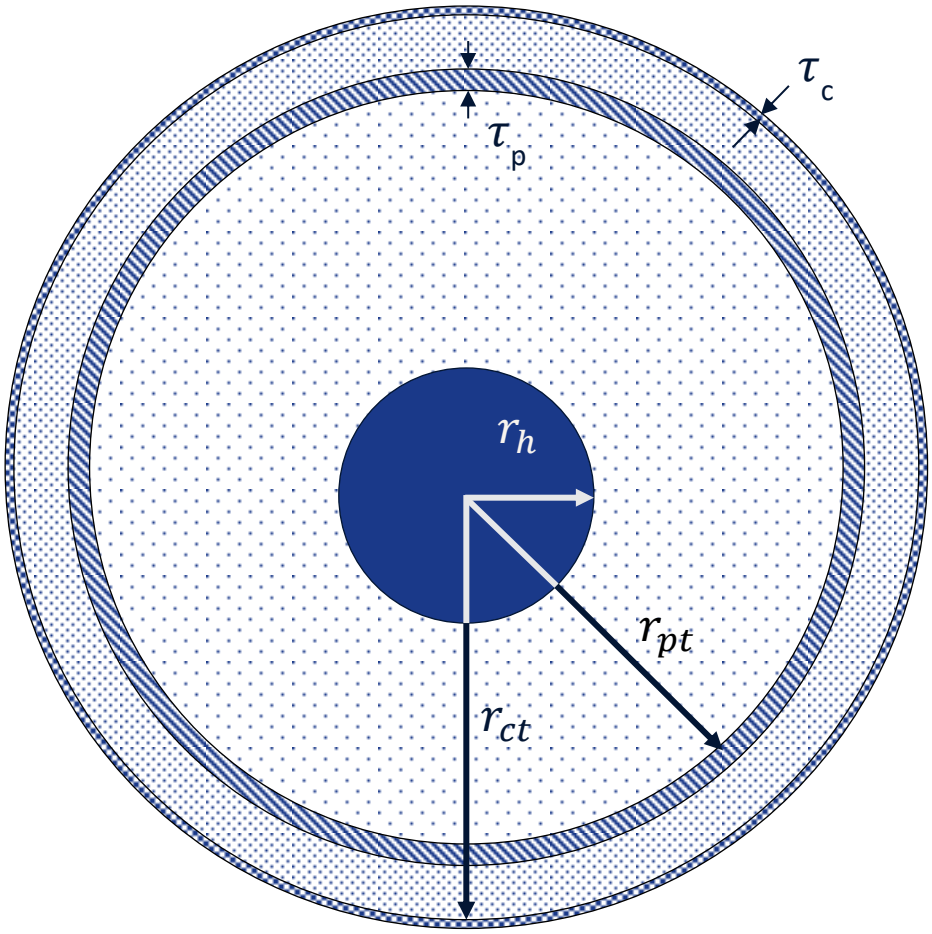

Figure 2.10 The experimental apparatus used to determine the PT and CT transients during the high pressure contact boiling experiments performed by Luxat [35]. The graphite heater was placed off center to promote a uniform temperature distribution around the PT.

Table 2.2 The set of experimental conditions used in high pressure contact boiling tests performed by Luxat [35]

Test ID	PT Pressure [MPa(g)]	Tank Subcooling [^{o}C]	Heater Power Rating [kW/m]
HPCB2	6.6	29.8	120
HPCB8	10.0	58.0	141
HPCB12	6.5	28.4	135
HPCB13	4.0	19.9	68
SUBC1	3.5	20.0	200
SUBC2	3.5	23.0	195

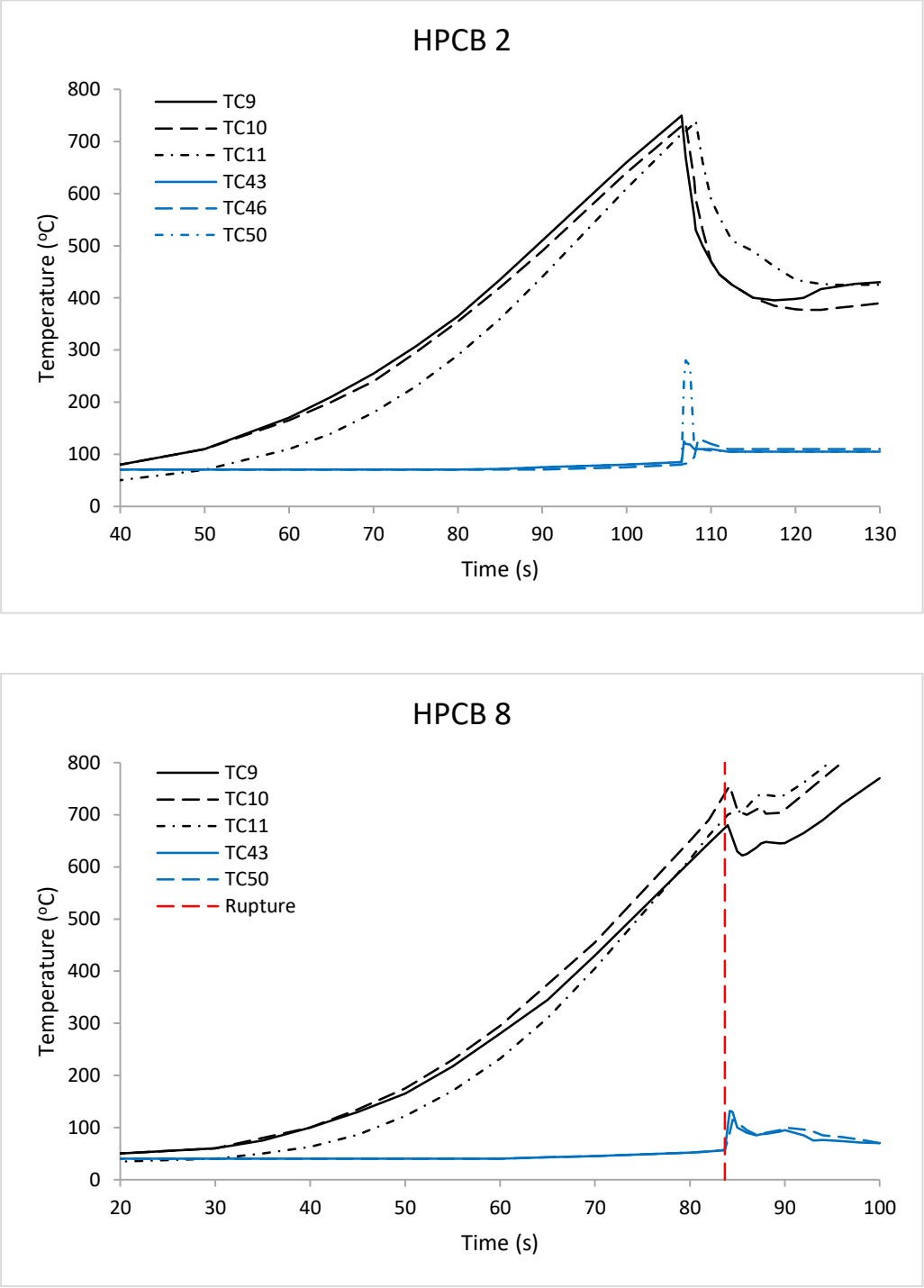

Figure 2.11 Thermocouple data for experiments HPCB2 and HPCB8, the PT failed prior to contact in HPCB8 at the 84 second mark (reproduced from [35])

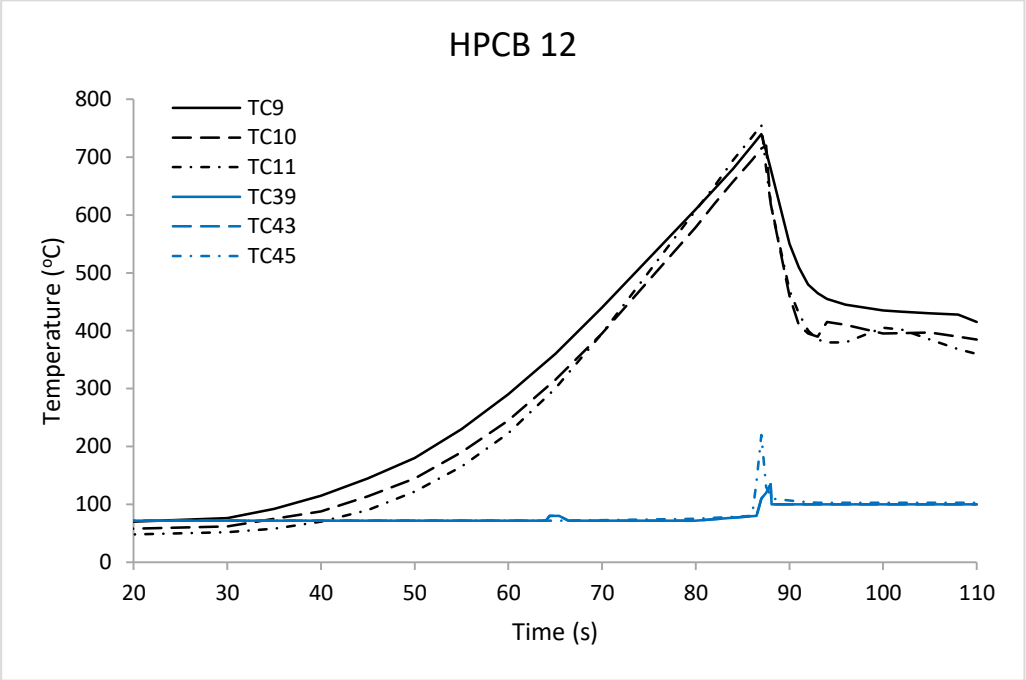

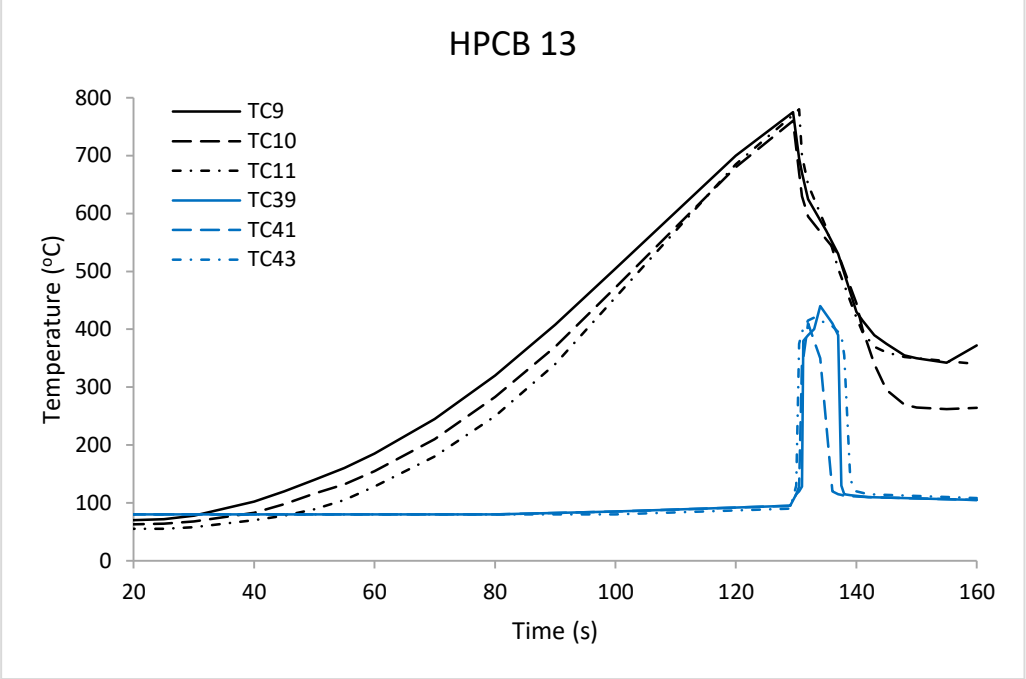

Figure 2.12 Thermocouple data for experiments HPCB12 and HPCB13 (reproduced from [35])

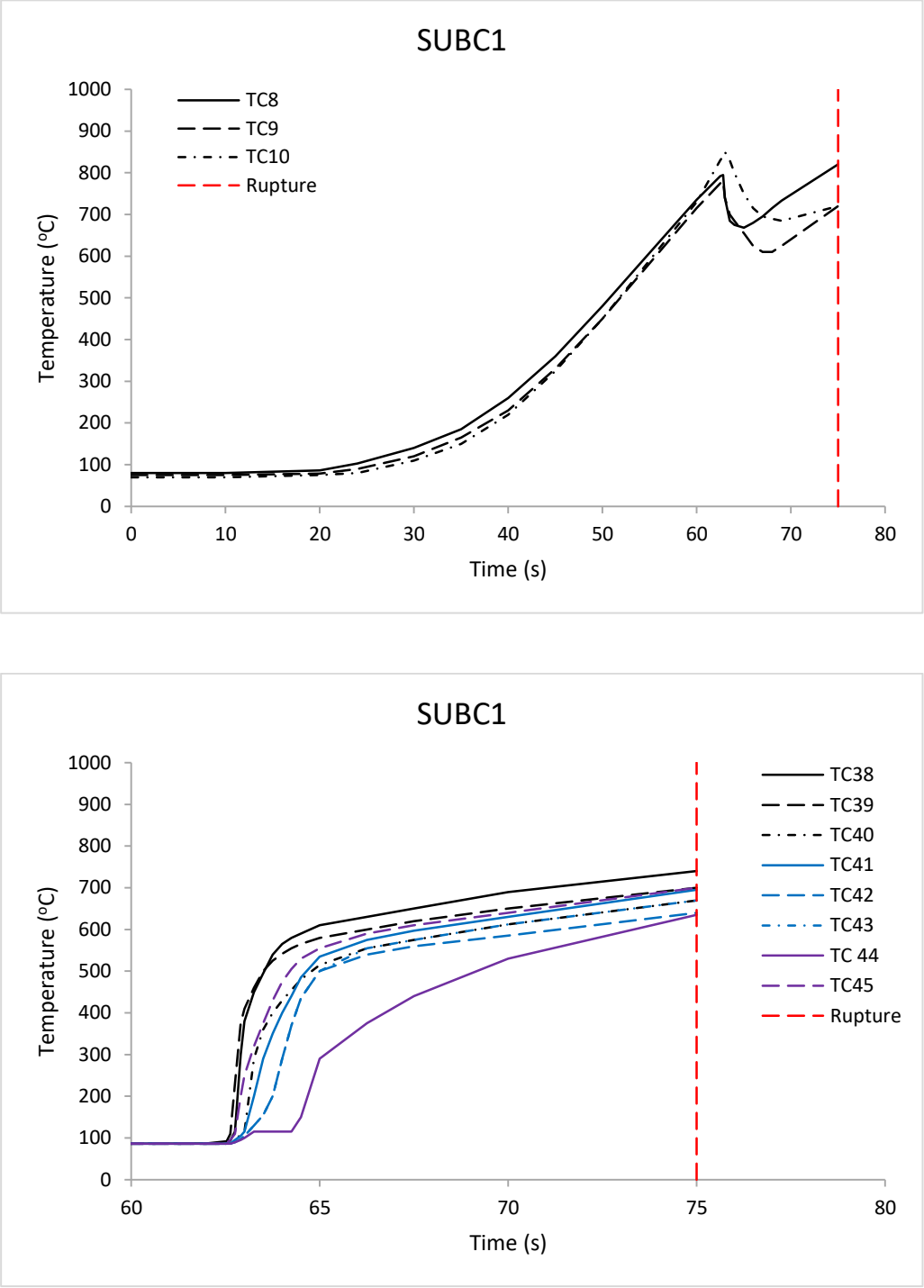

Figure 2.13 PT (top) & CT (bottom) thermocouple data recorded during experiment SUBC1, calandria tube failure occurred at the 75 second mark (reproduced from [35])

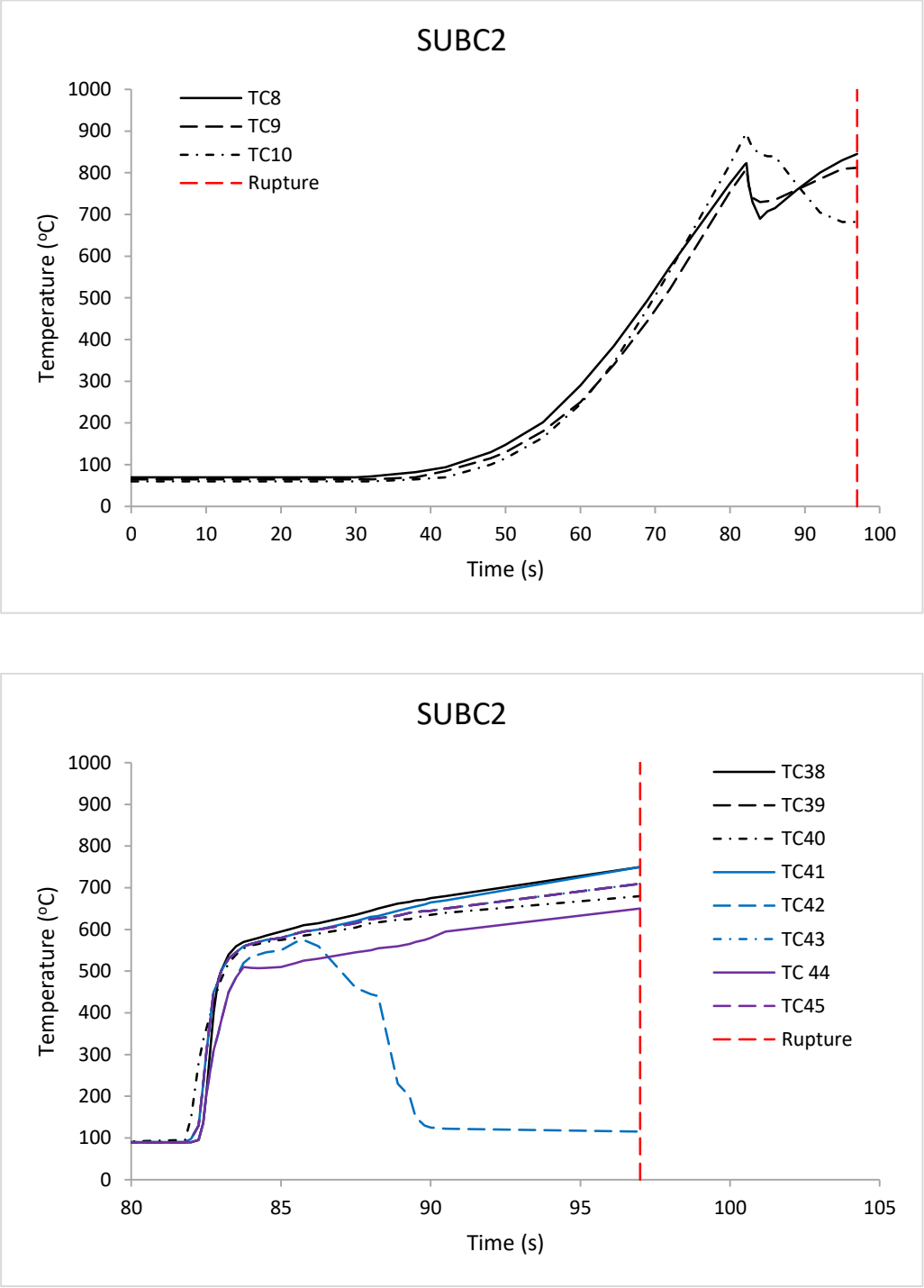

Figure 2.14 PT (top) & CT (bottom) thermocouple data recorded during experiment SUBC2, calandria tube failure occurred at the 97 second mark (reproduced from [35])

CHAPTER 3 - Initial Model Development

The model (provided in appendix B) was designed to run using either a single MATLAB file or through the use of a GUI. In either case there are 3 key functions that are called upon to calculate contact pressure, contact conductance, and heat transfer. The following section will describe the model design and the equations used during its execution.

3.1 Heat Transfer Equations

Pre-Contact

The equations that describe the heat transfer between the heater and pressure tube prior to contact are:

$$m'_h c_{ph} \frac{dT_h}{dt} = q'_h - h'_{rad}\left(T_h - T_{pt}\right) - \gamma' q'_h \quad (3.1)$$

$$m'_{pt} c_{ppt} \frac{dT_{pt}}{dt} = h'_{rad}\left(T_h - T_{pt}\right) - q'_{loss} \quad (3.2)$$

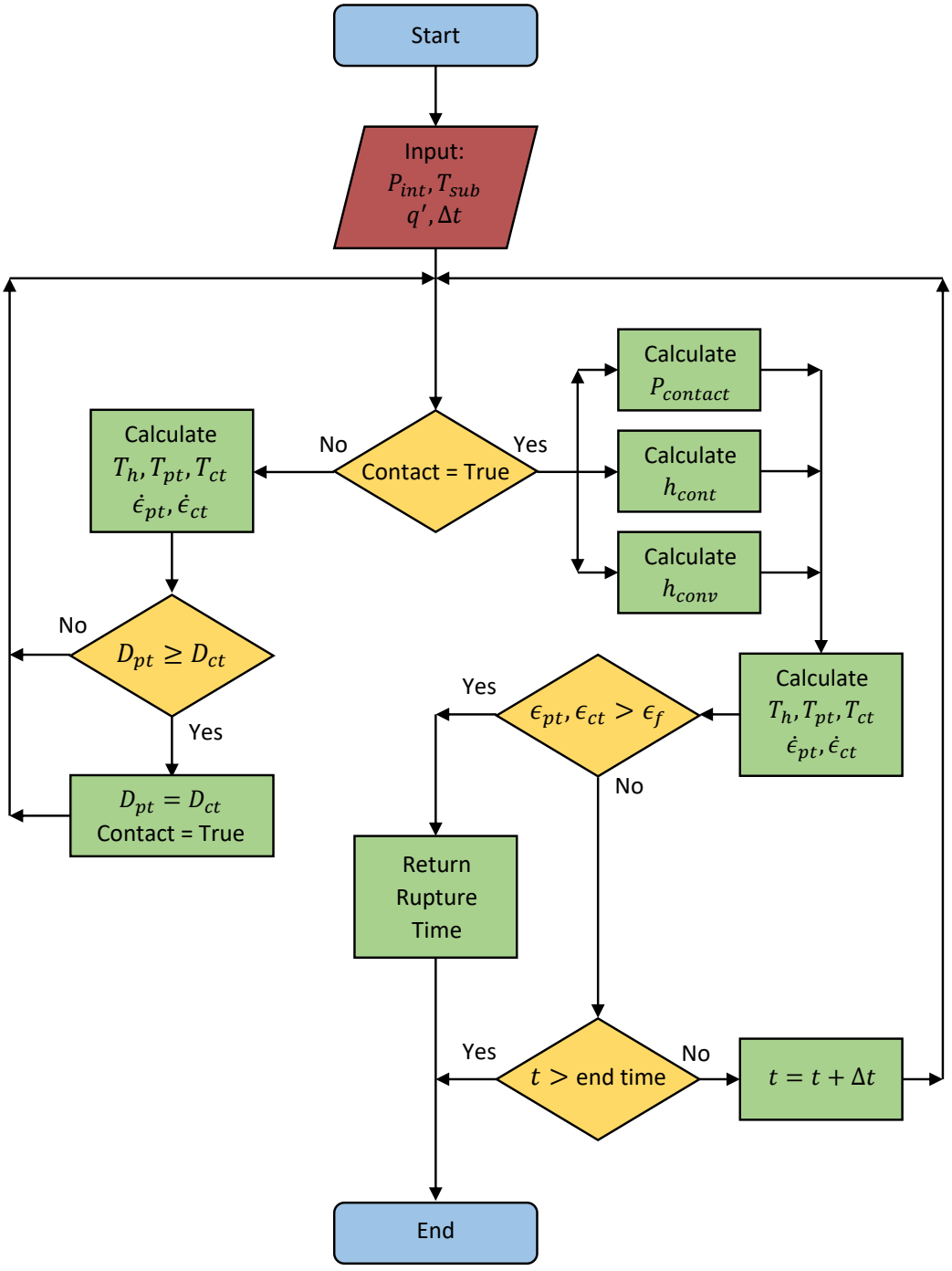

Figure 3.1 Overall flow control for the model presented in this thesis

Where the subscripts h and pt identify the component as the heater or pressure tube respectively. m' is the mass per unit length, c_p is the specific heat capacity, t is time, q' is the linear heat and h' is the linear heat transfer coefficient of the component. γ' and q'_{loss} refer respectively to the heat loss fraction and the axial heat loss through the end caps of the apparatus. Heat is transferred from the heater to the PT via radiation with the following heat transfer coefficient:

$$h'_{rad} = \frac{\pi\sigma_B(r_h\epsilon_h)\left(r_{pti}\epsilon_{pt}\right)\left(T_h^2 + T_{pt}^2\right)\left(T_h + T_{pt}\right)}{(r_h\epsilon_h)\left(1-\epsilon_{pt}\right) + \left(r_{pti}\epsilon_{pt}\right)} \quad (3.3)$$

σ_B is the Boltzmann constant, r is the radius and ϵ is the emissivity of the component. The differential equations above were integrated with respect to their own temperatures holding everything else constant to give:

$$T_h = T_{ho}\, exp(-b\Delta t) + \phi(1 - e^{-b\Delta t}) \quad (3.4)$$

$$b = \frac{h'_{rad}}{m'_h c_{ph}} \quad (3.5)$$

$$\phi = \frac{q'_h + h'_h T_{pt} - \gamma' q'_h}{h'_{rad}} \quad (3.6)$$

$$T_{pt} = T_{pto}\, exp(-b\Delta t) + \phi(1 - exp(-b\Delta t)) \quad (3.7)$$

$$b = \frac{h'_{rad}}{m'_{pt} c_{ppt}} \quad (3.8)$$

$$\phi = T_h - q'_{loss} \quad (3.9)$$

In comparing to experimental results the model assumes any losses attributed to γ or q'_{loss} are negligible.

Post-Contact

Once in contact the heater temperature equation remains unchanged but the q'_{loss} term is replaced by the heat transferred from the PT to the CT. A third equation must be introduced to account for the heat transfer from the CT to the moderator.

$$m'_{pt}c_{ppt}\frac{dT_{pt}}{dt} = h'_{rad}(T_h - T_{pt}) - h'_{eff}(T_{pt} - T_{ct}) \quad (3.10)$$

$$m'_{ct}c_{pct}\frac{dT_{ct}}{dt} = h'_{eff}(T_{pt} - T_{ct}) - h'_{conv}(T_{ct} - T_l) \quad (3.11)$$

$$h'_{conv} = 2\pi r_{ct}h_{conv} \quad (3.12)$$

h'_{eff} is the effective heat transfer coefficient from the inner wall of the PT to the outer surface of the CT and depends on the thermal conductivity (k) of both solids and the thermal contact conductance (h_{cont}) between them (see section 2.2).

$$h'_{eff} = \left(\frac{\tau_{pt}r_{cti}}{k_{pt}r_{pt}} + \frac{r_{cti}}{h_{cont}r_{pt}} + \frac{\tau_{ct}}{k_{ct}}\right)^{-1} \quad (3.13)$$

h'_{conv} is the convective heat transfer from the CT to the moderator which will depend on the boiling regime determined by the degree of wall superheat (section 2.4). T_l is the temperature of liquid at the CT surface and will be equal to the subcooled pool

temperature (T_{sub}) under pre-boiling conditions and saturation temperature (373 K) under nucleate and film boiling conditions. Solving the differential equations as previously:

$$T_{pt} = T_{pto}\, exp(-b\Delta t) + \phi(1 - exp(-b\Delta t) \quad (3.14)$$

$$b = \frac{h'_{rad} + h'_{eff}}{m'_{pt} c_{ppt}} \quad (3.15)$$

$$\phi = \frac{h'_{rad} T_h + h'_{eff} T_c}{h'_{pt} + h'_{eff}} \quad (3.16)$$

$$T_{ct} = T_{cto}\, exp(-b\Delta t) + \phi(1 - exp(-b\Delta t)) \quad (3.17)$$

$$b = \frac{h'_{eff} + h'_{conv}}{m'_{ct} c_{pct}} \quad (3.18)$$

$$\phi = \frac{h'_{eff} T_{pt} + h'_{conv} T_l}{h'_{eff} + h'_{conv}} \quad (3.19)$$

These equations provide a time step by time step calculation of temperature during the execution of the model.

3.2 Strain Rate and Contact Pressure

The strain rate ($\dot{\epsilon}$), as shown in section 2.1, is the fractional change in the tube's (PT or CT) diameter per second and is a function of the temperature and pressure difference between the interior and exterior of the tube. The increase in radius is calculated using:

$$r_f = r_i(\dot{\epsilon} t + 1) \quad (3.20)$$

and the change in thickness is:

$$\tau_f = \frac{\tau_i}{1 + \dot{\epsilon} t} \quad (3.21)$$

Pre-contact PT strain can be calculated using the simple application of equation (2.2).

Once the PT makes contact with the CT the program calls upon the contact pressure function. This function uses the assumption that the tubes do not separate after contact causing equation (2.2) and (2.6) to be equal. The equality allows us to solve for the CT hoop stress (σ_{ct}) and by extension the contact pressure. However, in order to solve for the CT strain rate we must first address the interdependence of equation (2.6) and (2.7). The internal stress in the Zircaloy-2 α-phase (σ_i) is dependent on the dislocation creep strain rate ($\dot{\epsilon}_d$) which is itself dependent on σ_i. This requires the use of an iterative method to solve for both parameters. An initial guess for contact pressure and σ_i is used to determine the hoop stress σ_{ct} and $\dot{\epsilon}_d$. This dislocation creep is in turn used to evaluate a new value for the internal stress (σ_{i_new}) and a comparison is made between the initial guess for σ_i and the calculated value. If the difference is larger than some predetermined limit (percent difference < 1% was chosen) the new guess for the internal stress (σ_{i_next}) is used to start the process over which is weighted towards the initial guess of σ_i:

$$\sigma_{i\_next} = 0.99\sigma_i + 0.01\sigma_{i\_new} \quad (3.22)$$

This weighting is used in order to damp oscillations that occur when attempting to converge on a value of σ_i. Once a value for σ_i has been determined it is used, along with the guessed contact pressure, to calculate the grain boundary sliding ($\dot{\epsilon}_{gb}$) completing the description of CT, and by assumption PT, strain rate. We then solve for contact pressure

(P_{c_new}) and compare to the initial guess. Again, if the percent difference between the initial guess and new value is larger than 1% a new guess (P_{c_next}) is obtained using:

$$P_{c\_next} = 0.99P_c + 0.01P_{c\_new} \quad (3.23)$$

The entire process is repeated until both the contact pressure and internal stress have sufficiently converged below a predetermined limit (1% difference) and the result is passed to the thermal contact conductance module of the model. The evaluation of contact conductance is a straightforward application of the equations provided in section 2.2 and will is not reviewed in this chapter.

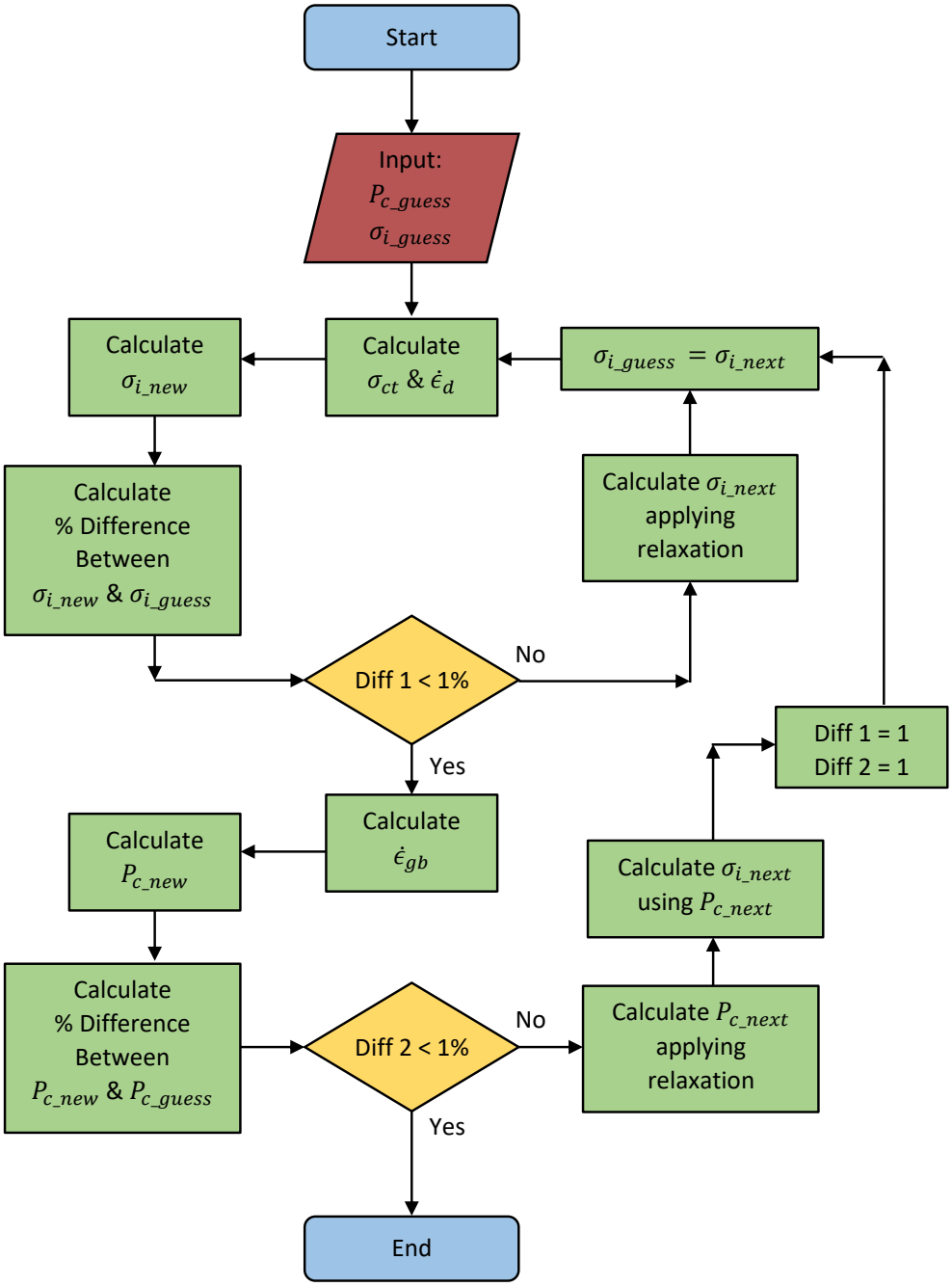

Figure 3.2 Overview of the iterative method used to estimate contact pressure

3.3 Boiling Heat Transfer

All thermophysical properties of water were obtained using XSteam for MATLAB [36]. The heat transfer function handles all heat transfer equations up to and including heater and pressure tube heat up, heat transfer through the contacting PT/CT, and heat transfer to the moderator. During initial contact the program determines which boiling regime the CT should be in based on the degree of wall superheat. While the CT is below saturation temperature equation (2.39) is used to evaluate h_{conv}. The mechanism of heat transfer will transition from natural convection to nucleate boiling (2.55) once the CT has exceeded ~105^{o}C. While in nucleate boiling the program continuously checks to see if the heat flux to the moderator exceeds the subcooled critical heat flux. In the event that CHF is exceeded h_{conv} will change to reflect film boiling conditions; described by equation (2.70). The CT temperature is allowed to rise without limit when it first enters into film boiling but once the temperature begins to decrease the program will check to see if at any point it drops below the minimum film boiling temperature. If this occurs the tube is considered to have quenched and h_{conv} returns to the nucleate boiling regime.

3.4 Model GUI

As mentioned at the beginning of the chapter a graphical user interface was created to make the model more user-friendly. The purpose of the GUI was to give the user an easy way to compare differences in the transient behaviour of various properties, involved in PT/CT contact boiling, based on changes to the initial conditions. To this end two plots remain on screen at all times allowing the evaluation of two separate sets

internal pressure, power and subcooling (Figure 3.3); a drop down menu lets the user switch between properties of interest (Figure 3.4).

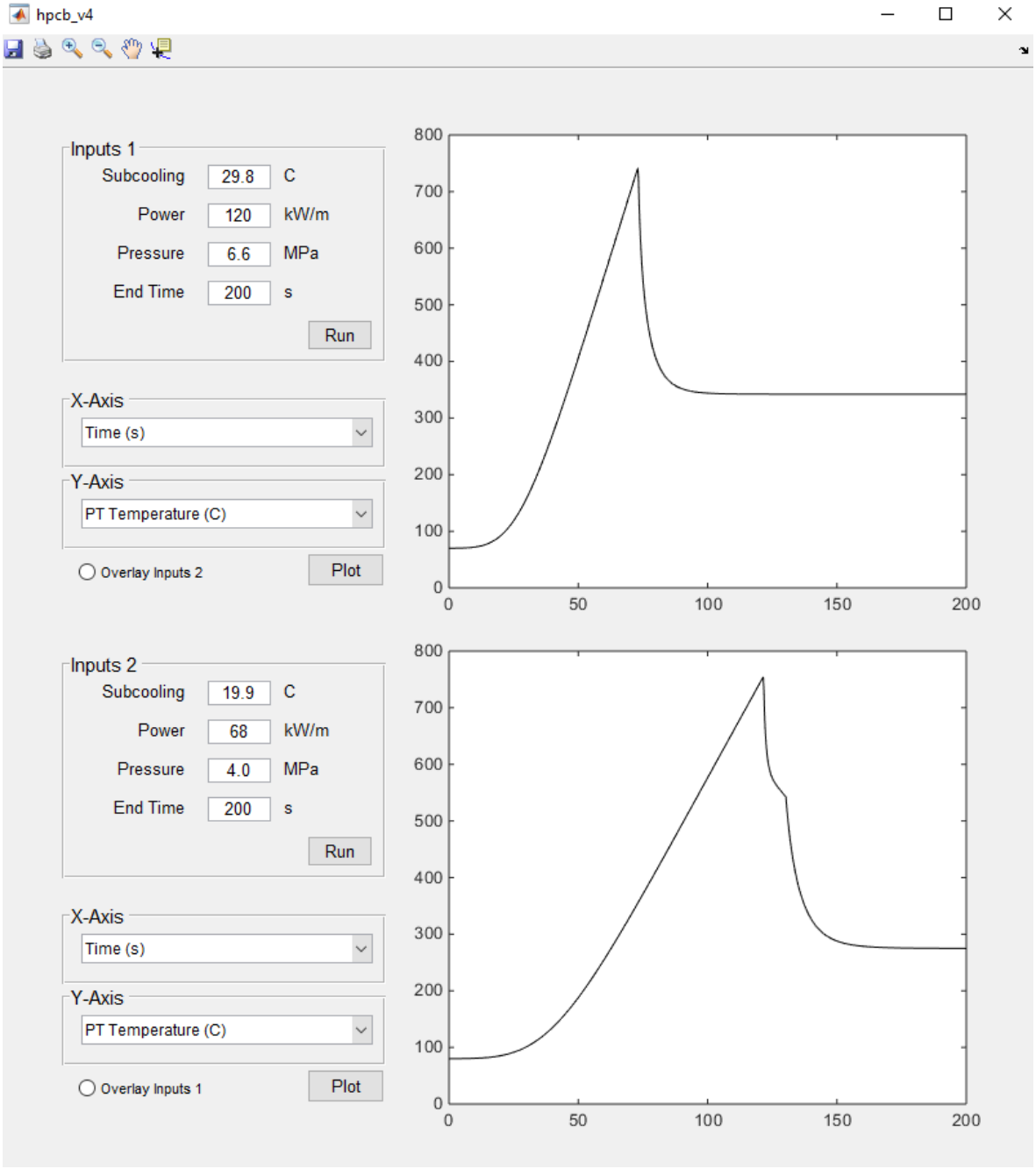

Figure 3.3 An example of the GUI showing the predicted PT temperature behaviours based on two separate inputs

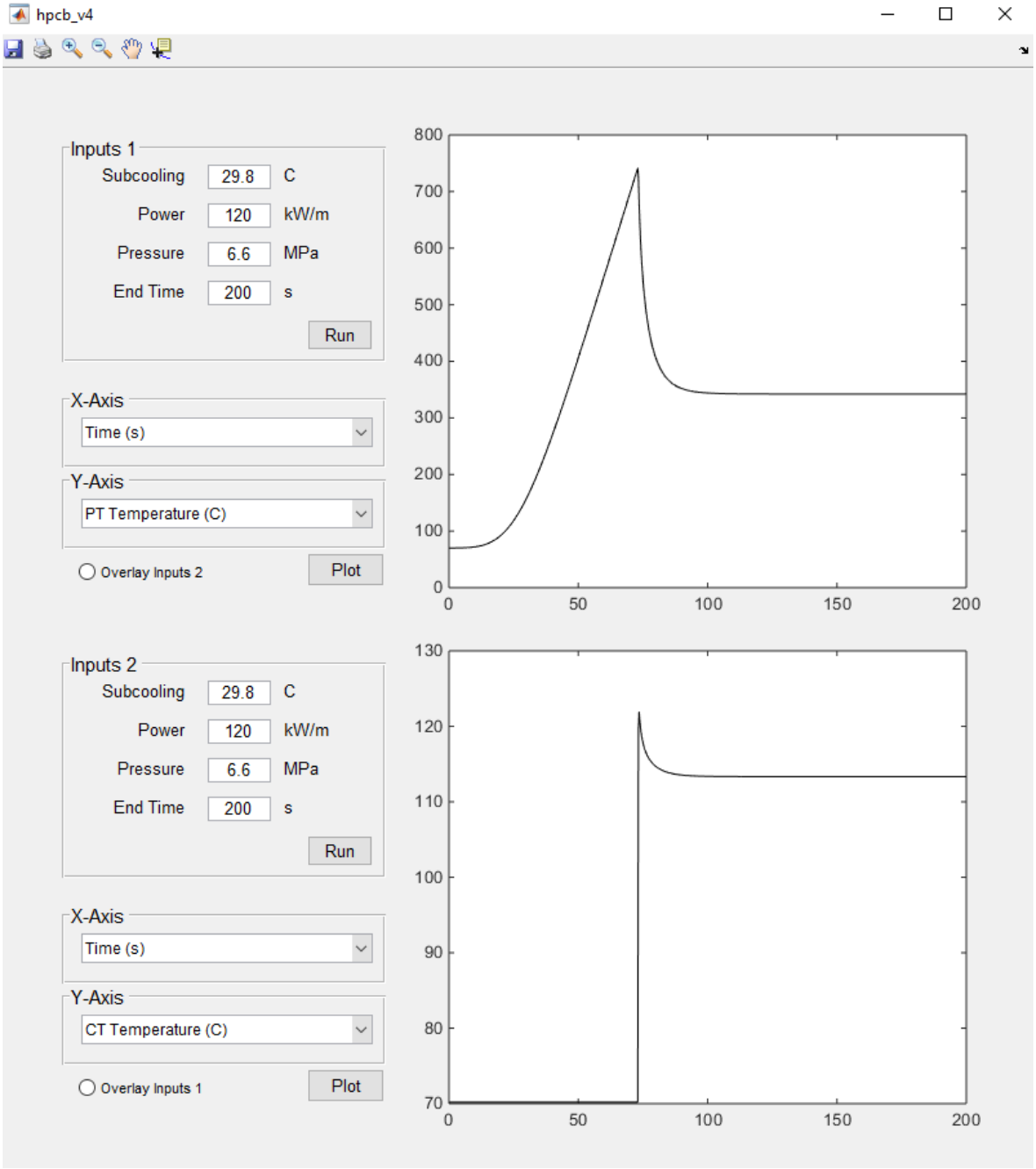

Figure 3.4 An example of the GUI showing the predicted PT (top) and CT (bottom) temperatures for a single set of initial conditions

CHAPTER 4 - Initial Results and Model Redesign

Initial model predictions are presented. Based on the results it appears that the model is unable to predict pre contact PT failure or CT quench after the initiation of film boiling. Suggestions are provided to address these limitations.

4.1 Initial Results and Limitations

To generate a PT/CT temperature transient prediction the model requires only 3 inputs from the user:

1. Internal Pressure (MPa)
2. Internal Channel Power (kW/m)
3. Pool Subcooling (^{o}C)

The following figures provide a comparison between the predicted and experimental temperature behaviours based on the 6 sets of experimental conditions outlined in section 2.6. The labels used by Luxat [35] to identify the experiments were adopted for use in this thesis.

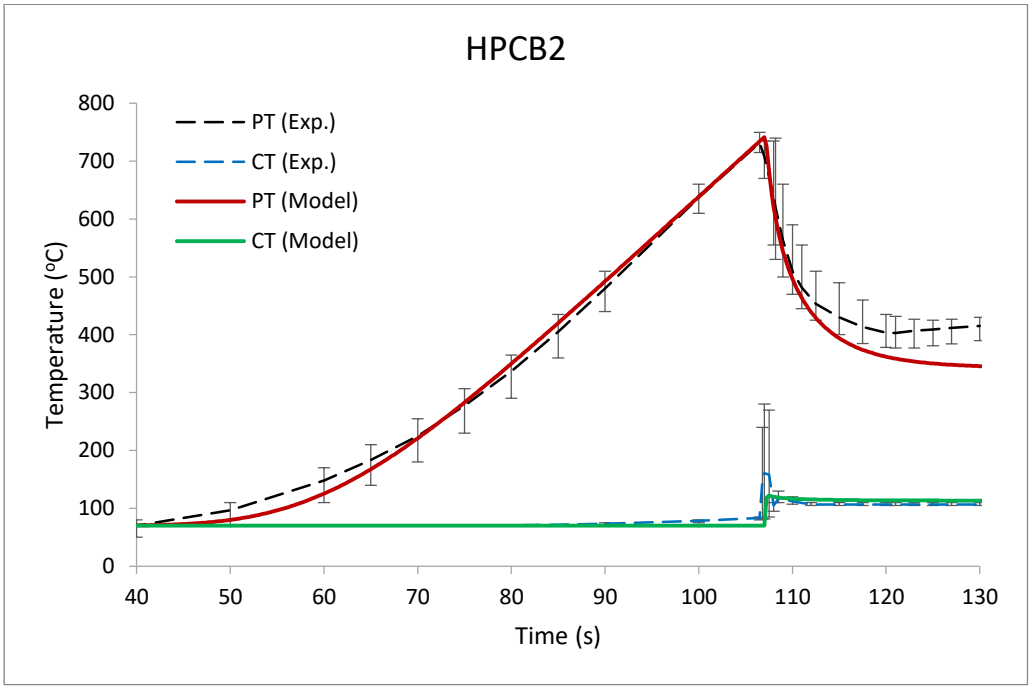

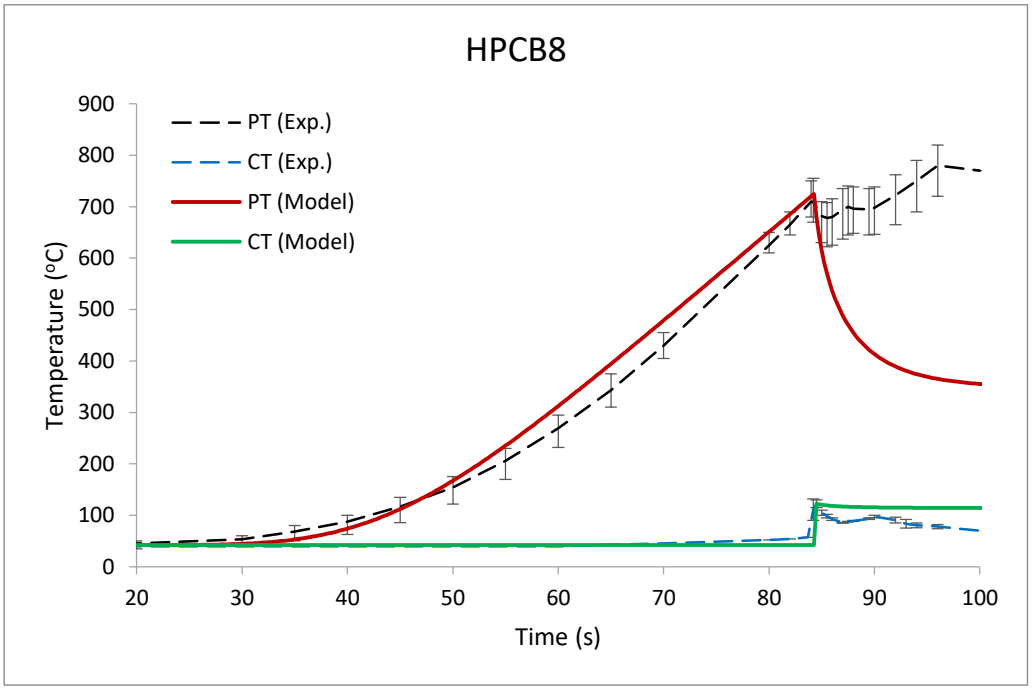

Figure 4.1 Model predicted PT and CT temperature behaviour based on the experimental conditions used for HPCB2 and HPCB8

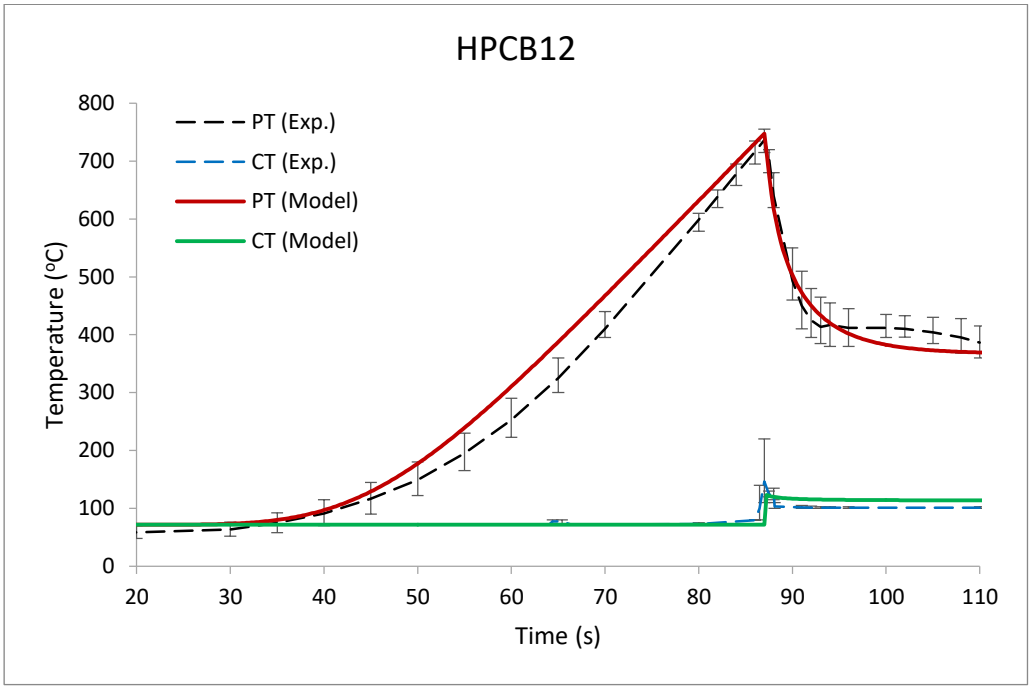

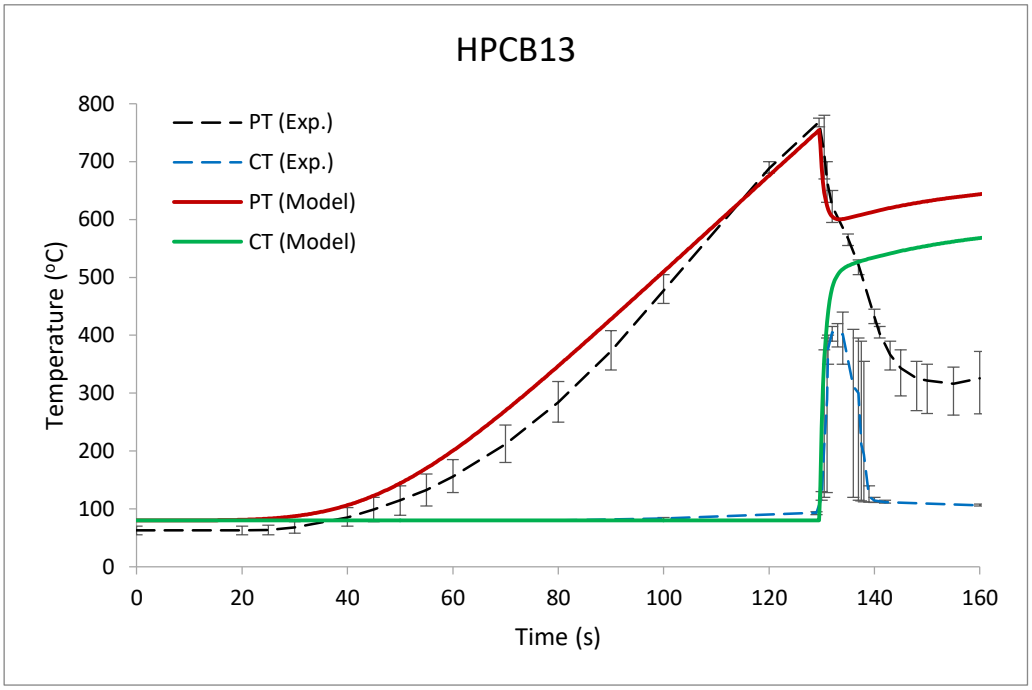

Figure 4.2 Model predicted PT and CT temperature behaviour based on the experimental conditions used for HPCB12 and HPCB13

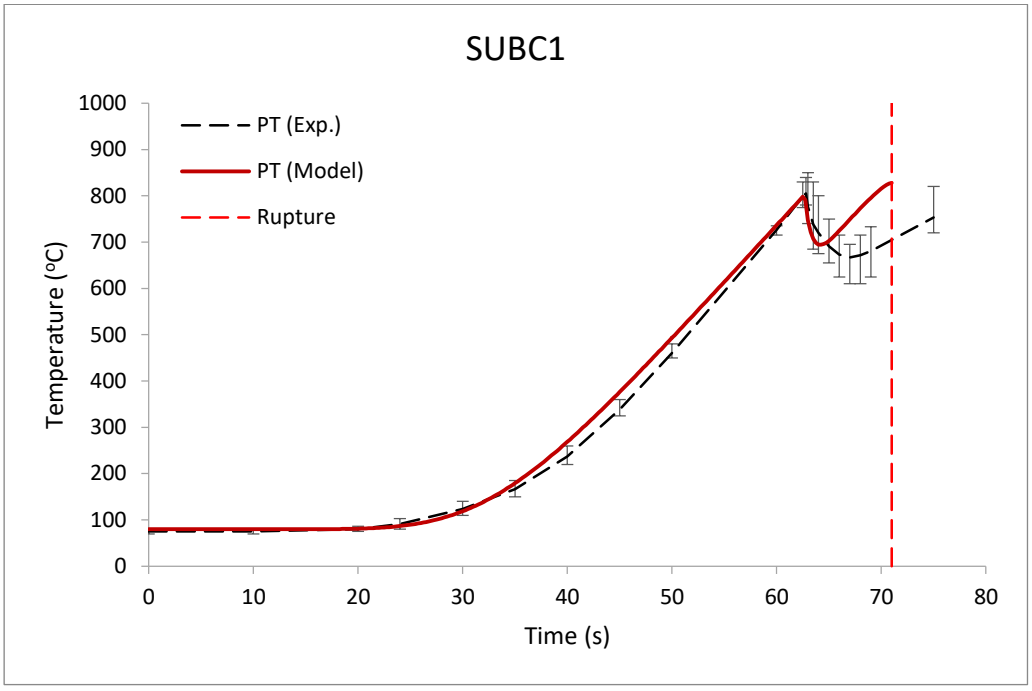

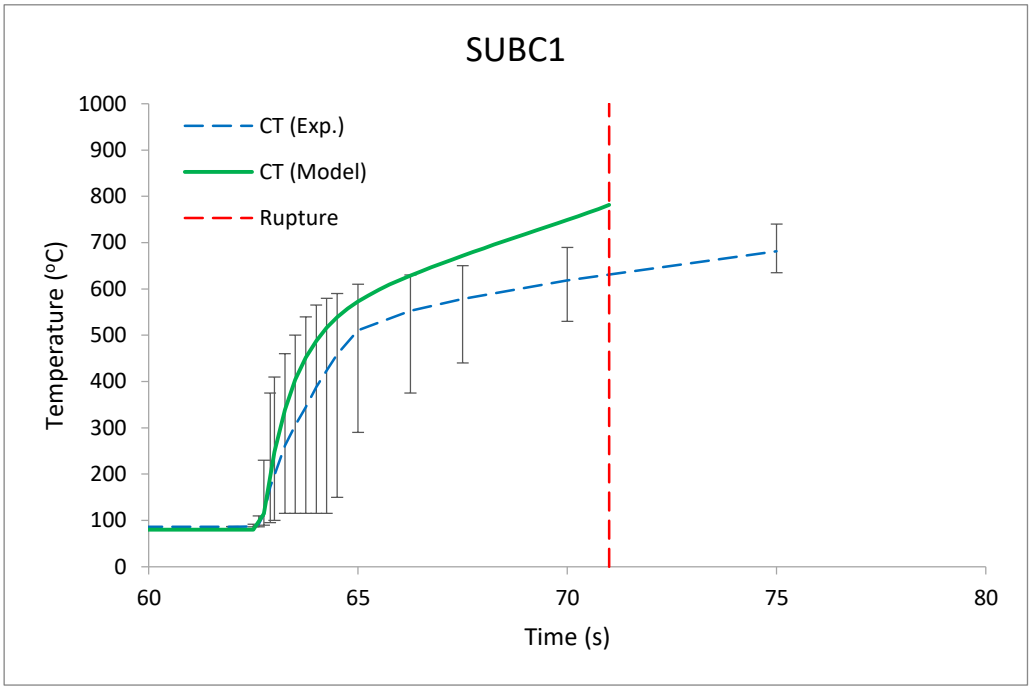

Figure 4.3 Model predicted PT (top) and CT (bottom) temperature behaviour based on the experimental conditions used for SUBC1

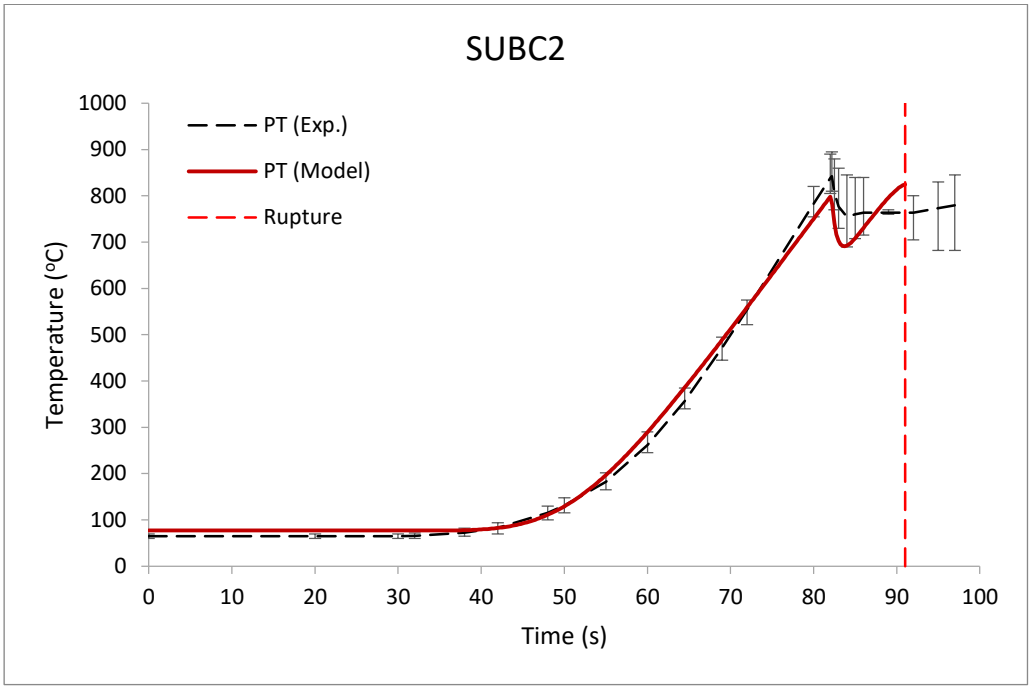

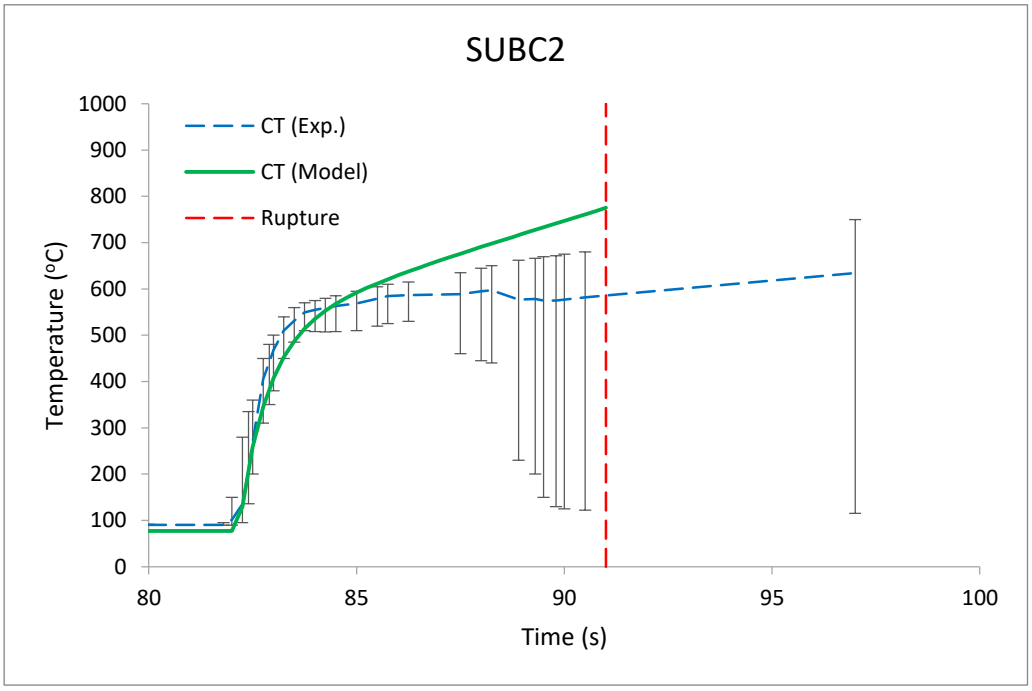

Figure 4.4 Model predicted PT (top) and CT (bottom) temperature behaviour based on the experimental conditions used for SUBC2

The model accurately estimates the PT/CT temperatures for cases of no film boiling (HPCB2/12) and sustained film boiling (SUBC1/2). However, the more nuanced behaviour of HPCB8 and HPCB13 fail to be predicted. For HPCB8 the PT failed prior to contact with the CT whereas the model predicts heat rejection via nucleate boiling immediately after contact. Failure before contact is likely a local phenomenon attributed to higher than average local temperatures resulting in increased strain. Since the current model is one dimensional, and returns average values of temperature and strain, it will be unable to predict PT failure before rupture unless significant changes are made.

For the case of HPCB13 the model predicts sustained film boiling but does not result in fuel channel failure. The model's inability to predict quench is likely the result of the Gillespie and Moyer film boiling HTC correlation. This correlation is based solely on the degree of pool subcooling and will not vary after film boiling is initiated. An attempt was made to develop a more detailed description of the film boiling HTC in order to more accurately predict the behaviour of HPCB13.

4.2 Revised Film Boiling Convective Heat Transfer

The following section is based on work performed by Jiang and Luxat [37] to describe the film thickness in steady state film boiling. In developing the revised film boiling HTC we assume that the film is of uniform thickness and completely convers the CT surface. During film boiling several mechanisms of heat transfer are at play and will be described.

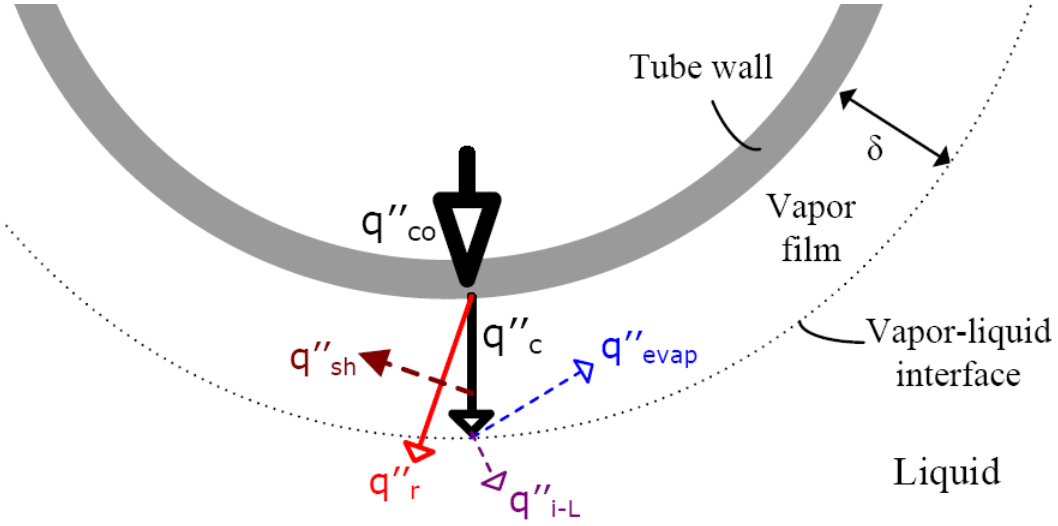

Figure 4.5 The various heat transfer mechanisms at play during film boiling [37]

4.2.1 Radiation and Conduction

Starting from the CT surface heat will be removed via conduction (q''_{cond}) and radiation (q''_{rad}) through the vapor of film.

$$q''_{cond} = \frac{k_g}{\delta_f}(T_{ct} - T_{sat}) \quad (4.1)$$

$$q''_{rad} = h_{rad,f}(T_{ct} - T_{sat}) \quad (4.2)$$

The conduction heat transfer coefficient will depend on the conductivity (k_f) and thickness (δ_f) of the vapor film and the radiation heat transfer coefficient is obtained in a similar fashion to the radiation HTC between the heater and PT.

$$h_{rad,f} = \frac{\sigma\epsilon_{ct}(r_f\epsilon_l)(T_{ct}^2 + T_{sat}^2)(T_{ct} + T_{sat})}{(r_{ct}\epsilon_{ct})(1-\epsilon_l) + (r_f\epsilon_l)} \quad (4.3)$$

The film radius (r_f) can be related to the CT radius by:

$$r_f = r_{ct} + \delta_f \quad (4.4)$$

4.2.2 Vapor Superheating and Liquid Evaporation

The energy leaving the CT interacts with the film as it is transferred to the bulk fluid. Part of this energy will go into to superheating (E_{sh}) the film based on the film mass, heat capacity and temperature.

$$E_{sh} = \rho_v V_v c_{p,v}(T_v - T_{sat}) \quad (4.5)$$

The film temperature is approximated as the average of the CT temperature and saturation temperature

$$T_v - T_{sat} = \frac{(T_{ct} + T_{sat})}{2} - T_{sat} = \frac{T_{ct} - T_{sat}}{2} \quad (4.6)$$

and the film volume is approximated as an annular cylinder.

$$V_v = \pi\left(r_f^2 - r_{ct}^2\right)L_a \quad (4.7)$$

Using the relationship (4.4) the film volume can be rewritten as:

$$V_v = \pi\left(\delta_f^2 + 2\delta_f r_{ct}\right)L_a \quad (4.8)$$

The heat flux due to superheating the film (q''_{sh}) can then be obtained by dividing E_{sh} by the time step used in the model and the outer area of the CT (A_{ct}).

$$A_{ct} = 2\pi r_{ct} L_a \quad (4.9)$$

$$q''_{sh} = \frac{\rho_v c_{p,v}(T_{ct} - T_{sat})}{2\Delta t}\delta_f\left(1 + \frac{\delta_f}{2r_{ct}}\right) \quad (4.10)$$

We must also account for the energy required to effect a phase change in the fluid at the CT surface. This evaporation energy (E_{evap}) is a product of the mass of generated vapor and the latent heat of vaporization.

$$E_{evap} = \rho_v V_v h_{fg} \quad (4.11)$$

Once again dividing by A_{ct} and Δt we obtain the heat flux that attributed to the evaporation of liquid at the CT surface is:

$$q''_{evap} = \frac{\rho_v h_{fg}}{\Delta t}\delta_f\left(1 + \frac{\delta_f}{2r_{ct}}\right) \quad (4.12)$$

4.2.3 Vapor-Liquid Heat and Mass Exchange

Finally we must account for the heat transferred to the bulk fluid as heat and mass are exchanged at the liquid vapor interface. Sideman [38] suggested that the heat flux between a gas bubble and pool of saturated liquid could be estimated using the equivalence theory for mass and potential flows. Using spherical coordinates Sideman equated the mass and heat transfer at steady state as:

$$U_r\delta\frac{\partial C}{\partial r} + U_\theta\frac{1}{r}\frac{\partial C}{\partial \theta} = \alpha\left[\frac{\partial^2 C}{\partial r^2} + \frac{2}{r}\frac{\partial C}{r}\right] \quad (4.13)$$

The above equation assumes axial symmetry and ignores conduction along the θ direction. C represents the energy density of the vapor.

$$C = \rho_v c_{p,v} T_v \quad (4.14)$$

The velocity in the radial (U_r) and θ direction are approximated based on the total bubble velocity as:

$$U_r \approx -3U \frac{r-R}{R} \cos(\theta) \quad (4.15)$$

$$U_\theta \approx \frac{3}{2} U \sin(\theta) \quad (4.16)$$

In order to solve equation (4.14) the assumption was made that most of the heat and mass transfer takes place within a small distance (δ) from the sphere surface. With this assumption Sideman used the approximation $\delta/R \ll 1$ causing the second term on the right hand side of equation (4.14) to reduce to zero at the bubble's surface ($r = R$). We also note that at the surface U_r vanishes and the differential equation reduces to:

$$\frac{3}{2} \frac{U \sin(\theta)}{R} \frac{\partial C}{\partial r^2} = \alpha \frac{\partial^2 C}{\partial r^2} \quad (4.17)$$

Making the following substitution:

$$\psi = y \sin^2(\theta) \quad (4.18)$$

$$\phi = \int_0^\theta \sin^3(\theta)\ d\theta \quad (4.19)$$

The differential equation was transformed into:

$$\frac{\partial C}{\partial \phi} = \frac{2R\alpha}{3U} \frac{\partial^2 C}{\partial \psi^2} \quad (4.20)$$

$$M = \frac{2R\alpha}{3U} \quad (4.21)$$

The boundary conditions assume the gas energy density at the bubble's surface is C_0 and 0 in the liquid medium.

$$C = 0 \quad \infty \geq \psi > 0 \quad \phi \geq 0 \quad (4.22)$$

$$C = C_0 \quad \psi = 0 \quad \phi \geq 0 \quad (4.23)$$

Sideman solved the above differential equation determining the local (N) and average flux (N_{av}). These values were then related to the heat flux at the gas liquid interface (q''_{v-l}).

$$N_{r=R} = \left(\frac{\partial C}{\partial r}\right)_{r=R} = \frac{\alpha C_0 \sin^2(\theta)}{\sqrt{\pi M \phi}} \quad (4.24)$$

$$N_{av} = \frac{1}{4\pi R^2}\int_0^{\pi} N_{r=R} 2\pi R^2 \sin(\theta)\ d\theta = \frac{2\alpha C_0}{\sqrt{\pi M 3}} \quad (4.25)$$

$$q''_{v-l} = \frac{N_{av}}{C_0}\rho_l c_{p,l}(T_{sat} - T_l) = 2k_l\sqrt{\frac{U}{2\pi R\alpha}}(T_{sat} - T_l) \quad (4.26)$$

Witte and Orozco [39] applied the same derivation to a vapor film on a horizontal cylinder and arrived at:

$$q''_{v-l} = 2k_l\sqrt{\frac{U}{\pi r_{ct}\alpha_l}}cos\left(\frac{\theta}{2}\right)\Delta T_{sub} \quad (4.27)$$

The model uses the stagnation point ($\theta = 0$) as a reference for the entire circumference of the CT.

4.2.4 Vapor Velocity

As can be observed in equation (4.27) q''_{v-l} is dependent on the vapor velocity (U). For the case of pool boiling U is taken as the sum of buoyancy driven flow (U_{sub}) and bubble rise velocity (U_{br}). U_{sub}, as seen in the description of natural convection, depends on the density gradient that develops in the fluid as the temperature difference between the film surface and bulk fluid increases.

$$U_{sub} = \sqrt{g\left(1 - \frac{\rho_v}{\rho_l}\right)L} \quad (4.28)$$

g is the acceleration due to gravity and ρ_v/ρ_l is the ratio of film to bulk fluid density. L is the characteristic length of the system in question and is taken as the CT diameter. A study on large diameter bubble rise, by Davies and Taylor [40], showed that U_{br} was related to the radius of curvature (r_{curv}) of the bubble nose:

$$U_{br} = \frac{2}{3}\sqrt{g r_{curv}} \quad (4.29)$$

Bubbles in the experiment were hemispherical in shape so Wallis [41] related the above equation to a volume contained in an object with a spherical cap sweeping 100^o and a flat tail.

$$U_{br} = 0.79\sqrt{g V_b^{\frac{1}{3}}} \quad (4.30)$$

This was then related to an equal volume, perfectly spherical, bubble which, we assume in this model, will share roughly the same radius as that of the CT it is enveloping, to give:

$$U_{br} = 1.00\sqrt{gr_{ct}} \quad (4.31)$$

The total vapor velocity is then:

$$U = \sqrt{gr_{ct}}\left[\sqrt{2\left(1 - \frac{\rho_v}{\rho_l}\right)} + 1\right] \quad (4.32)$$

4.2.5 Energy Balance

To reiterate, a stable film will develop if the heat removed from the CT is equal to the heat used to generate vapor, super heat the film and the heat lost at the vapor liquid interface.

$$q''_{cond} + q''_{rad} = q''_{sh} + q''_{evap} + q''_{v-l} \quad (4.33)$$

The program solves the above equality iteratively. First q''_{cond} and q''_{rad} are evaluated using a guessed δ_f.

$$A = q''_{cond} + q''_{rad} \quad (4.34)$$

We then solve for a new film thickness δ_{f_new} in the following polynomial.

$$\delta^2_{f\_new}\beta + \delta_{f\_new}2\beta r_{ct} + (q''_b - A) = 0 \quad (4.35)$$

where

$$\beta = \frac{\rho_f}{2\Delta t}\left(\frac{c_{p,f}(T_{ct} - T_{sat})}{2} + h_{fg}\right) \quad (4.36)$$

Similar to the contact pressure module δ_{f_new} is compared to the initial guess of δ_f and if the difference does not fall within a certain predetermined limit ($< 1\%$ difference) the model makes a new guess at the film thickness based on the initial guess and calculated value.

$$\delta_{f\_next} = 0.99\delta_f + 0.01\delta_{f\_new} \quad (4.37)$$

Using sufficiently small time steps (currently $\Delta t = 2$ ms) we can continuously monitor the film thickness and resulting film boiling HTC which will be equal to:

$$h_{conv} = \frac{k_v}{\delta_f} + \frac{\sigma\epsilon_{ct}(r_f\epsilon_l)(T_{ct}^2 + T_{sat}^2)(T_{ct} + T_{sat})}{(r_{ct}\epsilon_{ct})(1-\epsilon_l) + (r_f\epsilon_l)} \quad (4.38)$$

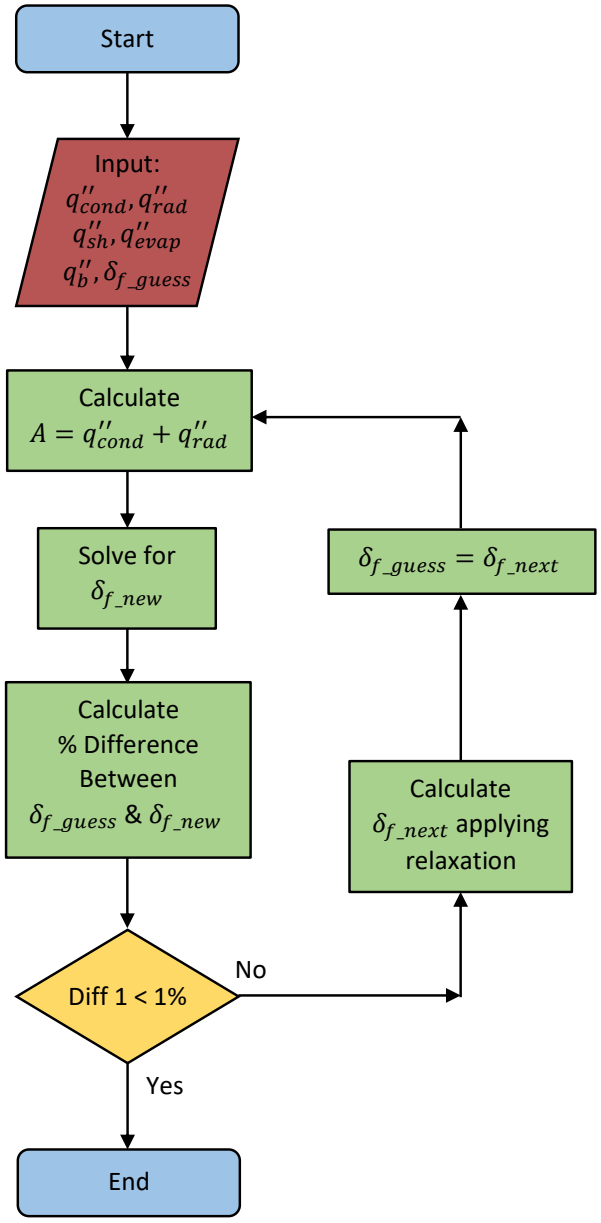

Figure 4.6 Overview of the iterative method used to estimate film thickness

CHAPTER 5 - Results and Discussion

The following plots show the new PT and CT temperature predictions obtained with the modified film boiling heat transfer coefficient. The modified model showed large improvement in its ability to predict the experimental results. A summary of simulated values is provide for parameters directly related to the development of film boiling and fuel channel failure including:

- PT and CT temperature
- Contact pressure
- Contact conductance
- Boiling convective HTC and film thickness

5.1 Temperature & Channel Failure

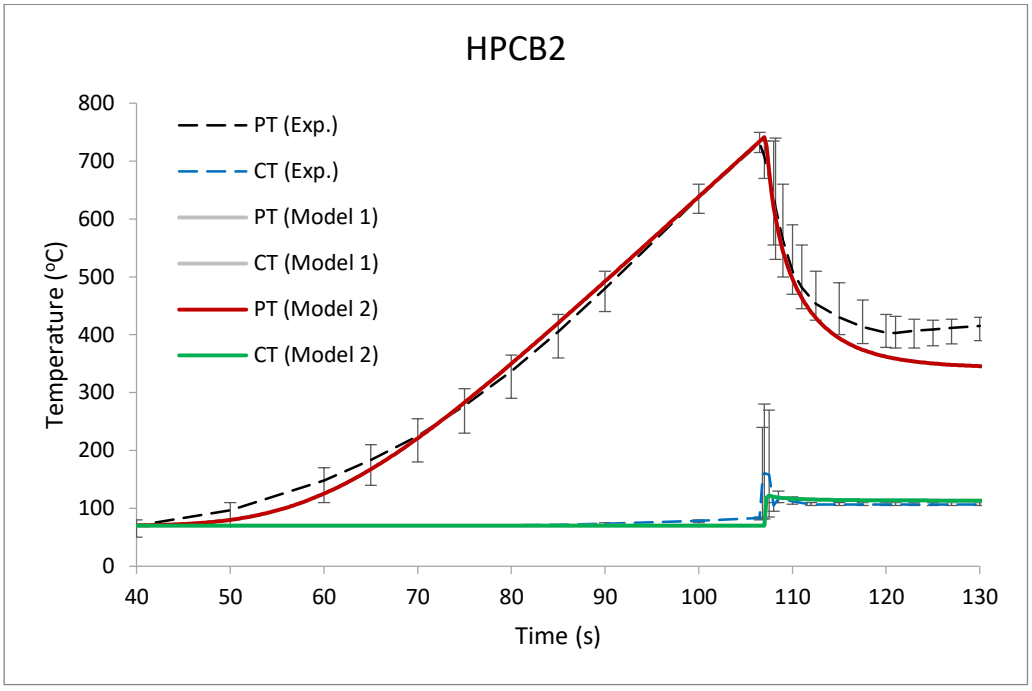

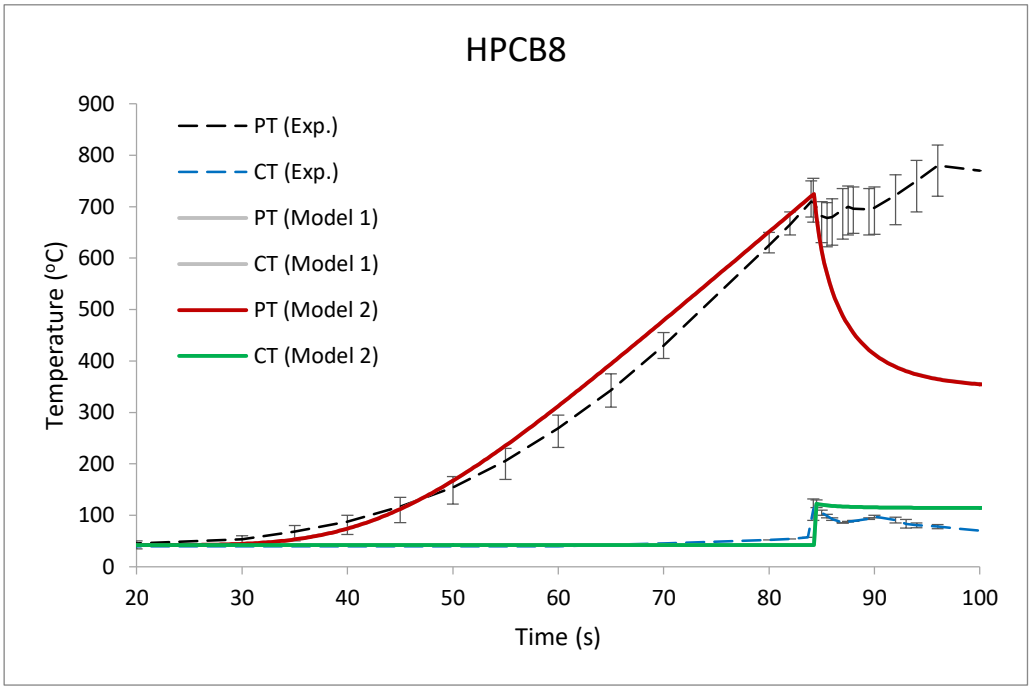

Figure 5.1 Revised model predictions for PT and CT temperature behaviour based on the experimental conditions used for HPCB2 and HPCB8

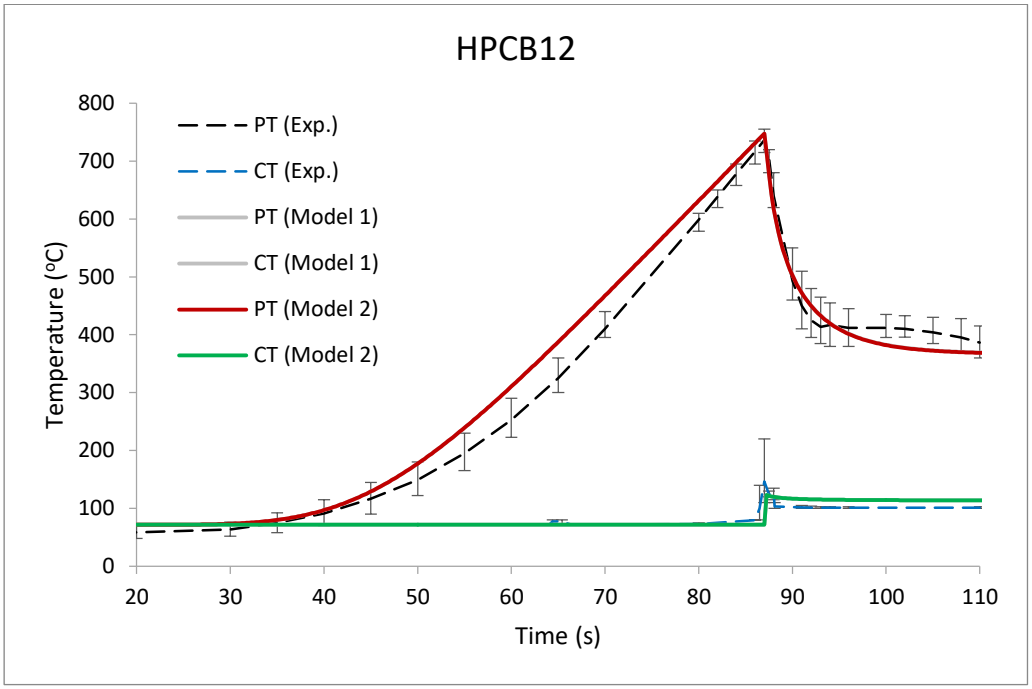

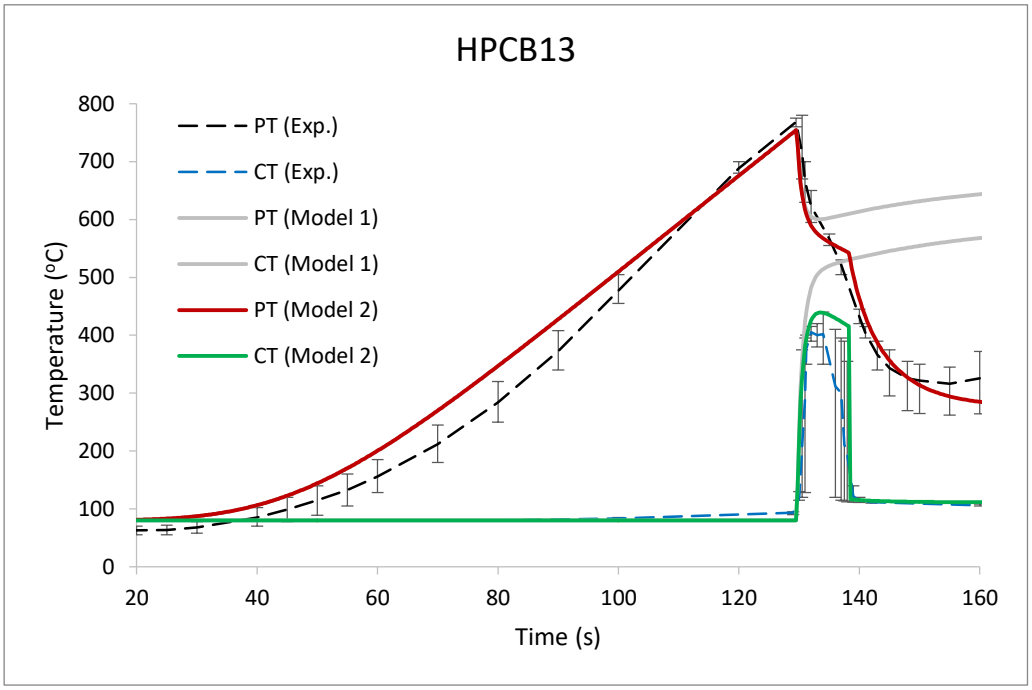

Figure 5.2 Revised model predictions for PT and CT temperature behaviour based on the experimental conditions used for HPCB12 and HPCB13

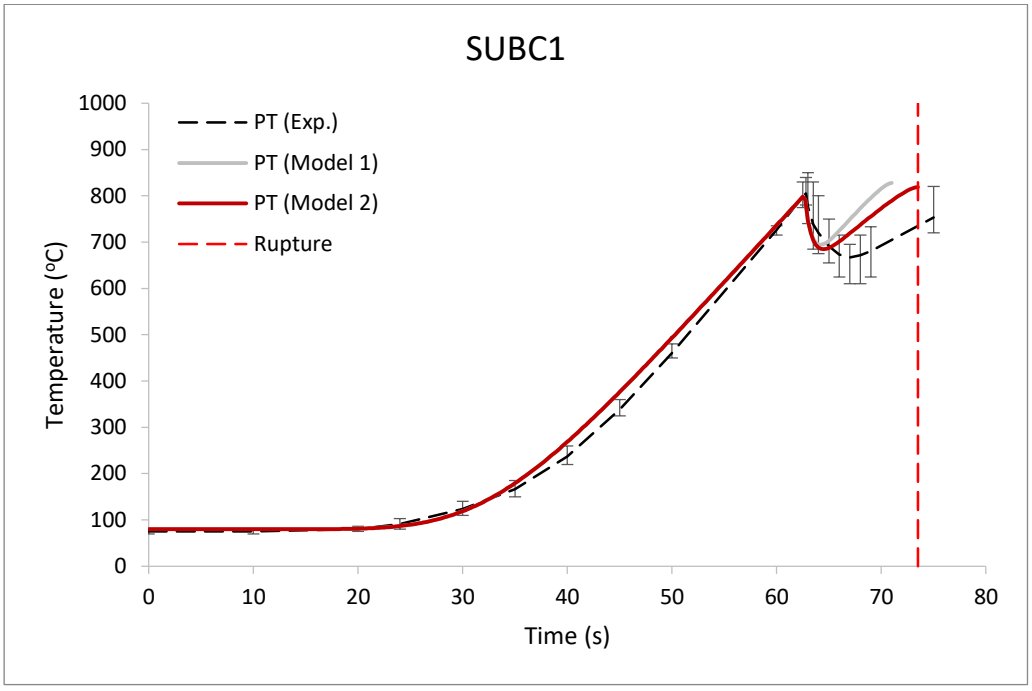

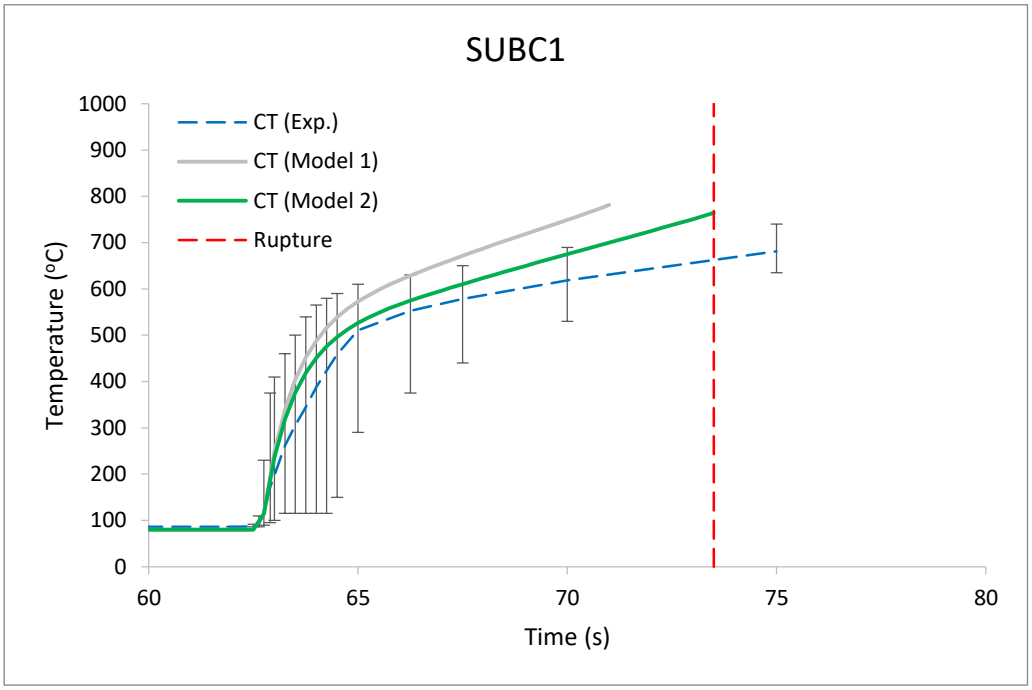

Figure 5.3 Revised model predictions for PT (top) and CT (bottom) temperature behaviour based on the experimental conditions used for SUBC1

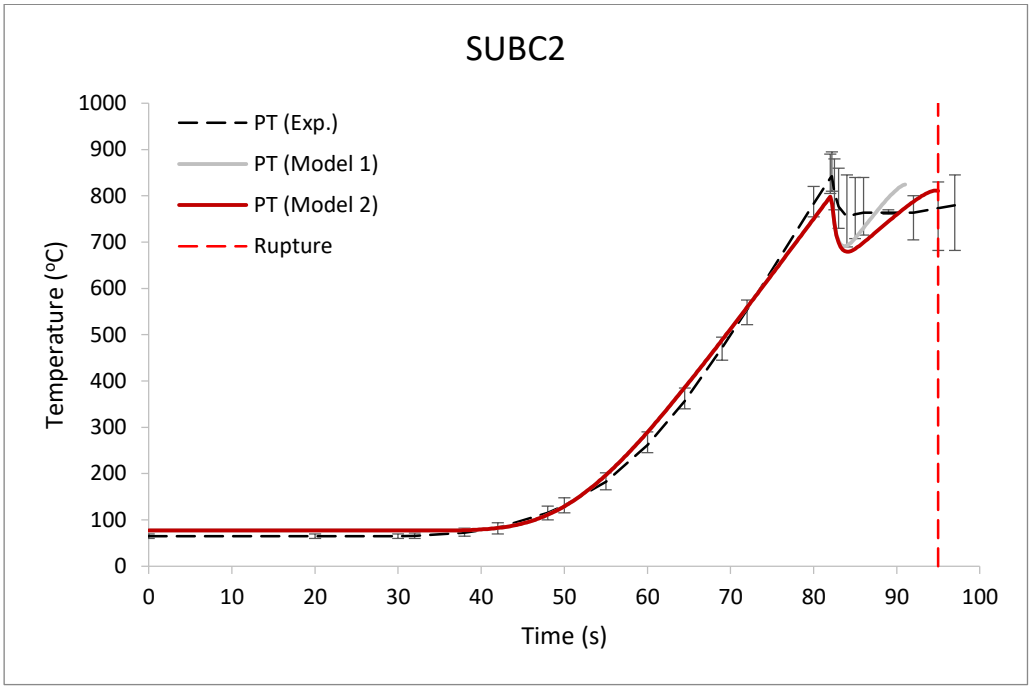

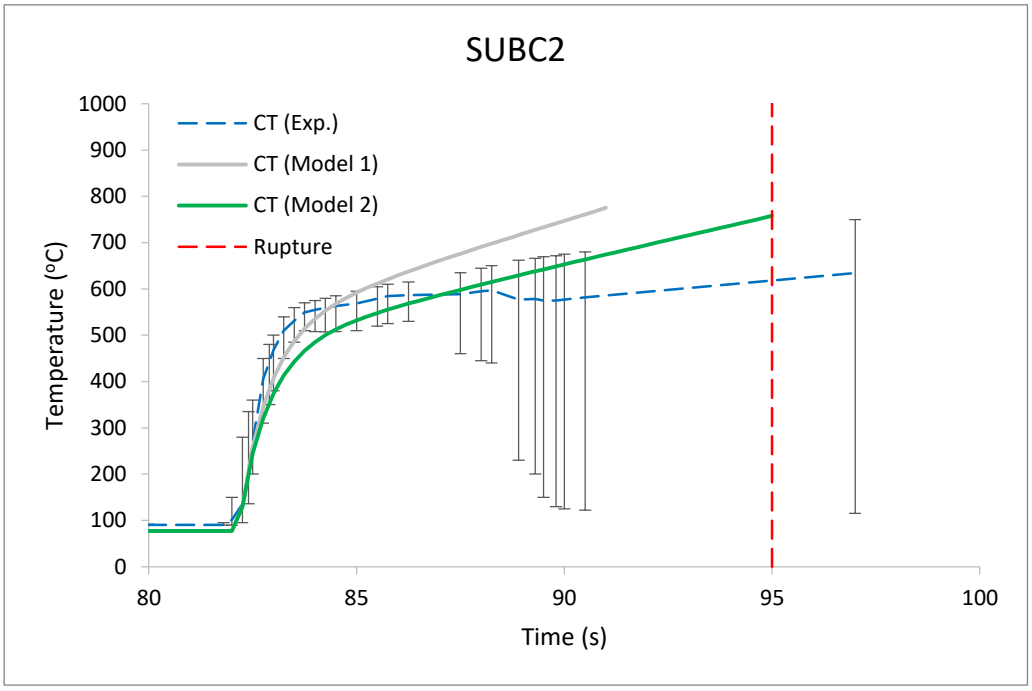

Figure 5.4 Revised model predictions for PT (top) and CT (bottom) temperature behaviour based on the experimental conditions used for SUBC2

Table 5.1 Experimental data for maximum and minimum PT contact temperatures along with model prediction, percent difference is with respect to the average of all thermocouple readings

	PT Contact Temperature (^{o}C)			
	Experiment (Min)	Experiment (Max)	Model	% Difference From Average
HPCB2	715	750	742	1.36
HPCB8	770	820	725	7.10
HPCB12	715	755	748	1.48
HPCB13	760	780	756	1.80
SUBC1	780	850	798	0.88
SUBC2	810	895	798	5.30

Table 5.2 Of the average thermocouple readings this is the maximum temperature achieved by the CT in each experiment compared to the model prediction

	Maximum Average CT Temperature (^{o}C)		
	Experiment	Model	% Difference
HPCB2	280	122	56.44
HPCB8	132	122	7.30
HPCB12	220	123	44.08
HPCB13	440	439	0.17
SUBC1	740	764	3.27
SUBC2	675	758	12.32

Table 5.3 Failure time, and failing tube in parenthesis, observed in experiment compared to that predicted by the model

	Time of Failure (s)		
	Experiment	Model	% Difference
HPCB2	--	--	--
HPCB8	84 (PT)	DNF	DNF
HPCB12	--	--	--
HPCB13	--	--	--
SUBC1	75 (CT)	73.5 (CT)	2.00
SUBC2	97 (CT)	95 (CT)	2.06

PT contact temperatures were within experimental observation for only half of the experiment. All instances where PT temperatures were found outside of experimental range resulted in lower than expected contact temperatures. That being said, the maximum difference between the model and experiment PT temperatures was 45^{o}C, (5.84 %) for HPCB8, the two other discrepancies were only 4 and 12^{o}C (1.46%) for HPCB13 and SUBC2 respectively.

Maximum CT temperatures were largely under predicted for experiments with limited to no film boiling (HPCB2/8/12) with an average difference of about ~50%. HPCB8 is, again, a unique case where the PT failed before contact which could have led to the low CT temperatures recorded. This discrepancy is likely due to the rigid restriction on the initiation of film boiling and the assumption of circumferentially uniform temperature. Although the model fails to predict these temperatures it is important to note

that short pulses (<1 second) of temperatures increases well below 600^{o}C will not result in fuel channel failure. For cases where film boiling was observed the model does a much better job at predicting maximum CT temperatures. The descending order was a 83^{o}C difference (12.32 %) for experiment SUBC2 followed by 24^{o}C (3.27 %) in SUBC1 and 1^{o}C in HPCB13. These differences were overestimations by the model and could be considered as conservative estimates.

The only observed case of quench was for test HPCB13 and the model accurately predicts sustained film boiling for a period of roughly 10 seconds. Predicted failure times were nearly identical to those observed experimentally both differing by about 2 seconds (~2 %) and are likely the result of the model's increased CT temperature predictions.

5.2 Contact Pressure

At the moment of contact the pressure exerted by the PT on the CT should match the internal pressure of the PT since the two tubes, for all intents and purposes, have formed a single composite tube. It won't be until the CT begins to strain that a change in contact pressure will be observed. This is the exact behaviour predicted by the model in the following figures.

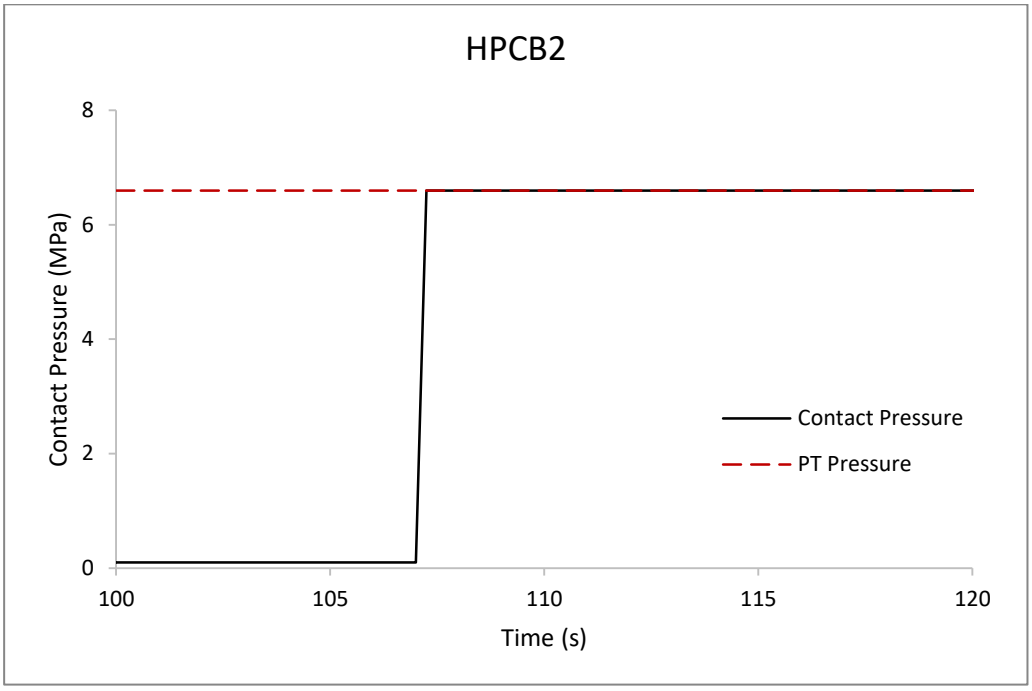

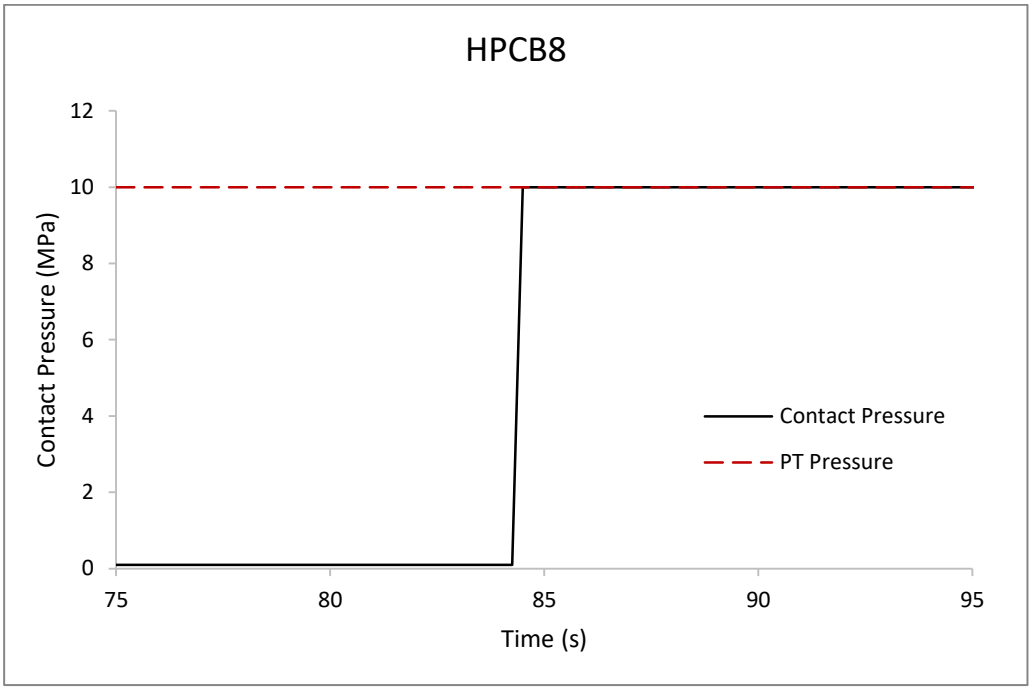

Figure 5.5 Estimated contact pressure transient compared to internal PT pressure for HPCB2 and HPCB8

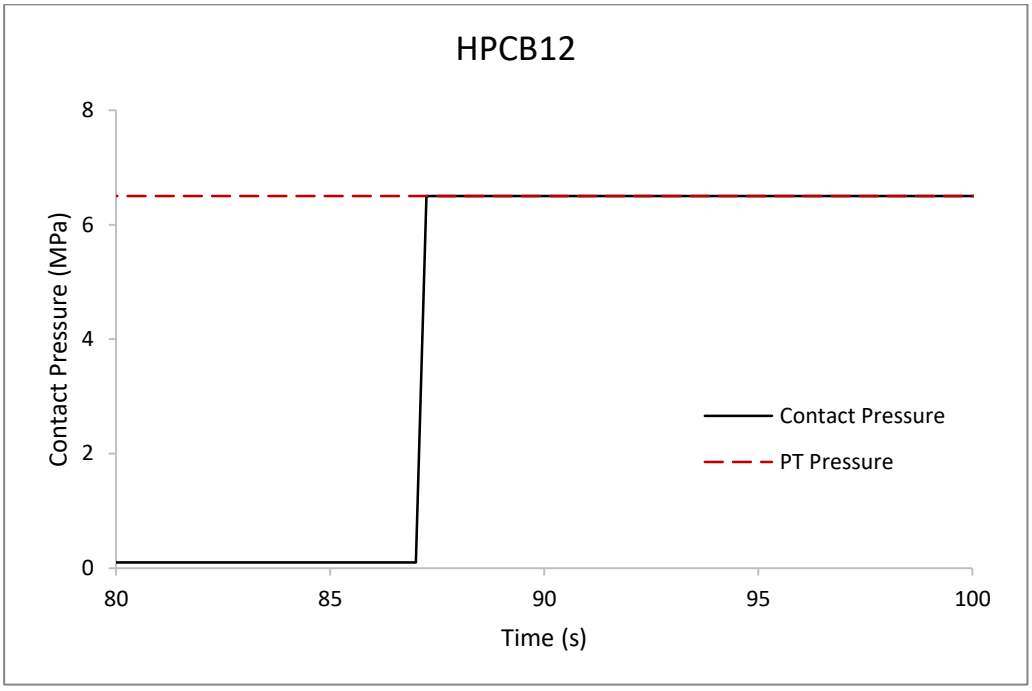

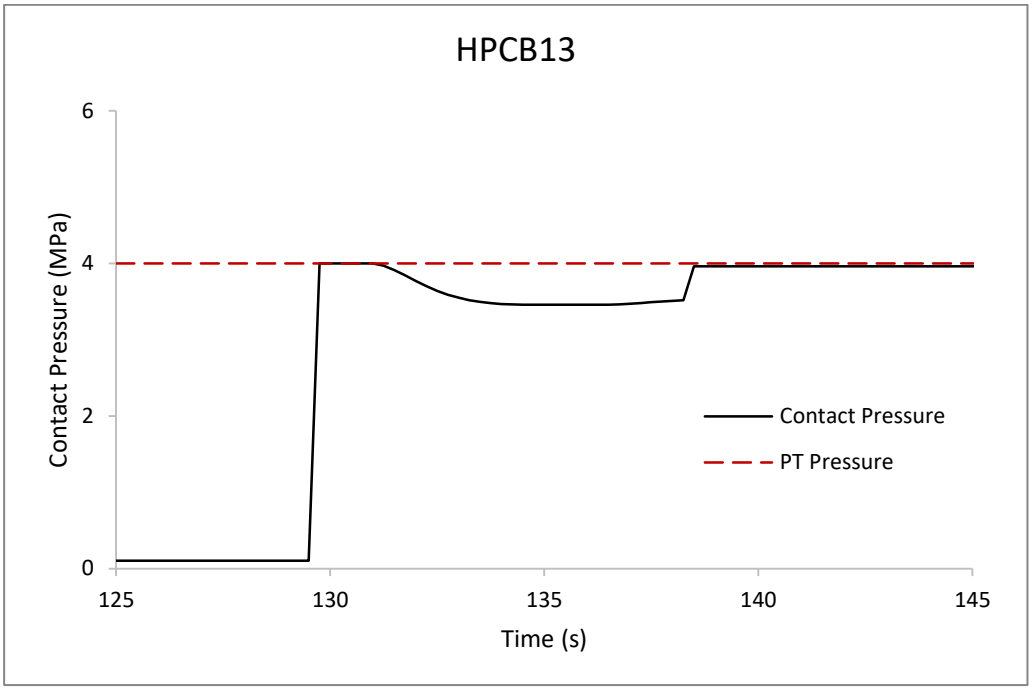

Figure 5.6 Estimated contact pressure transient compared to internal PT pressure for HPCB12 and HPCB13

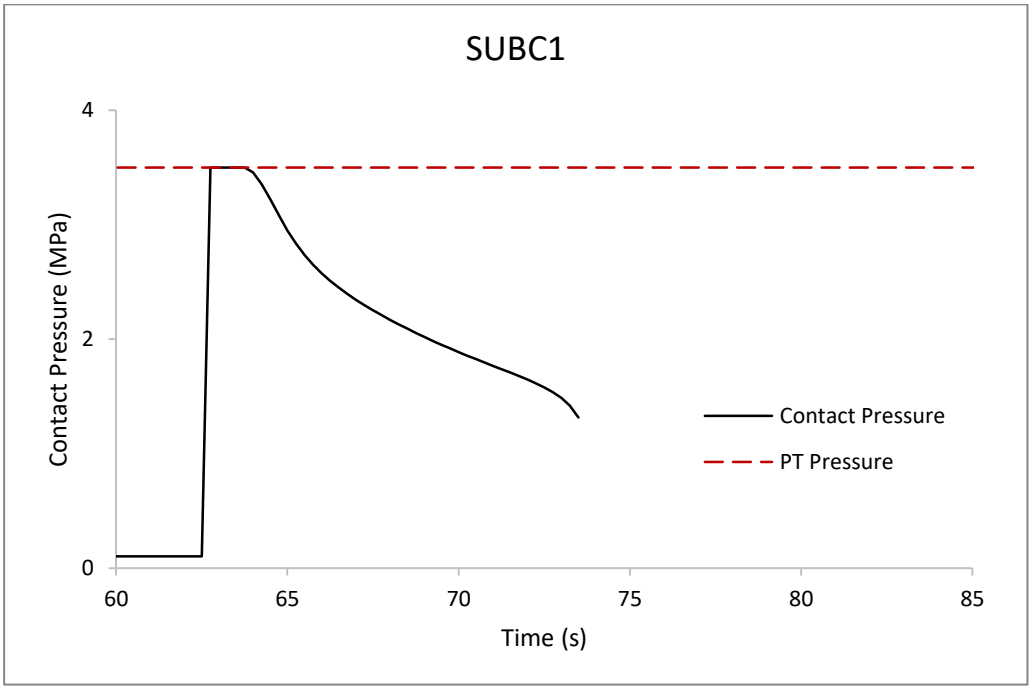

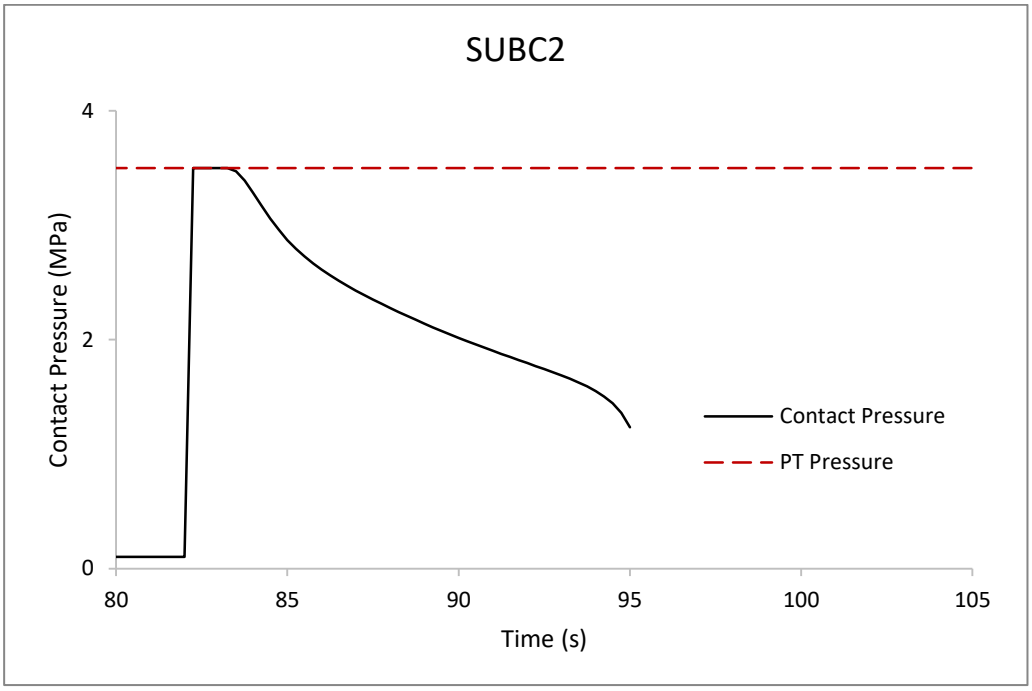

Figure 5.7 Estimated contact pressure transient compared to internal PT pressure for SUBC1 and SUBC2

Luxat [35] suggested that the contact pressure could be approximated using a pressure redistribution factor (a_{pc}).

$$P_{contact} = a_{pc}P_{pt} + (1 - a_{pc})P_a \quad (5.1)$$

Predictions for a_{pc} based on the PT and CT temperatures are provided in Figure 5.8. Accounting only for the cases where contact pressure decreased we can see that the model correctly predicts the behaviour of contact pressure with respect to CT temperature.

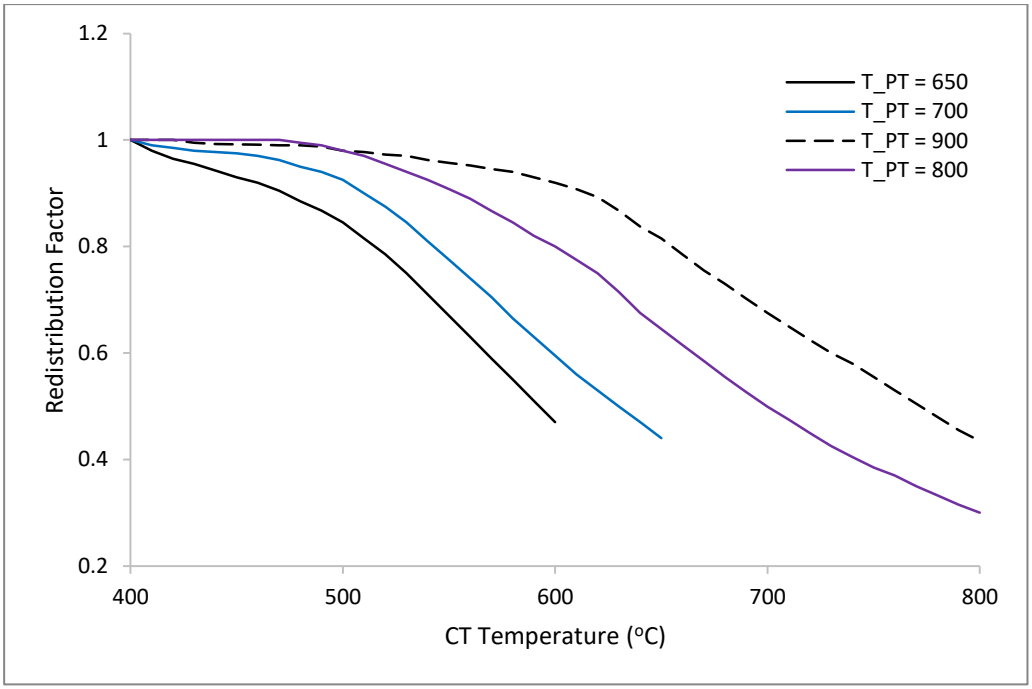

Figure 5.8 Pressure redistribution factor as a function of CT temperature provided by Luxat

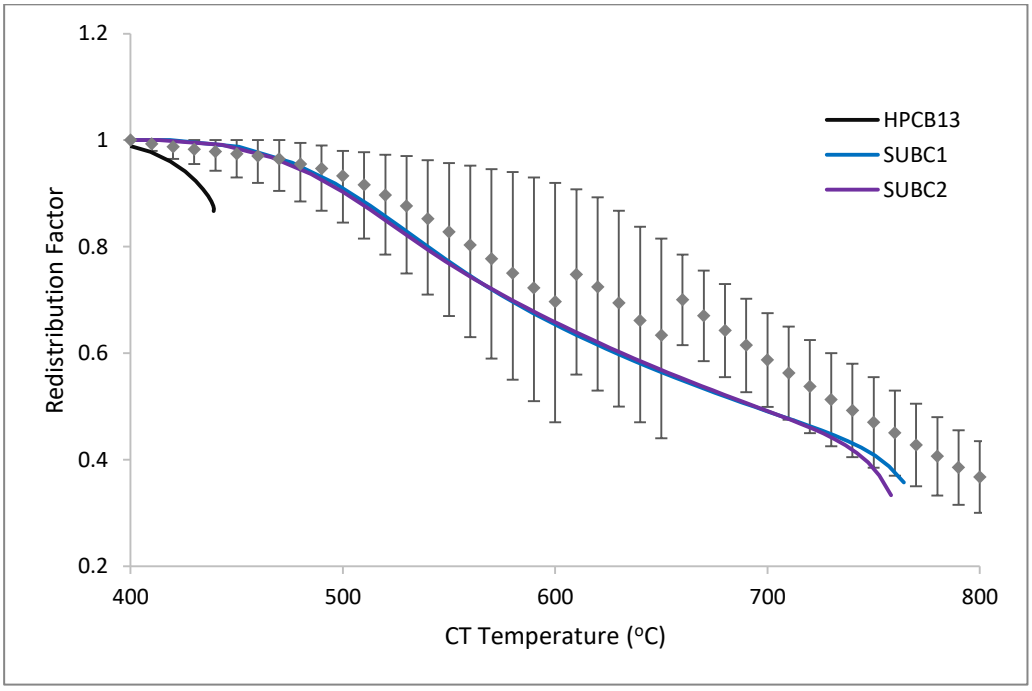

Figure 5.9 Comparison of model predicted pressure redistribution factor with data provided by Luxat [35]

5.3 Contact Conductance

CATHENA is a software package that was developed by Atomic Energy of Canada Limited to simulate two phase flow in a piping network. Among other capabilities it is able to predict temperature transients similar to those described in this thesis. Although access to the code itself is restricted research performed by El-Hawary et al. [42], for the Canadian Nuclear Safety Commission, describes how CATHENA estimates the contact conductance in PT/CT ballooning contact. The contact conductance is estimated using a step function that consists of "a high value immediately upon contact, that is pressure dependent, and a much lower value for the longer term" [42]. Exact values

are not specified but Luxat [35] suggested that initial contact conductance could be upwards of 11 kW/m^2/K.

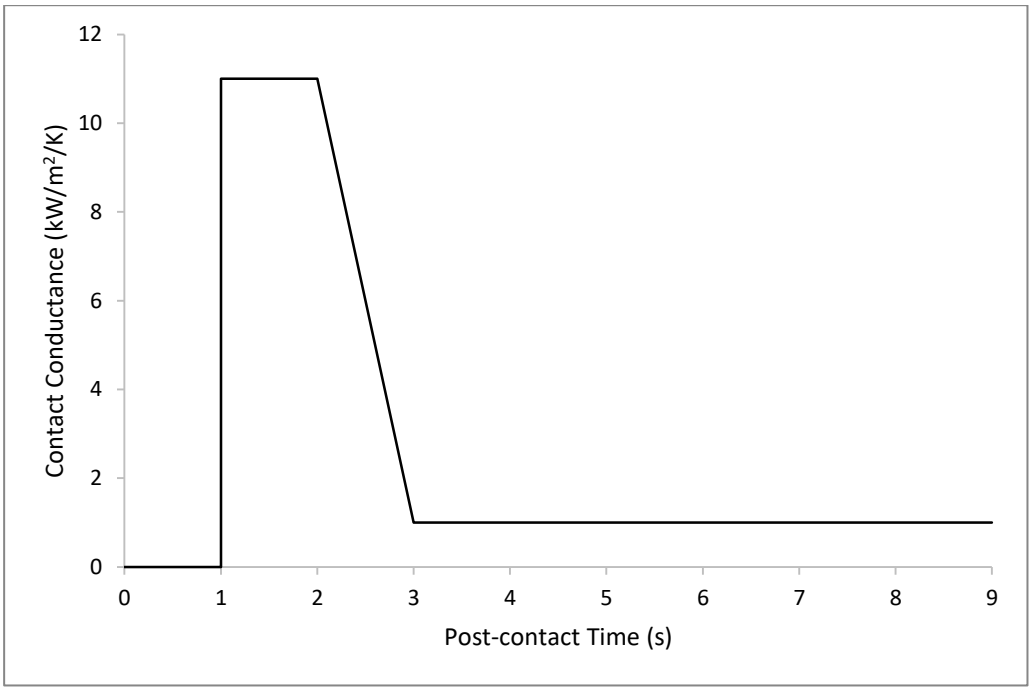

Figure 5.10 General behaviour of contact conductance used in CATHENA software (reproduced from [42])

Predicted contact conductance values shown in Figure 5.11 to Figure 5.13 follow a similar trend, with initial values being much larger than those calculated a few seconds after contact. The main difference is that the period of initially high contact conductance is much shorter than assumed in CATHENA, lasting for about half a second. We also notice that for cases of sever CT strain (SUBC1 and SUBC2) the contact conductance begins to increase rapidly.

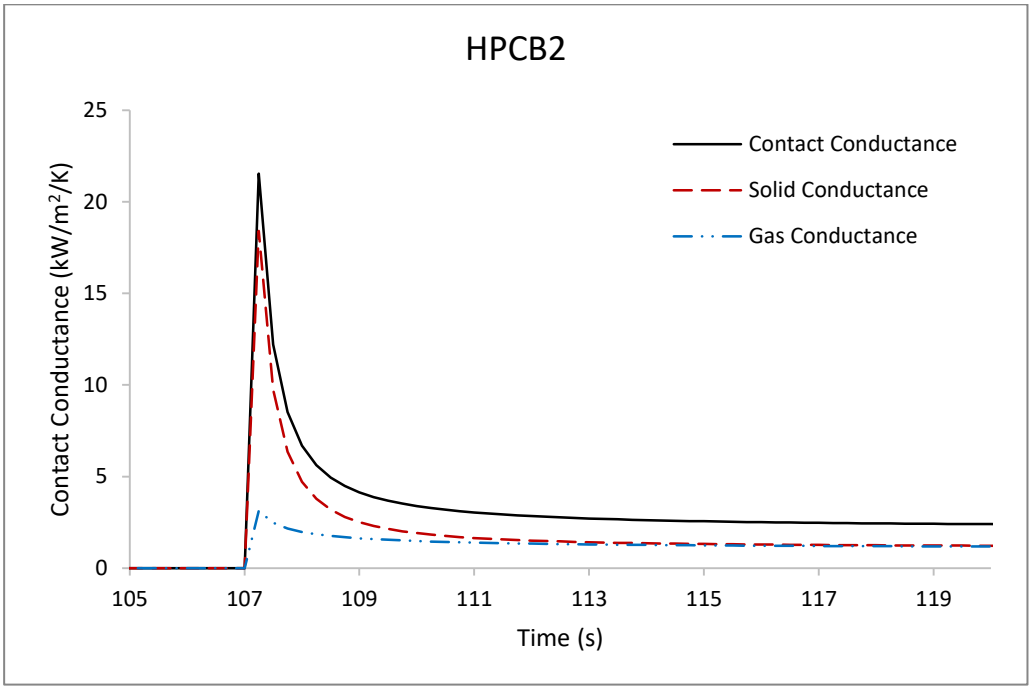

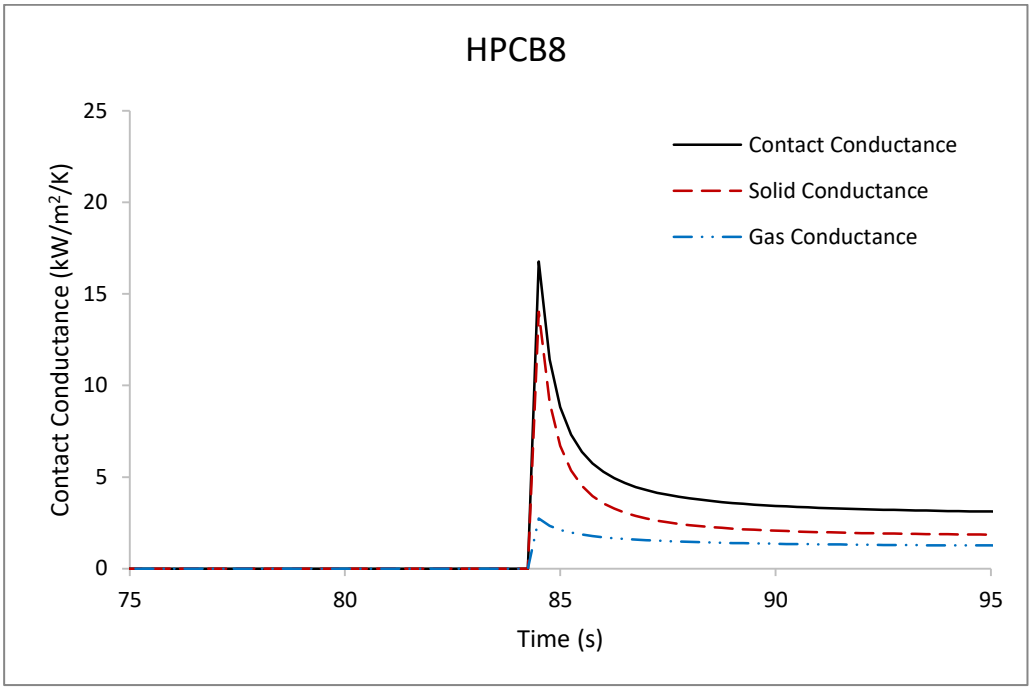

Figure 5.11 Total contact conductance (gas + solid) predicted by the model for HPCB2 and HPCB8

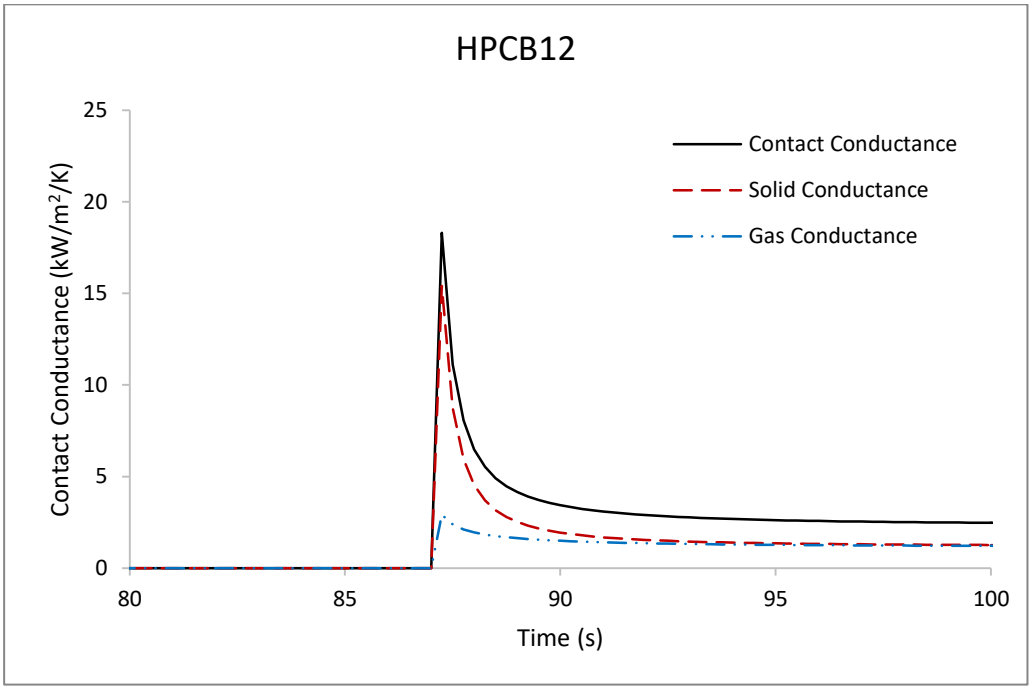

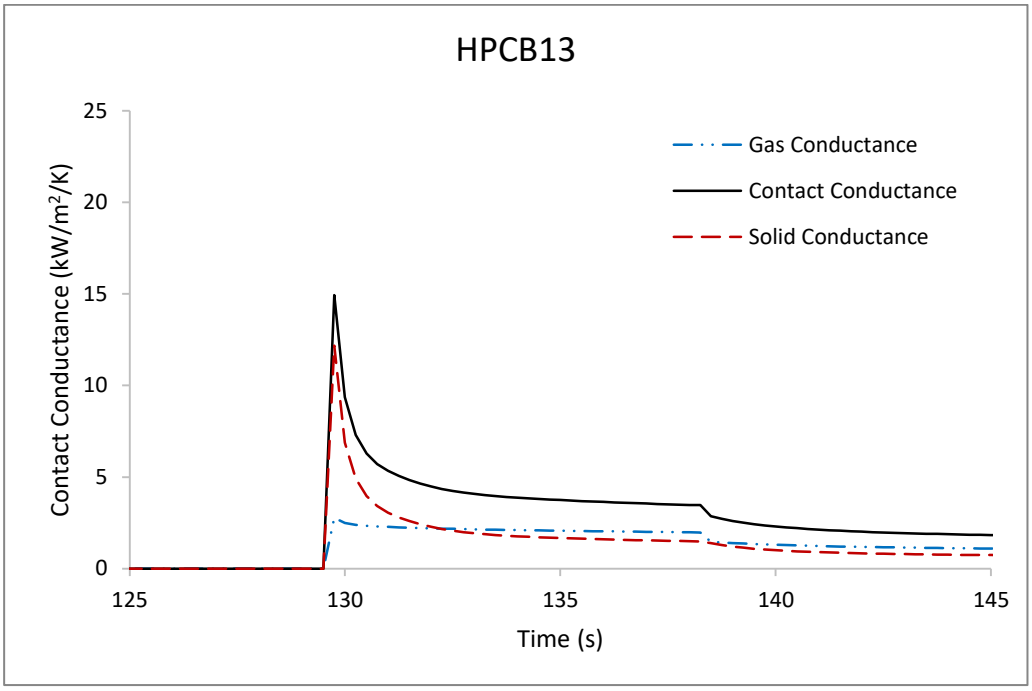

Figure 5.12 Total contact conductance (gas + solid) predicted by the model for HPCB12 and HPCB13

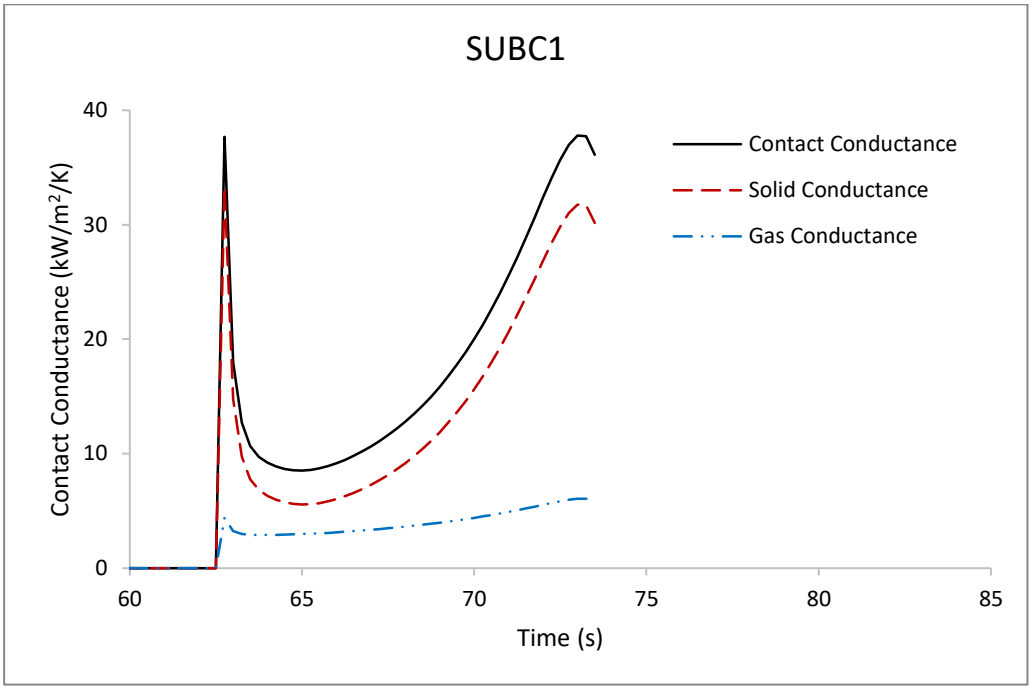

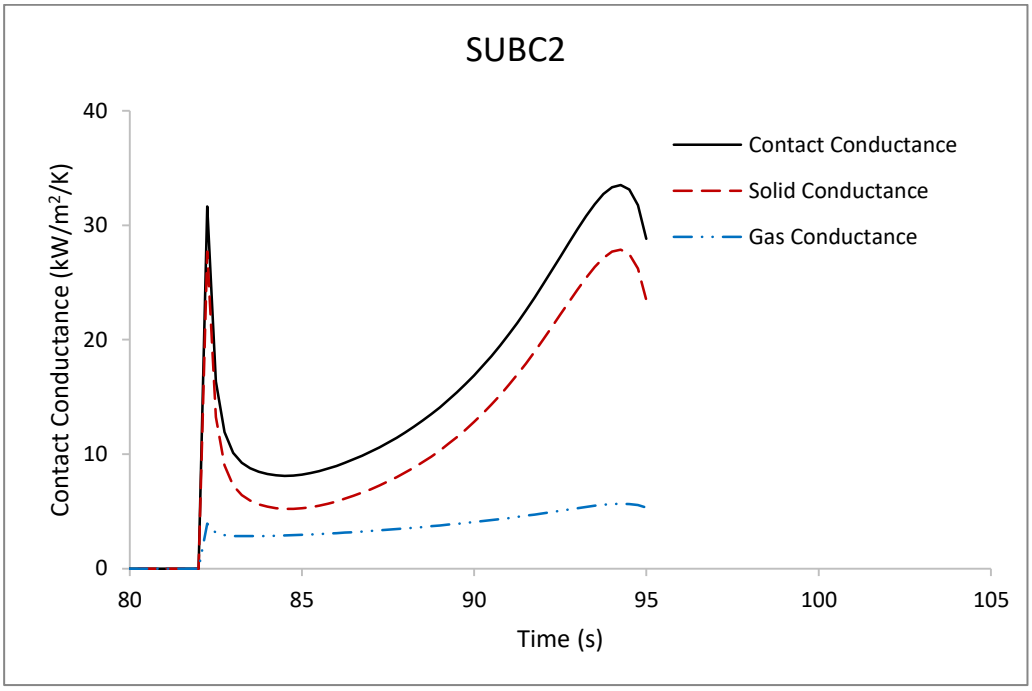

Figure 5.13 Total contact conductance (gas + solid) predicted by the model for SUBC1 and SUBC2

This behaviour is the direct result of increasing contact pressure to hardness ratio. Yovanovich [8] suggested that as the pressure to hardness ratio increased the contact asperities would begin to deform resulting in an increased solid contact area. In turn this would result in higher contact conductance. The figure below is an example of the pressure to hardness ratio transient for experiment SUBC1.

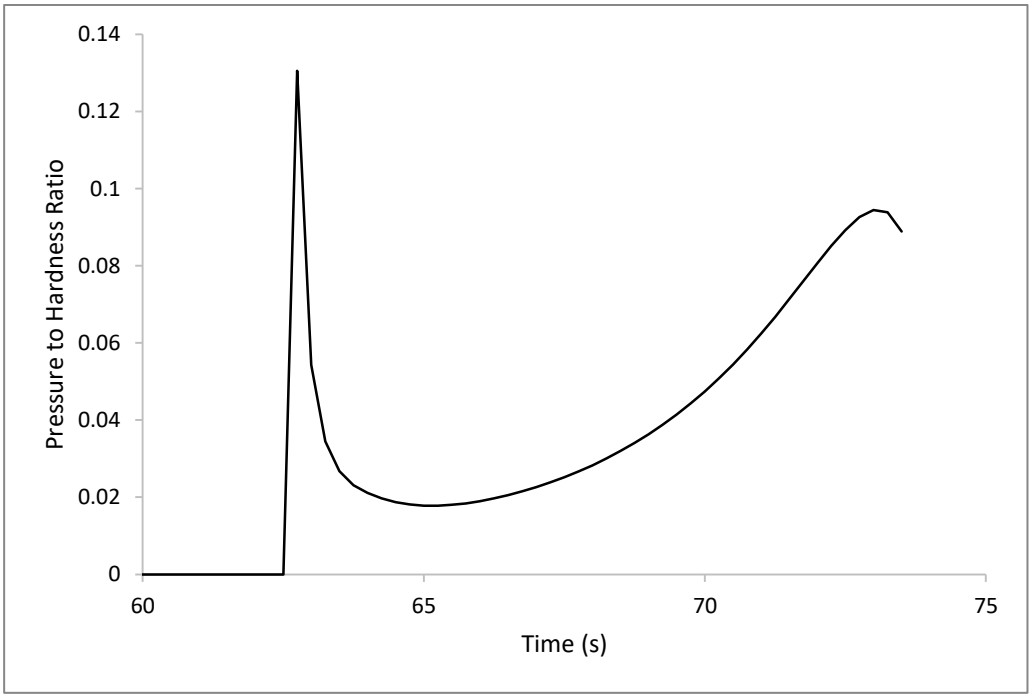

Figure 5.14 Contact pressure to hardness ratio for SUBC1

5.4 Boiling Water Convective HTC & Film Thickness

Luxat [35] suggested that the nucleate pool boiling HTC would be somewhere between 25-50 $kW/m^2/K$. For experiments where film boiling was not observed the predicted values behaved similarly to the contact conductance values, where there is a period of initially high HTC value followed by a lower steady state value. This is a result

of the large temperature difference between the PT and CT at the moment of contact. Steady state values are in the range of 20-25 kw/m^2/K for HPCB2/8 & 12. Once HPCB13 quenches, approximately 10 seconds after contact, the steady sate nucleate boiling HTC is about 13 kw/m^2/K. The figure below shows nucleate boiling convective HTC for all experiments on an adjusted time scale.

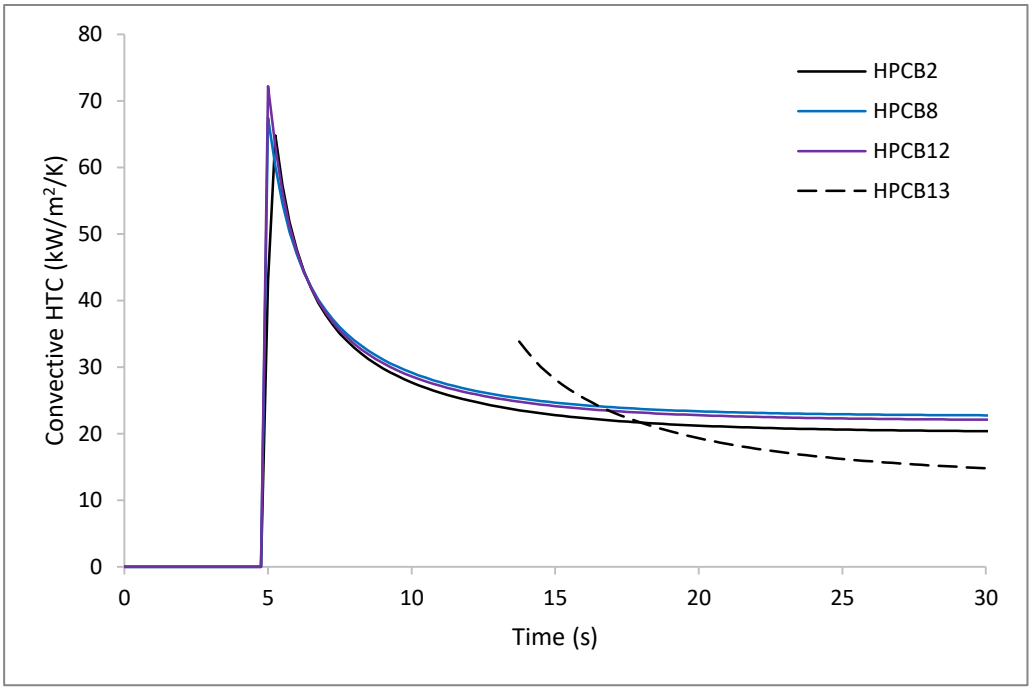

Figure 5.15 The calculated nucleate boiling convective HTC for all applicable simulations

The revised film boiling HTC can be compared to the value predicted by Gillespie and Moyer. In Figure 5.16 we can see that if the CT does not quench, as in SUBC1/2, the calculated value of h_{conv} will approach the correlation value. A single line representing

the correlation is used since the degree of subcooling for HPCB13 and SUBC1/2 is roughly the same (~20^{o}C).

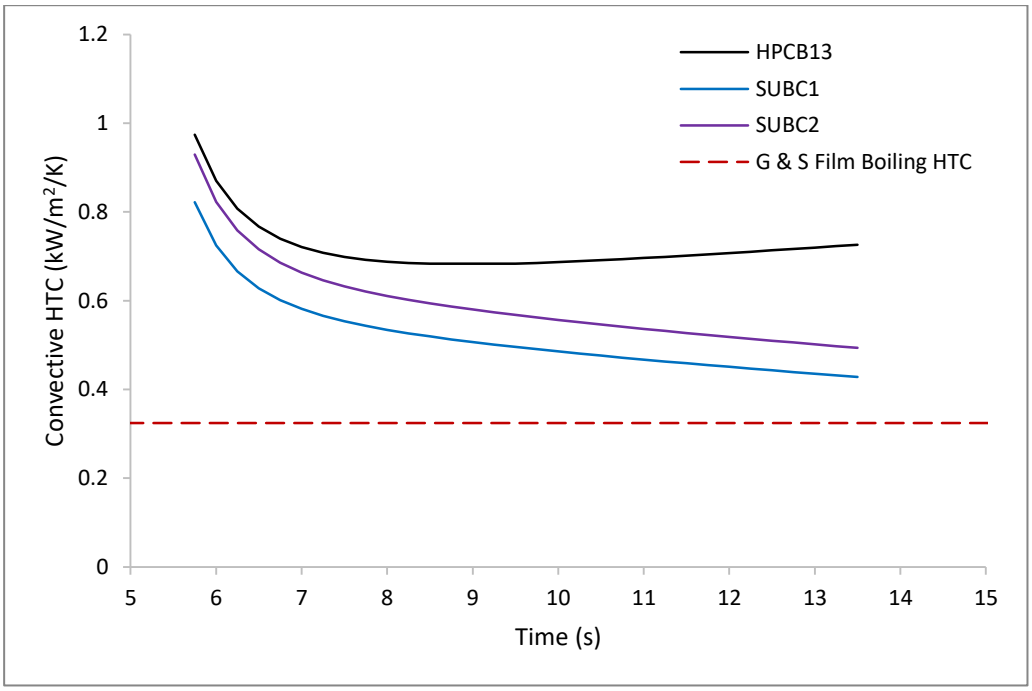

Figure 5.16 Calculated film boiling HTC for all applicable simulations

In comparing the film thickness predicted by this model to those obtained by Jiang and Luxat [37] we notice a large difference between the two. A tentative explanation for this discrepancy could be the use of constant CT diameter in the model described by Jiang. In Figure 5.17 we see that values for film thickness are provided for CT temperatures upwards of 800^{o}C, which is above the temperature required to induce strain. As can be seen in equation (4.32) as the CT diameter increases so too will the bubble rise velocity which, in turn, increases the rate at which energy is removed from the film. This limits the energy available to superheat and expand the film and would result in reduced

film thickness. A second explanation is that the model provided by Jiang focused on the development of stable film boiling where all three instances of observed film boiling had continually changing film thickness.

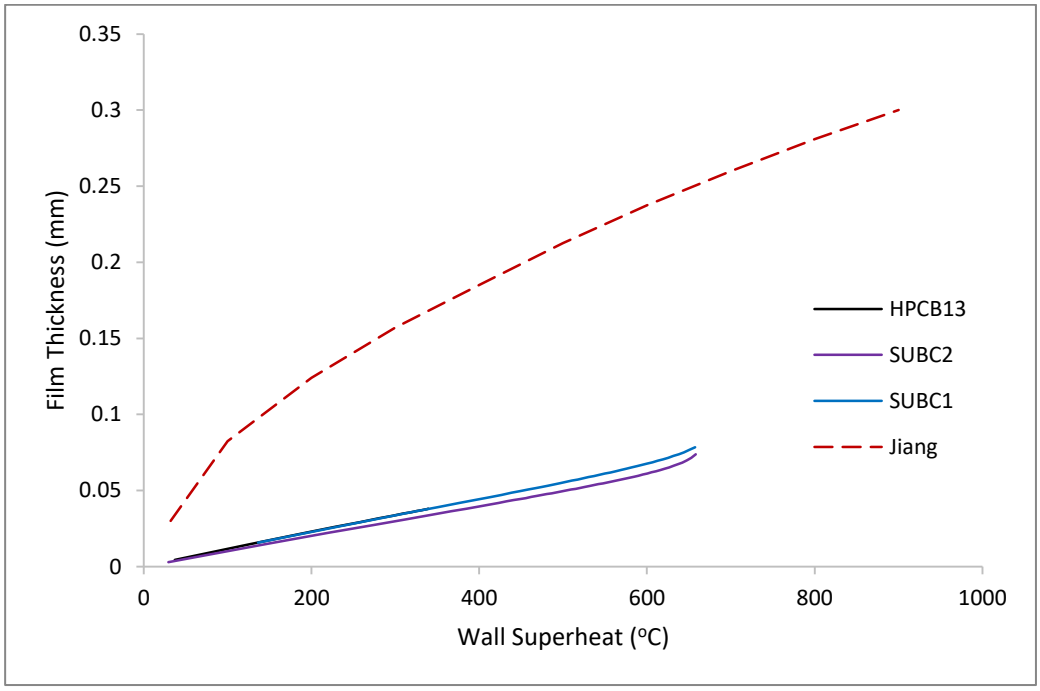

Figure 5.17 Comparison of film thickness between the model outlined in this thesis and the one provided by Jiang [37]

5.5 CT Temperature Sensitivity to Contact Conductance and Convective HTC

The initiation of film boiling, and therefore the risk of channel failure, is dependent on the intensity of the heat flux from the inner PT to wall, through the CT, to subcooled pool. This heat flux is not only dependent on the temperature difference between the PT and CT but the resistance to heat transfer between the contacting tubes.

We can examine the variation in the PT and CT temperature with respect to certain parameters by performing a sensitivity analysis and determine the risk of not predicting film boiling when in reality it would occur (false negative). This section will focus on the variation in CT temperature at the moment of contact as a function of contact conductance and convective HTC as well as their components. Equation used for sensitivity analysis can be found in appendix A.

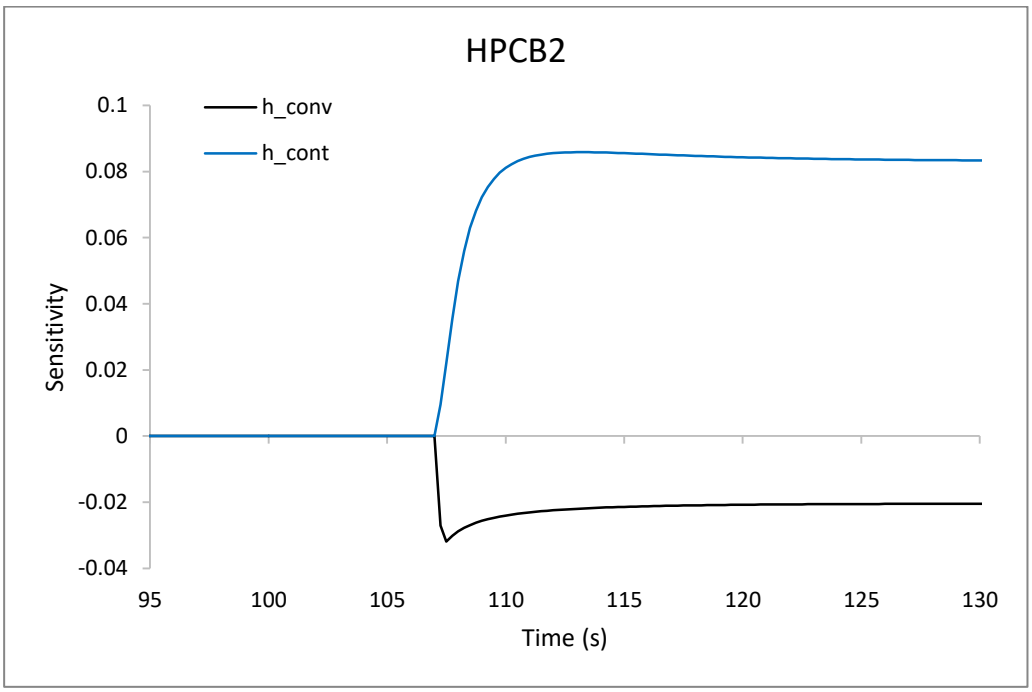

Figure 5.18 Sensitivity of CT temperature to convective HTC and contact conductance for HPCB2. Units are in ^{o}C per kW/m^{2}/K

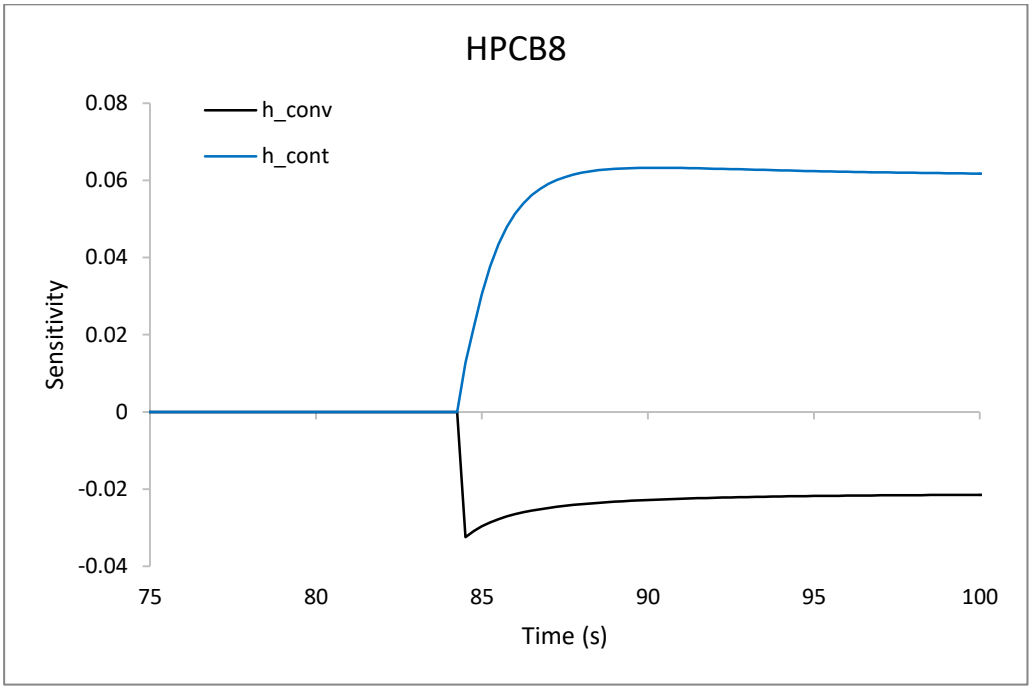

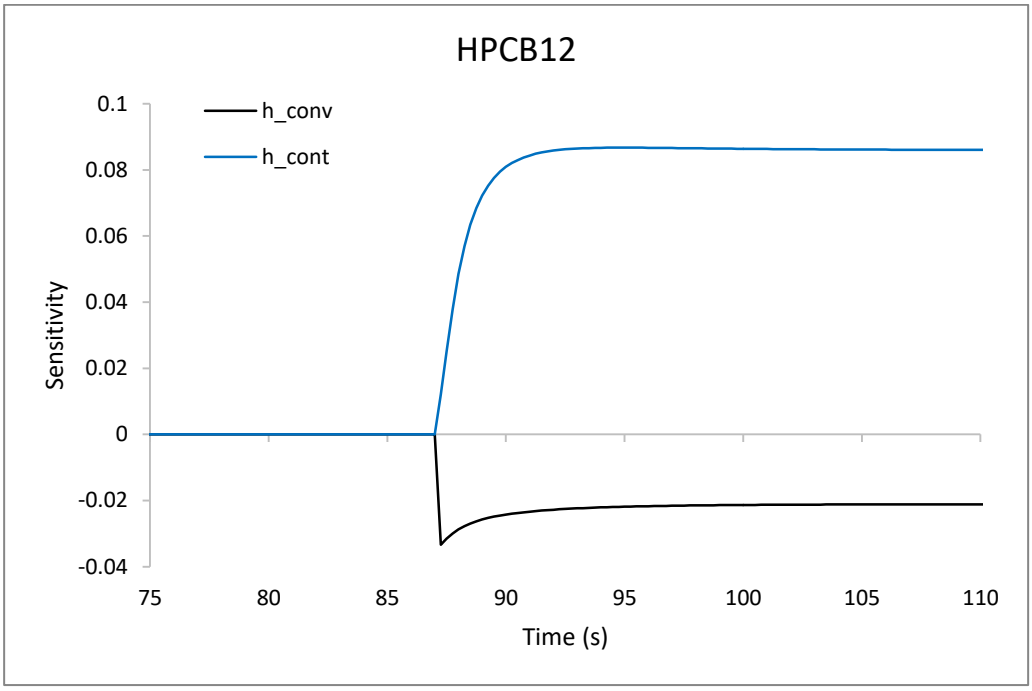

Figure 5.19 Sensitivity of CT temperature to convective HTC and contact conductance for HPCB8 and HPCB12. Units are in ^{o}C per kW/m^{2}/K

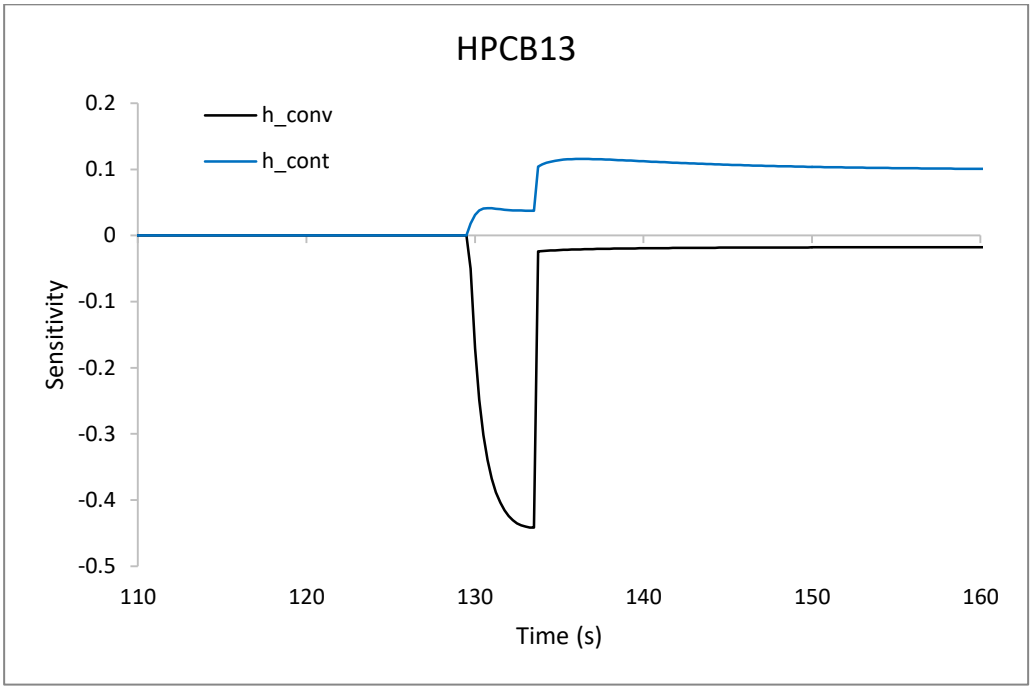

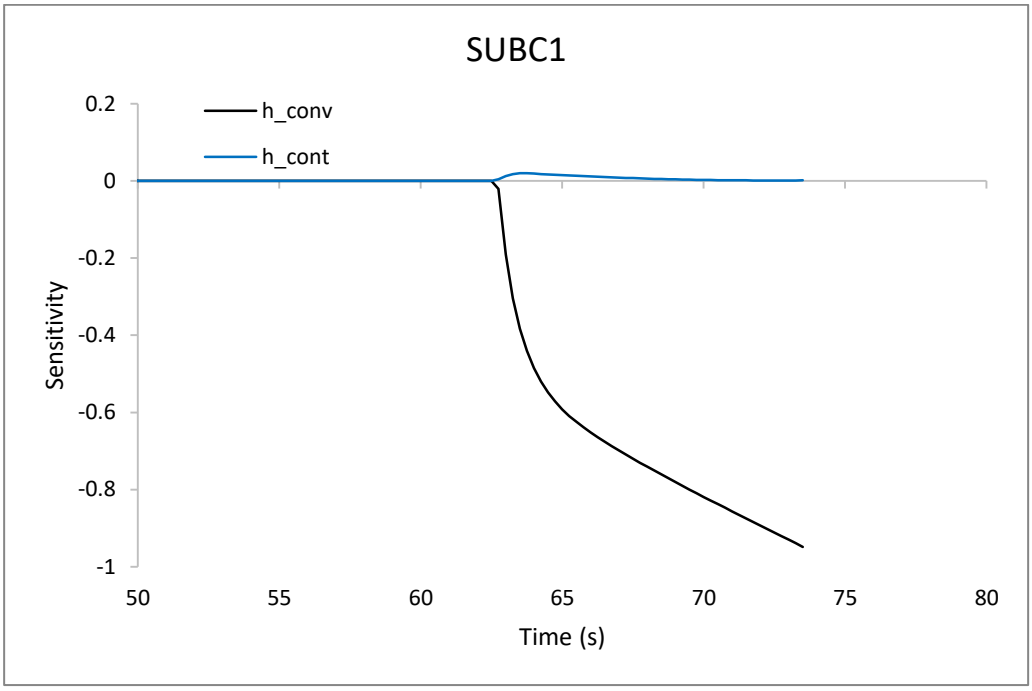

Figure 5.20 Sensitivity of CT temperature to convective HTC and contact conductance for HPCB13 and SUBC1. Units are in ^{o}C per kW/m^{2}/K

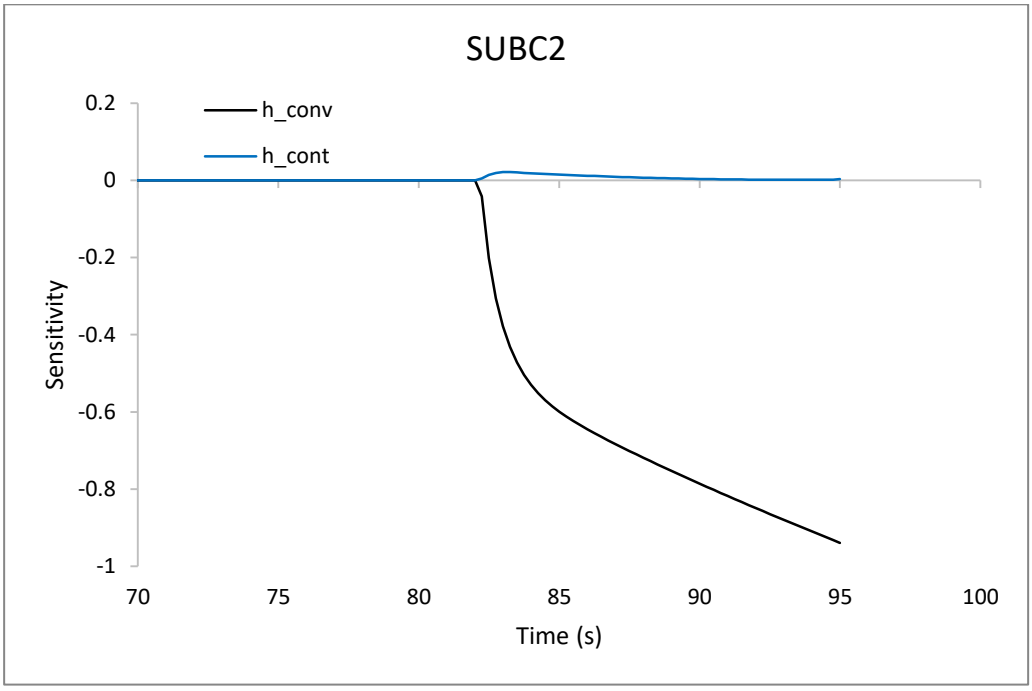

Figure 5.21 Sensitivity of CT temperature to convective HTC and contact conductance for SUBC2, units are in ^{o}C per kW/m^2/K

Results in the above figures indicate that the CT temperature is more sensitive to the convective HTC compared to the contact conductance once film boiling has been initiated. We see that the CT temperature can vary anywhere between by 0.5 to 1 degree for every 1 kW/m^2/K change in film boiling HTC. This is to be expected based on the range of HTC values predicted for film boiling in Figure 5.17, a change of 1 kW/m^2/K would mean a doubling or, in extreme cases tripling, in heat flux which would significantly impact CT temperatures. This point is further reinforced by the observation of rapid CT temperature decrease upon quench in HPCB13. For cases where film boiling was not initiated we see that the CT temperature is more sensitive to contact conductance varying by about 1^{o}C for every 10 kW/m^2/K increase. The contact conductance is

dependent on several properties that can be difficult to determine; more specifically the surface roughness and average asperity slope.

The current form of the model uses an assumed, constant, roughness of 11 μm and average asperity slope of 0.12 based on a model created by Cziraky and Luxat [43] to predict high pressure contact conductance. Their results showed that the ratio of roughness to average asperity slope would directly affect the ratio of peak to steady state contact conductance. The value of roughness and slope were chosen in an attempt to match the expected behaviour shown in Figure 5.10.

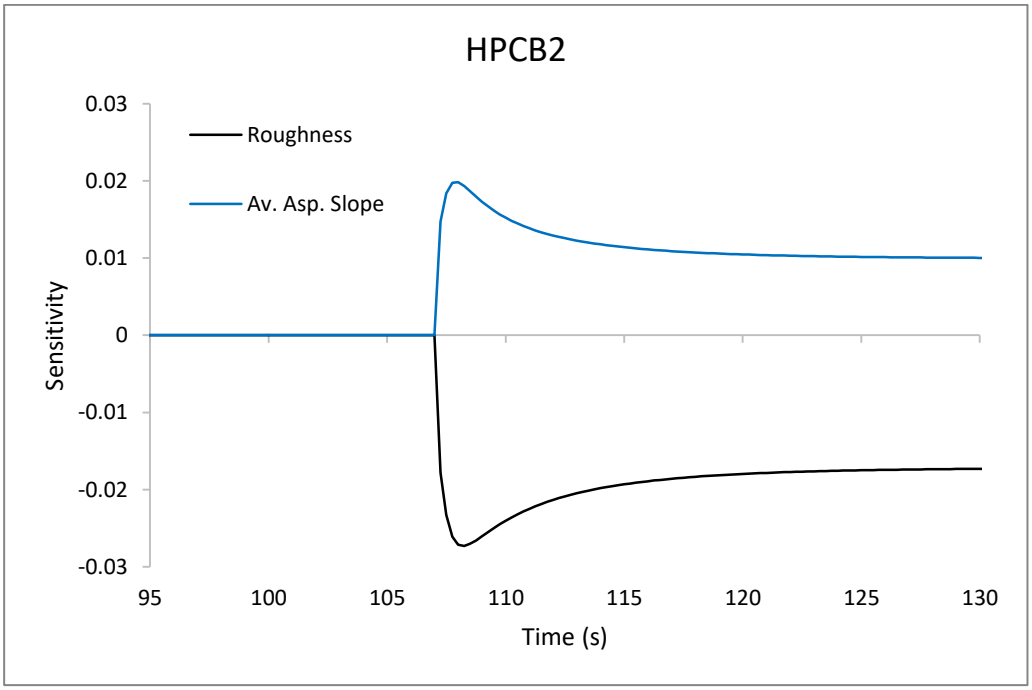

Figure 5.22 Sensitivity of CT temperature to change in average surface roughness or average asperity slope for HPCB2, units are in ^{o}C/μm and ^{o}C per 1% increase in slope

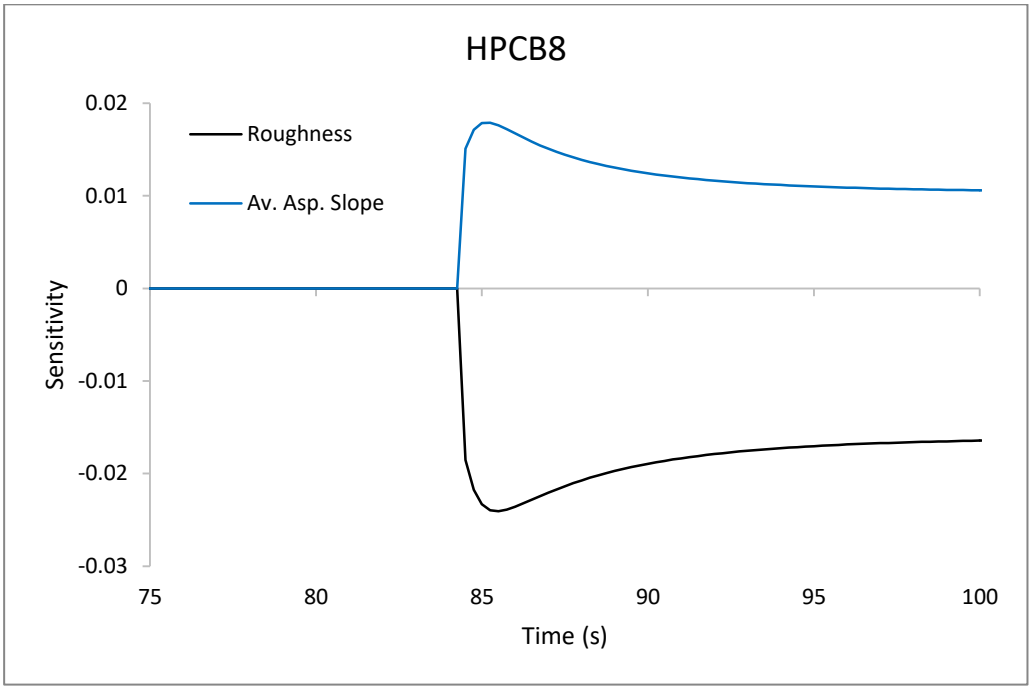

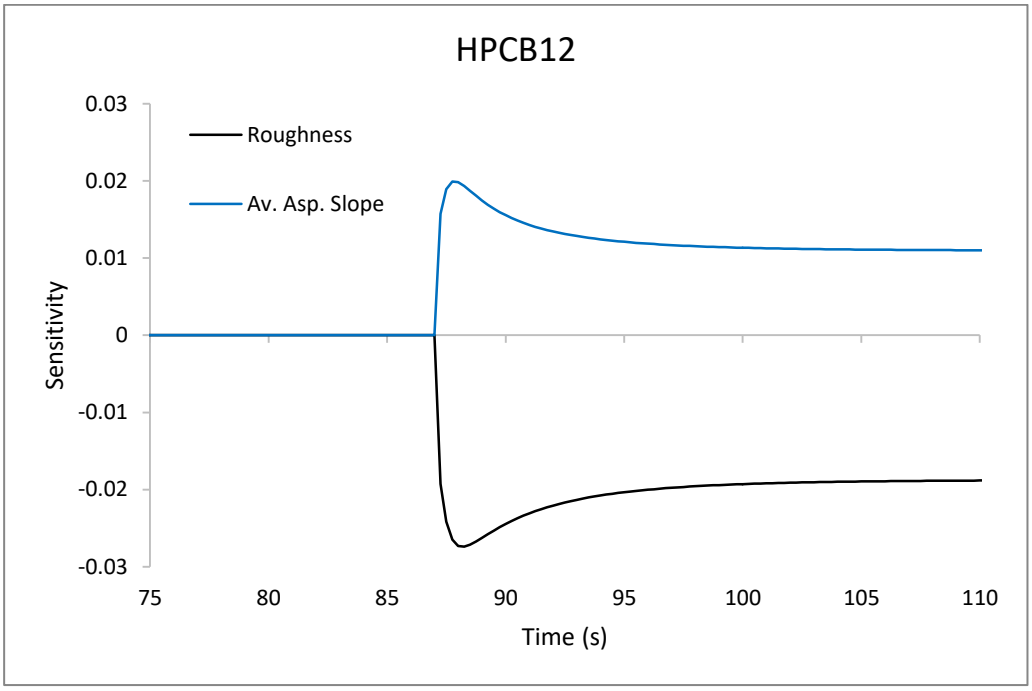

Figure 5.23 Sensitivity of CT temperature to change in average surface roughness or average asperity slope for HPCB8 and HPCB 12, units match Figure 5.22

Results show the CT temperature sensitivity is at its highest at the moment of contact, with variations of about 1^{o}C per ~30 μm change in roughness and 2^{o}C for every 1 unit increase in average asperity slope. In both cases this variation is minimal. Considering the surface roughness, a 30 μm variation in roughness would mean a 300% error in the value used for this model. Furthermore, the maximum allowable defect depth in PT manufacturing is 13 μm and should serve as an upper limit to surface roughness. This means the CT temperature variation that can be attributed to a change in roughness is limited to ± 0.43^{o}C. For the average asperity slope, in order to change the CT temperature by 50^{o}C the average inclination of the asperities would have increase from 7^{o} to 88.86^{o} at which point the surface would be broken into a set of discrete heights. At any rate with such a drastic difference in surface profile yielding low temperature variations we should be safe in approximating the average asperity slope and roughness on the values used by Cziraky and Luxat [43].

One final component of the contact conductance that should be accounted for is contact pressure to hardness (P/H) ratio. The maximum P/H ratio for each experiment is shown in Figure 5.24 and at no point does it exceed 0.08. Figure 5.25 shows the effect a 100% maximum increase to P/H ratio would have on CT temperature. The largest observed difference would be an increase of ~1.7^{o}C in HPCB2 which is not appreciable enough to result in false negative prediction of film boiling.

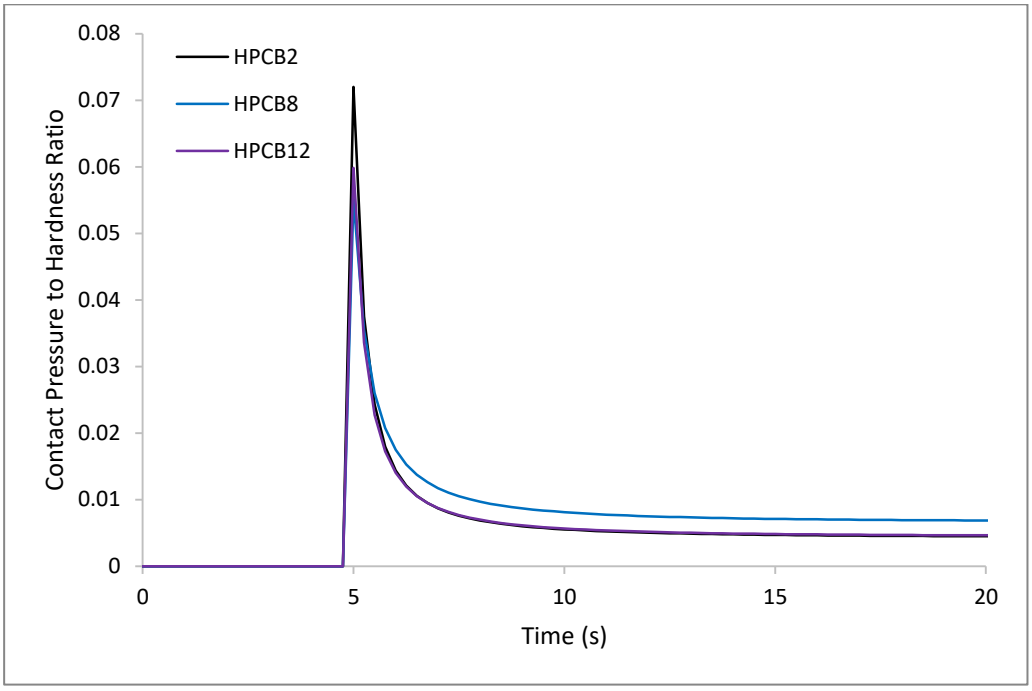

Figure 5.24 The contact pressure to hardness (P/H) ratio for HPCB2/8 & 12

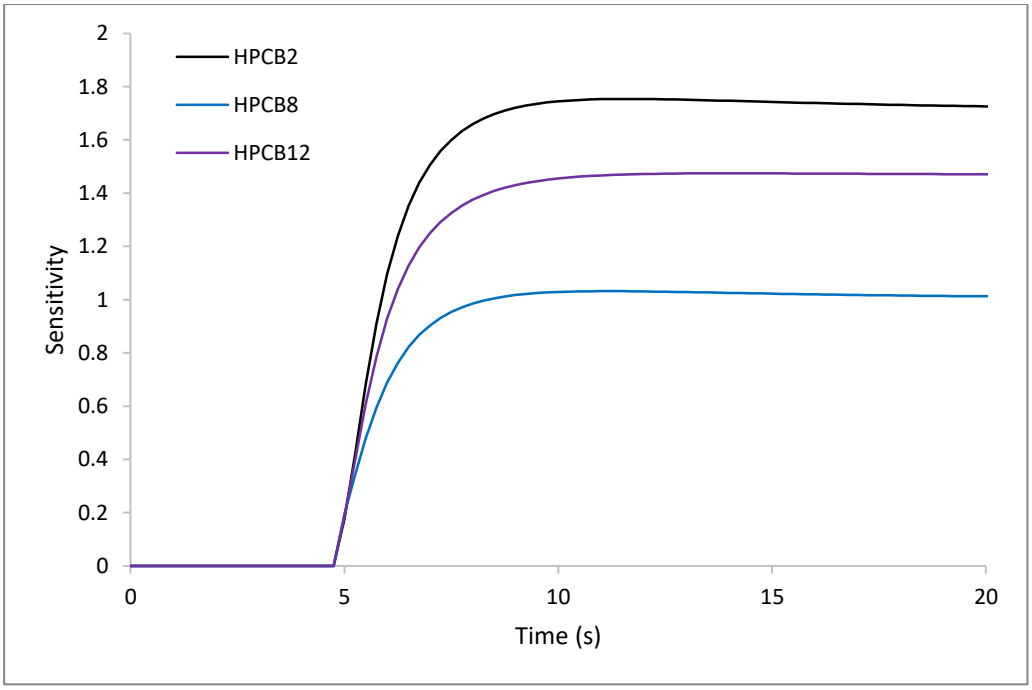

Figure 5.25 Sensitivity of CT temperature per 100% increase in P/H ratio

The P/H ratio is dependent on the contact pressure which in turn is dependent on the strain rate and temperature of the contacting tube and the internal pressure of the pressure tube. Based on the contact times observed in the model it is unlikely that strain rate is being estimated incorrectly and the values for the P/H ratio should be correct.

CHAPTER 6 - Conclusion and Suggestion for Future Work

The model outlined in this thesis was able to accurately estimate the thermal and mechanical data collected for 5 out of 6 pressure tube / calandria tube ballooning contact experiments. This included the prediction of quench roughly 10 seconds after the initiation of film boiling in HPCB13 and the failure time of SUBC1 and SUBC2. The largest deviation between the experimental pressure tube contact temperatures and those obtained using the model was about 7% and was related to an experiment where the PT ruptured before contact (HPCB8). Maximum calandria tube temperatures were underestimated for experiments where film boiling did not develop but fell within 13% of expected values when film boiling was observed. Based on sensitivity analysis the predicted CT temperatures are not conditional on the selection of surface roughness or average asperity slope. The largest contributor to CT temperature increase at the moment of contact was the contact pressure to hardness ratio. This value is dependent on the strain rate of the PT and CT which, in turn, are dependent on the PT and CT temperature as well as internal pressure of the PT. Judging by the correct prediction of contact time it is

unlikely that the strain rate is being evaluated incorrectly and thus the P/H ratio should be correct throughout the simulation. It is unlikely that the model will make false negative predictions with respect to the development of film boiling.

The current version of the model was unable to predict PT failure before CT contact as observed in HPCB8. The inability of the model to anticipate this behaviour is likely due to the limited nature of the chosen failure criteria and the assumption circumferentially uniform thermal and mechanical properties. In consideration of the former, the failure criteria used in the model required that a tube deform by 2.7 times its original size in order to be considered "failed". It would be physically impossible for the PT to deform to this degree without making contact with the CT. Shewfelt approached tube failure by breaking the circumference into infinitely small sections and evaluating strain based on local temperatures which brings us to the second limitation of the model. Temperatures, and a variety of other properties such as the convective heat transfer coefficient, are assumed to be circumferentially uniform around both the PT and CT. If the model was converted to account for the transverse heat exchange it is possible it would be able to predict pre contact failure.

Improvements to the model could be made when considering the change from 1 dimension to 2. Not only would a circumferential temperature distribution allow for a local description of creep strain but it could better describe the development of film boiling. The model currently assumes a uniform temperature, even thickness film, develops around the CT the moment critical heat flux is exceeded. In reality film boiling would likely begin at the stagnation point and eventually work its way around the sides of

the tube ending in wrap around film boiling. This could result in more accurate maximum CT temperature predictions. Furthermore, to more accurately represent the in reactor behaviour of the PT and CT the model should be revised to account for fuel bundle weight. Allowing a bundle to make contact with the PT would result in both increased local PT temperatures strain as a result of increased stress at the point of bundle/tube contact.

Bibliography

[1] B. Rouben, "Reactor-Physics Analysis Basis for Current CANDU," Atomic Energy of Canada Limited, Mississauga, 2002.

[2] B. Nangia, G. Fountain, D. Gammage, D. Pun-Quach and J. Robertson, "Strategies for Optimizing CANDU Plant Operations," Amec Foster Wheeler, Toronto, 2015.

[3] "Enhanced CANDU 6 Technical Summary," SNC Lavalin, Mississauga.

[4] N. J. Spinks, "CANDU Nuclear Power Reactors," Thermopedia, 2011.

[5] R. S. Shewfelt, L. W. Lyall and D. P. Godin, "A High Temperature Creep Model for Zr-2.5 wt% Nb Pressure Tubes," *Journal of Nuclear Materials,* pp. 228-235, 1984.

[6] "Ceramic Composition and Properties," Encyclopedia Britannica.

[7] R. S. Shewfelt and L. W. Lyall, "A High Temperature Creep Model for Zircaloy-2 Calandria Tubes," COG, 1988.

[8] M. M. Yovanovich, "New Contact and Gap Conductance Correlations for Conforming Rough Surfaces," in *16th Thermophysics Conference*, Palo Alto, 1981.

[9] M. Bahrami, M. M. Yovanovich and J. R. Culham, "Thermal Joint Resistance of Conforming Rough Surfaces with Gas-Filled Gaps," *Journal of Thermophysics and*

Heat Transfer, vol. 18, no. 3, pp. 318-326, 2004.

[10] "SCDAP/RELAP5/MOD3.2 Code Manual Volume IV - A Library of Materials Properties fo Light Wate Reactor Accident Analysis," Idaho National Engineering and Environmental Laboratory, Idaho, 1997.

[11] S. Song and M. M. Yovanovich, "Relative Contact Pressure: Dependence on Surface Roughness and Vickers Microhardness," *Journal of Thermophysics and Heat Transfer*, vol. 2, no. 1, pp. 43-47, 1988.

[12] V. P. Carey, "Liquid-Vapor Phase Change Phenomena," Hemisphere, 1992.

[13] S. W. Churchill and R. Usagi, "A General Expression for the Correlation of Rates of Transfer and Other Phenomena," *A.I.Ch.E. Journal*, vol. 18, no. 6, pp. 1121-1128, 1972.

[14] S. W. Churchill and H. H. Chu, "Correlating Equations for Laminar and Turbulent Free Convection from a Horizontal Cylinder," *International Journal of Heat and Mass Transfer*, vol. 18, no. 9, pp. 1049-1053, 1975.

[15] R. C. Bosworth, Heat Transfer Phenomena, New York: John Wiley, 1952, p. 101.

[16] W. M. Rohsenow, "A Method of Correlating Heat Transfer Data for Surface Boiling of Liquids," Massachusetts Institute of Technology Division of Industrial Cooperation, Massachusetts, 1951.

[17] W. Fritz, *Physik. Zeitschr,* vol. 36, p. 370, 1935.

[18] B. B. Mikic and W. M. Rhosenow, "A New Correlation of Pool Boiling Data Including the Effect of Heating Surface Characteristics," *Transactions of the American Society of Mechanical Engineering Journal of Heat Transfer,* vol. 91, no. 2, pp. 245-250, 1969.

[19] I. L. Pioro, W. Rohsenow and S. S. Doerffer, "Nucleate Pool-Boiling Heat Transfer. II: Assesment of Prediction Methods," *International Journal of Heat and Mass Transfer,* vol. 47, no. 23, pp. 5045-5057, 2004.

[20] P. K. Sarma, V. Srinivas, K. V. Sharma, T. Subrahmanyam and S. Kakac, "A Correlation to Predict Heat Transfer Coefficient in Nucleate Boiling on Cylindrical Heating Elements," *International Journal of Thermal Sciences,* vol. 47, no. 3, pp. 347-354, 2008.

[21] V. M. Borishansky, "Correlation of the Effect of Pressure on Critical Heat Flux and Heat Transfer Rates using Theory of Thermodynamic Similarity," in *Problems of Heat Transfer and Hydraulics of Two-Phase Media*, New York, Pergamon Press, 1969, pp. 16-37.

[22] P. K. Sarma, V. Srinivas, K. V. Sharma and V. Dharma Rao, "Correlation for Heat Transfer in Nucleate Boiling on Horizontal Cylindrical Surfaces," *Heat Transfer Engineering,* vol. 31, no. 6, pp. 449-457, 2010.

[23] N. Zuber, "Hydrodynamic Aspects of Boiing Heat Transfer," United States Atomic Energy Commission, Los Angeles, 1959.

[24] V. P. Carey, "Liquid Vapor Phase Change Phenomena," Taulor and Francis Inc., 2007.

[25] H. Lamb, Hydrodynamics, New York: Dover Publishing, 1957.

[26] L. M. Milne-Thompson, Theoretical Hydrodynamics, New York: Macmillan Co., 1950.

[27] H. J. Ivey and D. J. Morris, "On the Relevance of Vapor-Liquid Exchange Mechanisms for Subcooled Boiling Heat Transfer at High Pressure," U.K. Report AEEW-R-137, Winfrith, 1962.

[28] G. Gillespie and R. Moyer, "An Experimental Determination of Heat Transfer from Large Cylinders: Film Boiling in Subcooled Water," AECL, 1984.

[29] W. S. Bradfield, "On the Effect of Subcooling on Wall Superheat in Pool Boiling," *Transactions of the American Society of Mechanical Engineering Journal of Heat Transfer*, vol. 89, no. 3, pp. 269-270, 1967.

[30] N. Ohnishi, K. Ishijima and S. Tanzawa, "A Study of Subcooled Film-Boiling Heat Transfer Under Reactivity-Initiated Accident Conditions in Light Water Reactor," *Nuclear Science and Engineering*, vol. 88, no. 3, pp. 331-341, 1984.

[31] M. R. Adler, "The Influence of Water Purity and Subcooling on the Minimum Film Boiling Temperature," University of Illinois, 1979.

[32] L. H. Leung and D. Groeneveld, "Compendium of Thermalhydraulics Correlations and Fluid Properties," CANDU Owners Group, 1991.

[33] M. Mori, S. Toda, M. Ochiai and S. Saito, "Transient Cooling Process of Fuel Rod in Reactivity Initiated Accident," *Journal of Nuclear and Science Technology,* vol. 17, no. 6, pp. 413-424, 1980.

[34] R. S. Shewfelt, "Ballooning of CANDU Pressure Tubes - Model Assesment," Atomic Energy of Canada Limited, Pinawa, 1990.

[35] J. Luxat, "Analysis of High Pressure Contact Boiling Tests," Ontario Power Generation, 2001.

[36] M. Holmgren, ""X Steam for Matlab"," 2006.

[37] J. T. Jiang and J. C. Luxat, "Mechanistic Modeling of Pool Film-Boiling and Quench on a CANDU Calandria Tube following a Critical Break LOCA," in *Proceedings of the Internation Youth Nuclear Congress*, Interlaken, 2008.

[38] S. Sideman, "The Equivalence of the Penetration and Potential Flow Theories," *Industrial & Engineering Chemistry,* vol. 58, no. 2, pp. 54-58, 1966.

[39] L. C. Witte and J. Orozco, "The Effect of Vapor Velocity Profile Shape on Flow Film Boiling from Submerged Bodies," *ASME Journal of Heat Transfer,* pp. 191-197, 1984.

[40] R. M. Davies and G. Taylor, "The Mechanics of Large Bubbles Rising through Extended Liquids and through Liquids in Tubes," *Proceedings of the Royal Society of London. Series A, Mathematical and Physical Sciences,* vol. 200, no. 1062, pp. 375-390, 1950.

[41] G. B. Wallis, One-dimensional Two-phase Flow, McGraw-Hill, 1969.

[42] M. El-Hawary, J. Szymanski, A. Tanase, A. Delja, A. Oussoren and P. Neal, "New Contact Boiling Experiments to Evaluate Calandria Tube Strin Acceptance Criteria," in *35th Annual Conference of the Canadian Nuclear Society*, Saint John, 2015.

[43] A. Cziraky and J. C. Luxat, "Pressure Tube-Calandria Tube Thermal Contact Conductance," McMaster Univeristy, Hamilton, 2009.

[44] "Thermophysical Properties Database of Materials for Light Water Reactors and Heavy Water Reactors," International Atomic Energy Agency, Vienna, 1999-2005.

[45] S. K. Boetcher, "Natural Convection Heat Transfer From Horizontal Cylinders," in *Thermal Engineering and Applied Science*, Springer, 2014.

[46] I. L. Pioro, "Experimental Evaluation of Constants for the Rohsenow Pool Boiling

Correlation," *International Journal of Heat and Mass Transfer,* vol. 42, no. 11, pp. 2003-2013, 1999.

[47] S. G. Kandlikar, "A Theoretical Model to Predict Pool Boiling CHF Incorporating Effects of Contact Angle and Orientation," *Journal of Heat Transfer,* vol. 123, no. 6, pp. 1071-1080, 2001.

[48] I. L. Mostinski, "Calculation of Heat Transfer and Critical Heat Flux in Boiling Liquids on the Law of Corresponding States," *Teploenergetika,* vol. 10, no. 4, pp. 66-71, 1963.

Appendix A - Equations for Sensitivity Analysis

To determine a function's sensitivity to specific parameter we can simply differentiate that function with respect to the desired parameter. With that in mind we begin with the general form of the equation describing PT and CT temperature.

$$T_{i+1} = T_i e^{-b\Delta t} + \phi(1 - e^{-b\Delta t}) \quad (A.1)$$

Where the values of b and ϕ will change based on the tube in question and whether contact has been made.

Pre-Contact PT

$$b_{pt} = \frac{h'_{rad}}{m'_{pt} c_{p,pt}} \qquad \phi_{pt} = T_h - q'_{loss} \quad (A.2)$$

$$b_{ct} = 0 \qquad \phi_{ct} = 0 \quad (A.3)$$

Post-Contact PT

$$b_{pt} = \frac{h'_{rad} + h'_{eff}}{m'_{pt} c_{p,pt}} \qquad \phi_{pt} = \frac{h'_{rad} T_h + h'_{eff} T_{ct}}{h'_{rad} + h'_{eff}} \quad (A.4)$$

$$b_{ct} = \frac{h'_{eff} + h'_{conv}}{m'_{ct} c_{p,ct}} \qquad \phi_{ct} = \frac{h'_{eff} T_{pt} + h'_{conv} T_l}{h'_{eff} + h'_{conv}} \quad (A.5)$$

Section 5.4 and 5.5 focuses on the post-contact CT temperature sensitivity with respect to h'_{eff}, h'_{conv} and h_{cont}. The equations used for this analysis follow.

Temperature w.r.t. Effective HTC

$$\frac{\partial T_{ct}}{\partial h'_{eff}} = -\frac{b_{ct}\Delta t e^{-b_{ct}\Delta t}}{h'_{eff}+h'_{conv}}[T_{cto}-\phi_{ct}] + \frac{h'_{conv}\left(T_{pt}-T_l\right)}{\left(h'_{conv}+h'_{eff}\right)^2}[1-e^{-b_{ct}\Delta t}] \quad (A.6)$$

Temperature w.r.t. Convective HTC

$$\frac{\partial T_{ct}}{\partial h'_{conv}} = -\frac{b_{ct}\Delta t e^{-b_{ct}\Delta t}}{h'_{eff}+h'_{conv}}[T_{cto}-\phi_{ct}] + \frac{h'_{eff}\left(T_l-T_{pt}\right)}{\left(h'_{conv}+h'_{eff}\right)^2}[1-e^{-b_{ct}\Delta t}] \quad (A.7)$$

Temperature w.r.t. Contact Conductance

We note that the contact conductance is part of the effective heat transfer coefficient.

$$h'_{eff} = \left[\frac{\tau_{pt}r_{ct}}{k_{pt}r_{pt}} + \frac{r_{ct}}{h_{cont}r_{pt}} + \frac{\tau_{ct}}{k_{ct}}\right]^{-1} \quad (A.8)$$

Using this relationship we can rewrite b_{ct} and ϕ_{ct} in terms of the contact conductance.

$$b_{ct} = \frac{h'_{conv}(Bh_{cont}+C)+Ah_{cont}}{(Bh_{cont}+C)m'_{ct}c_{p,ct}} \quad (A.9)$$

$$\phi_{ct} = \frac{h'_{conv}T_l(Bh_{cont}+C)+Ah_{cont}T_{pt}}{h'_{conv}(Bh_{cont}+C)+Ah_{cont}} \quad (A.10)$$

$$A = k_{pt}r_{pt} \quad (A.11)$$

$$B = \tau_{pt}r_{ct}k_{ct} + \tau_{ct}k_{pt}r_{pt} \quad (A.12)$$

$$C = r_{ct}k_p k_{ct} \quad (A.13)$$

The sensitivity of CT temperature to contact conductance is then:

$$\frac{\partial T_{ct}}{\partial h_{cont}} = \frac{-AC\Delta t e^{-b_{ct}\Delta t}[T_{cto} - \phi_{ct}]}{m'_{ct}c_{p,ct}(Bh_{cont} + C)^2} - \frac{ACh'_{conv}(T_{pt} - T_l)(1 - e^{-b_{ct}\Delta t})}{\left(Ah_{cont} + h'_{conv}(Bh_{cont} + C)\right)^2} \quad (A.14)$$

Further we can determine the sensitivity of CT temperature based on any parameter (ξ) related to the contact conductance by taking the derivative of the contact conductance related to that value.

$$\psi = \frac{\partial h_{cont}}{\partial \xi} \quad (A.15)$$

$$\frac{\partial T_{ct}}{\partial \xi} = \frac{-AC\psi\Delta t e^{-b_{ct}\Delta t}[T_{cto} - \phi_{ct}]}{m'_{ct}c_{p,ct}(Bh_{cont} + C)^2} - \frac{AC\psi h'_{conv}(T_{pt} - T_l)(1 - e^{-b_{ct}\Delta t})}{\left(Ah_{cont} + h'_{conv}(Bh_{cont} + C)\right)^2} \quad (A.16)$$

Values for ψ were evaluated for RMS surface roughness, average asperity slope and pressure to hardness ratio.

$$h_{cont} = \frac{1.25mk_s}{\sigma_{rms}}\left(\frac{P}{H}\right)^{0.95} + \frac{k_g}{1.184\sigma_{rms}\left(-\ln\left(\frac{3.132P}{H}\right)\right)^{0.547} + \alpha\beta\Lambda} \quad (A.17)$$

Surface Roughness

$$\psi_{\sigma_{rms}} = -\frac{1.25mk_s}{\sigma_{rms}^2}\left(\frac{P}{H}\right)^{0.95} - \frac{Dk_g}{(\sigma_{rms}D + \alpha\beta\Lambda)^2} \quad (A.18)$$

$$D = 1.184\left(-\ln\left(\frac{3.132P}{H}\right)\right)^{0.547} \quad (A.19)$$

Average Asperity Slope

$$\psi_m = \frac{1.25 k_s}{\sigma_{rms}} \left(\frac{P}{H}\right)^{0.95} \quad (A.20)$$

Pressure to Hardness Ratio

$$\gamma = \frac{P}{H} \quad (A.21)$$

$$\psi_\gamma = \frac{1.1875 m k_s}{\sigma_{rms} \gamma^{0.05}} + \frac{0.647648 k_g \sigma_{rms}}{\gamma E^{0.453} (\alpha\beta\Lambda + 1.184 \sigma_{rms} E^{0.547})^2} \quad (A.22)$$

$$E = -\ln\left(\frac{3.132P}{H}\right) \quad (A.23)$$

Appendix B - MATLAB Code

Main Program Shell

```
clc;clear;close all;
format long

% ------------------------------------------------------------------------
% READ IN EXPERIMENTAL VALUES AND MATERALS PROPERTIES
% ------------------------------------------------------------------------

ex_values = dlmread('Input\exvalues.txt','\t');

% Values should be entered in a tab delimited notepad file. A single row
per experiment with subcooling in column 1, linear power in column 2 and
internal pressure in column 3.

% ------------------------------------------------------------------------
% TIME PARAMETERS AND CREATION OF DATA STORAGE MATRICES
% ------------------------------------------------------------------------

timestep = 1/512;
end_time = 200;
num_exp = length(ex_values);

data_rec = 0.25;
mat_length = (end_time/data_rec)+1;

x                       = zeros(num_exp,ceil(mat_length));
azim_stress_ct_mat      = x;
azim_stress_pt_mat      = x;
c_press_mat             = x;
ct_flux_mat             = x;
diam_ct_mat             = x;
diam_pt_mat             = x;
h_gas_mat               = x;
h_solid_mat             = x;
h_conv_mat              = x;
strain_rate_mat         = x;
strain_tot_mat          = x;
temp_ct_mat             = x;
temp_h_mat              = x;
temp_pt_mat             = x;
thickness_ct_mat        = x;
thickness_pt_mat        = x;
time_mat                = x;
film_thickness_mat      = x;
h_total_mat             = x;
```

```
q_chf_sc_mat            = x;
j                       = ones(1,num_exp);
jay                     = j;
temp_mfb                = j;

% -------------------------------------------------------------------------
% The following numbers give to plot_type will plot the following as a
% function of time:
%       1.   PT and CT Hoop stress.
%       2.   Contact pressure.
%       3.   PT/CT diameter.
%       4.  h_conv.
%       5.   Gas, solid and total contact conductance
%       6.   PT and CT temperatures.
%       7.   Strain rate and total strain.
%       8.   Film Thickness.

      plot_type = 1;
% -------------------------------------------------------------------------

% -------------------------------------------------------------------------
% INITIATE PROGRAM LOOP
% -------------------------------------------------------------------------

for i = 1:num_exp

%Reset params for each experiment

diam_pt             = 0.10338;
thickness_pt        = 0.004;
thickness_ct        = 0.0014;
diam_ct             = 0.1292;
h_conv              = 0;
saturation_temp     = 373.0;
temp_h1             = saturation_temp - ex_values(i,1);
temp_sub            = ex_values(i,1);
temp_bulk           = temp_h1;
temp_pt1            = temp_h1;
temp_pt2            = temp_h1;
temp_ct1            = temp_h1;
temp_ct2            = temp_h1;
temp_l              = temp_h1;
azim_stress_pt      = 0;
strain              = 0;
strain_rate         = 0;
c_press             = 0.1013;
ct_flux             = 0;
contact             = 0;
contact2            = 0;
temp_pt_contact     = 0;
contact_time        = 0;
plane_separation    = diam_ct-(diam_pt+(2*thickness_pt));
h_total             = 0;
```

```
h_solid             = 0;
film_thickness      = 1;
sigma_i             = 1;
int                 = 0;
Ed1                 = 0;
Ed                  = 0;
sigma_i1            = 1;
temp_mfb(i)         = 6.3*temp_sub+290;
h_gas               = 0;
q_mod               = 0;
q_chf_sc            = 0;
total_strain        = 0;
ph_ratio            = 0;
hardi               = 0;
sigma_pt            = 0;
min_Y               = 0;

for time = 0:timestep:end_time

% ------------------------------------------------------------------------
% CONTACT PRESSURE IF CONTACT OCCURS
% ------------------------------------------------------------------------

if contact == 1

plane_separation = (diam_ct - diam_pt - (2*thickness_pt))/2;

[c_press, int, sigma_i,...
 Ed1, Ed, sigma_i1, sigma_pt,...
 sigma_ct, strain_rate] = contact_pressure (    ex_values(i,3),...
                                                c_press,...
                                                sigma_i,...
                                                diam_ct,...
                                                thickness_ct,...
                                                temp_ct1,...
                                                temp_ct2,...
                                                timestep,...
                                                temp_pt2,...
                                                thickness_pt,...
                                                int,...
                                                diam_pt,...
                                                Ed1,...
                                                Ed,...
                                                sigma_i1,...
                                                sigma_pt,...
                                                strain_rate);
```

```
% ------------------------------------------------------------------------
% CONTACT CONDUCTANCE IF CONTACT OCCURS
% ------------------------------------------------------------------------
[h_total, h_solid,...
 h_gas, min_Y, ph_ratio, hardi] = contact_conductance ( temp_pt2,...
                                                        temp_ct2,...
                                                        c_press,...
                                                        min_Y);

end

temp_pt1 = temp_pt2;
temp_ct1 = temp_ct2;

% ------------------------------------------------------------------------
% HEAT TRANSFER CALCULATIONS
% ------------------------------------------------------------------------

[temp_pt2, temp_ct2,...
 temp_sub, h_conv,...
 contact2, temp_h1,...
 ht_pt, film_thickness,...
 temp_l, ct_flux, q_chf_sc] = heat_transfer (   time,...
                                                contact,...
                                                temp_pt1,...
                                                temp_ct1,...
                                                temp_l,...
                                                timestep,...
                                                thickness_pt,...
                                                thickness_ct,...
                                                diam_pt,...
                                                h_total,...
                                                diam_ct,...
                                                temp_sub,...
                                                temp_bulk,...
                                                h_conv,...
                                                temp_h1,...
                                                ex_values(i,2),...
                                                contact2,...
                                                film_thickness,...
                                                temp_mfb(i),...
                                                ct_flux);

% ------------------------------------------------------------------------
% STRAIN CALCULATION OF PT AND CT
% ------------------------------------------------------------------------
if contact == 0

azim_stress_pt = (ex_values(i,3)-c_press)*(diam_pt/2)/thickness_pt;
strain_rate = ((5.7e7*((azim_stress_pt)^1.8)* exp(-29200./(temp_pt2))));
strain = strain_rate*(timestep);
diam_pt = diam_pt * (1+strain);
thickness_pt = thickness_pt/(1+strain);
```

```
elseif contact == 1

strain = strain_rate*timestep;
diam_ct = diam_ct*(1+strain);
thickness_pt = thickness_pt/(1+strain);
thickness_ct = thickness_ct/(1+strain);
diam_pt = diam_ct - (2*thickness_pt);

end

azim_stress_pt = ((ex_values(i,3)-c_press)*(diam_pt/2)/thickness_pt);
azim_stress_ct = ((c_press-0.1013)*(diam_ct/2)/thickness_ct);

total_strain = strain + total_strain;

% FLAG FOR CONTACT OF PT AND CT ----------------------------------------

if (diam_pt+(2*thickness_pt)) >= diam_ct

if contact == 0

temp_pt_contact = temp_pt2;
contact_time    = time;
contact         = 1;
jay(i)          = j(1,i);
c_press         = ex_values(i,3);
total_strain    = 0;

end

end

% ------------------------------------------------------------------------
% STORE DATA FOR PLOT
% ------------------------------------------------------------------------

if mod(time,data_rec) == 0

azim_stress_ct_mat(i,j(1,i))     = azim_stress_pt;
azim_stress_pt_mat(i,j(1,i))     = azim_stress_ct;
c_press_mat(i,j(1,i))            = c_press;
diam_ct_mat(i,j(1,i))            = diam_ct;
diam_pt_mat(i,j(1,i))            = diam_pt + (2*thickness_pt);
h_conv_mat(i,j(1,i))             = h_conv;
h_gas_mat(i,j(1,i))              = h_gas;
h_solid_mat(i,j(1,i))            = h_solid;
h_total_mat(i,j(1,i))            = h_total;
temp_ct_mat(i,j(1,i))            = temp_ct2-273;
temp_h_mat(i,j(1,i))             = temp_h1-273;
temp_pt_mat(i,j(1,i))            = temp_pt2-273;
strain_rate_mat(i,j(1,i))        = strain_rate;
```

```
strain_tot_mat(i,j(1,i))          = total_strain;
film_thickness_mat(i,j(1,i))      = film_thickness*1000;

j(1,i) = j(1,i) + 1;

end

if total_strain > 2.7

rupture_time = time;
disp('Ruptured at:')
disp(time)
break

end

end

end

time_mat = 0:data_rec:end_time;

grand_mat = cat(1, azim_stress_ct_mat, azim_stress_pt_mat,...
                c_press_mat, diam_ct_mat, diam_pt_mat,...
                h_conv_mat, h_gas_mat, h_solid_mat, h_total_mat,...
                temp_ct_mat, temp_pt_mat, strain_rate_mat,...
                strain_tot_mat, film_thickness_mat, time_mat);

plot_it(grand_mat,plot_type,j,jay,temp_mfb,num_exp);
```

Heat Transfer

```
function [temp_pt2, temp_ct2, temp_sub,...
          h_conv, contact2,...
          temp_h2, ht_pt, tf,...
          temp_l,ct_flux,q_chf_sc] = heat_transfer (  time,...
                                                      contact,...
                                                      temp_pt1,...
                                                      temp_ct1,...
                                                      temp_l,...
                                                      timestep,...
                                                      thickness_pt,...
                                                      thickness_ct,...
                                                      diam_pt,...
                                                      h_contact,...
                                                      diam_ct,...
                                                      temp_sub,...
                                                      temp_bulk,...
                                                      h_conv,...
                                                      temp_h1,...
                                                      q_heater,...
                                                      contact2,...
                                                      tf,...
                                                      temp_mfb,...
                                                      ct_flux)

temp_sat = 373;

if temp_ct1 < 375 && contact2~=2

Pr_L = (XSteam('Cp_pT',1,temp_ct1-273)*1000*...
            XSteam('my_pT',1,temp_ct1-273))/...
                  XSteam('tc_pT',1,temp_ct1-273);

if temp_ct1 > temp_bulk

beta = (1-(XSteam('rho_pT',1,temp_ct1-273)/...
            XSteam('rho_pT',1,temp_bulk-273)))/(temp_ct1 - temp_bulk);

Gr_L = (9.8*((pi*diam_ct/2)^3)*(temp_ct1-...
            temp_bulk)*beta)/((XSteam('my_pT',1,temp_bulk-...
                  273)/XSteam('rho_pT',1,temp_bulk-273))^2);

Ra_L = Pr_L * Gr_L;

else

Ra_L = 0;

end
```

```
h_conv = ((XSteam('tc_pT',1,temp_bulk-273)/(1000*(pi*diam_ct/2)))*...
            ((0.6 + ((0.387*(Ra_L^(1/6)))/(((1 + ...
                  ((0.559/Pr_L)^(9/16)))^(8/27)))))^2));
elseif contact2~=2 && temp_ct1 >= temp_sat + 5

p_c = 220.6;
p_R = 1.013/p_c;
f_pr = (1.8*(p_R^0.17)) + (4*(p_R^1.2)) + (10*(p_R^10));
Gamma = 0.106*(p_c^0.69)*f_pr;
h_conv = ((Gamma^(10/3))*((temp_ct1-temp_sat)^(7/3)))/1000;

end

masslength_pt   = 9.164;
masslength_ct   = 3.901;
masslength_h    = 2.608;
spec_heat_pt    = 0.350;
spec_heat_ct    = 0.350;
spec_heat_h     = 0.711;
diam_h          = 0.038;
emissivity_h    = 0.9;
emissivity_pt   = 0.8;
emissivity_ct   = 0.8;
emissivity_w    = 0.993;
boltzmann       = 5.6696e-11;
q_chf_sc        = 99999999;
q_loss          = 0;
loss_frac       = 0;

zirc2nb_conduct = @(T) 27.3952 + ((((9687.14*T)-0.126187E8))/...
                        ((T-1067.64)^2 + 0.397548E6));
conduct_pt = zirc2nb_conduct(temp_pt1)/1000;

zircaloy_conduct = @(T) 12.767 - ((5.4348E-4)*T) + ((8.9818E-6)*(T^2));
conduct_ct = zircaloy_conduct(temp_ct1)/1000; %kW/m.K

% ------------------------------------------------------------------------
% HEATER TEMPERATURE
% ------------------------------------------------------------------------

% Heat transfer general formula
new_temp = @(T0,bee,fi) ...
            ((T0*exp(-bee*timestep)) + fi*(1-exp(-bee*timestep)));

a = diam_h * emissivity_h;
b = diam_pt * emissivity_pt;
c = ((temp_h1^2) + (temp_pt1^2));
d = (temp_h1 + temp_pt1);
f = (1 - emissivity_pt);

h = a * b * c * d;
```

```
k = (a * f) + b;

ht_radiation = pi * boltzmann * (h/k); %Radiation heat transfer

if contact == 0
    ht_pt        = ht_radiation*(0.4); %Account for heater heatup
else
    ht_pt        = ht_radiation;
end

b_h = ht_radiation / (masslength_h * spec_heat_h);
phi_h  = temp_pt1 + ((q_heater*(1-loss_frac))/ht_radiation);
temp_h2 = new_temp(temp_h1,b_h,phi_h);

% ------------------------------------------------------------------------
% PRE CONTACT PT AND CT TEMPERATURE
% ------------------------------------------------------------------------

if contact == 0

b_pt = ht_pt / (masslength_pt * spec_heat_pt);
phi_pt = temp_h1 - q_loss;
temp_pt2 = new_temp(temp_pt1,b_pt,phi_pt);
temp_ct2 = temp_ct1;
ct_flux = 0;

elseif contact == 1

% ------------------------------------------------------------------------
% POST CONTACT PT AND CT TEMPERATURE
% ------------------------------------------------------------------------

a      = (thickness_pt*(diam_ct))/(conduct_pt*diam_pt);
b      = diam_ct/((h_contact)*diam_pt);
c      = thickness_ct/conduct_ct;
h_eff  = 1/(a+b+c);
h_effp = (pi*diam_ct*h_eff);

phi_pt   = ((ht_pt * temp_h1) + (h_effp * temp_ct1))/(ht_pt + h_effp);
b_pt     = (ht_pt + h_effp)/(masslength_pt*spec_heat_pt);
temp_pt2 = new_temp(temp_pt1,b_pt,phi_pt);

% CALANDRIA TUBE TEMPERATURE

% This assumes constant pressure in the film and moderator ------------
hV_p    = XSteam('hV_p',1);
hL_p    = XSteam('hL_p',1);
rhoV_p  = XSteam('rhoV_p',1);
rhoL_p  = XSteam('rhoL_p',1);
tcV_p   = XSteam('tcV_p',1)/1000;
tcL_p   = XSteam('tcL_p',1)/1000;
CpL_p   = XSteam('CpL_p',1);
```

```
CpV_p    = XSteam('CpV_p',1);
hfg      = XSteam('hV_p',1)-XSteam('hL_p',1);
%-------------------------------------------------------------------------

r_ct = (diam_ct/2) + thickness_ct;
h_fg = hV_p-hL_p;
temp_f = (temp_ct1 + temp_bulk)/2;
C_p = XSteam('Cp_pT',1,temp_f-273);
st = XSteam('st_T',temp_bulk-273);

q_chf_sat  = 0.119*h_fg*(rhoV_p^0.5)*((st*9.8*((rhoL_p-rhoV_p)))^0.25);
q_chf_sc_sat   = 1 + (0.1*((C_p*temp_sub)/h_fg)*((rhoL_p/rhoV_p)^0.75));
q_chf_sc = q_chf_sc_sat * q_chf_sat;

ct_flux = h_conv*(temp_ct1-temp_l);

if (ct_flux>0.95*q_chf_sc || contact2 == 2) && contact2 ~= 1

diff = 1;
count = 0;
tf_new = 0;
limit2 = 0.01;

while diff > limit2

count = count + 1;

a = emissivity_ct*emissivity_w*(r_ct +...
      tf)*((temp_ct1^2)+(temp_sat^2))*(temp_ct1 + temp_sat);

b = (emissivity_w*(r_ct + tf)) +...
       ((emissivity_ct*(1-emissivity_w))*r_ct);

h_rad = (boltzmann*a)/b;

h_c = tcV_p/tf;
A = (h_rad + h_c)*(temp_ct1 - temp_sat);
alpha_l = tcL_p/(rhoL_p*CpL_p);
U_inf = sqrt(9.8*(r_ct))*(sqrt(2*(1-rhoV_p/rhoL_p))+1);
Gamma = 2*tcL_p*sqrt(U_inf/(pi*r_ct*alpha_l))*temp_sub;
Beta = (rhoV_p/(2*timestep))*((CpV_p*(temp_ct1 - temp_sat)/2)+ hfg);

a = Beta;
b = Beta*2*r_ct;
c = (Gamma - A)*r_ct;
p = [a b c];

r = roots(p)

for i = 1:length(p)-1;
if isreal(r(i)) == 1 && r(i) > 0
```

```
tf_new = r(i);
end
end
diff = abs((tf-tf_new)/tf);
if diff>limit2
tf = 0.99*tf + 0.01*tf_new;
end

end

h_conv = (h_rad + h_c);
h_convp = pi*(2*r_ct)*h_conv;
contact2 = 2;

else

h_convp = pi*(2*r_ct)*h_conv;

end

b_ct = (h_effp+h_convp)/(masslength_ct * spec_heat_ct);
phi_ct = ((h_effp*temp_pt1) + (h_convp*temp_l))/(h_effp + h_convp);
temp_ct2 = new_temp(temp_ct1,b_ct,phi_ct);

if temp_ct1>temp_ct2 && temp_ct2<(temp_mfb+273)
contact2 = 1;
tf = 0;
end

end

if temp_ct2 >= 373
    temp_l = 372;
end

end
```

Contact Pressure

```
function [c_press, int2, sigma_i, Ed1,
          Ed, sigma_i1, sigma_pt, sigma_ct,
          strain_rate] = contact_pressure (     pressure_pt,...
                                                c_press,...
                                                sigma_i,...
                                                diam_ct,...
                                                thickness_ct,...
                                                temp_ct1,...
                                                temp_ct2,...
                                                timestep,...
                                                temp_pt2,...
                                                thickness_pt,...
                                                int,...
                                                diam_pt,...
                                                Ed1,...
                                                Ed,...
                                                sigma_i1,...
                                                sigma_pt,...
                                                strain_rate)

limit = 0.01;
diff1 = 1;
ext_press = 0.1013;
int2 = int;

while diff1>limit

%LOOPING FOR SIGMA_I ----------------------------------------------------

sigma_ct = ((c_press - ext_press)*(diam_ct/2))/thickness_ct;
diff2 = 1;

while diff2>limit

Ed = 22000*((sigma_ct-sigma_i)^5.1)*exp(-34500/(temp_ct2));
func = @(Ep,S,T) (110*Ep - ((3.5E10)*(S^1.8)*exp(-34500/(T))));

int2 = int + ...
      ((timestep)/2)*(func(Ed,sigma_i,temp_ct2)+func(Ed1,sigma_i1,temp_c
t1));

sigma_inew = 1.4 + int2;

diff2 = abs(sigma_i-sigma_inew)/sigma_i;

%relaxation
if diff2 > limit
sigma_i=0.99*sigma_i + 0.01*sigma_inew;
end
```

```
end

Egb = 140*(sigma_ct^1.3)*exp(-19000/(temp_ct2));
strain_rate = Ed + Egb;
sigma_pt = (strain_rate/(5.7E7*exp(-29200/(temp_pt2))))^(1/1.8);
c_pressnew = pressure_pt - ((sigma_pt*thickness_pt)/(diam_pt/2));

diff1 = abs(c_press-c_pressnew)/c_press;

%relaxation
if diff1 > limit
c_press = 0.99*c_press + 0.01*c_pressnew;
end

end

Ed1 = Ed;
sigma_i1 = sigma_i;

end
```

Contact Conductance

```
function [total_conductance, h_solid,
          h_gas, min_Y, ph_ratio,
          hardi] = contact_conductance (  temp_pt2,...
                                          temp_ct2,...
                                          c_press,...
                                          min_Y)

av_roughness  = 11E-6;
av_asp_slope  = 0.12;
vick_ind      = -0.267;
reference_mfp = 2.8497434E-7;
ref_temp      = 500;
ref_press     = 0.101300;
To            = 273;
Molec_mass_g  = 44;
Molec_mass_s  = 91;
mew           = Molec_mass_g/Molec_mass_s;

% SOLID CONDUCTANCE ------------------------------------------------------

% PT/CT CONDUCTIVITY
zirc2nb_conduct = @(T) 27.3952 + ((((9687.14*T)-0.126187E8))/...
                        ((T-1067.64)^2 + 0.397548E6));

zircaloy_conduct = @(T) 12.767 - ((5.4348E-4)*T) + ((8.9818E-6)*(T^2));

conduct_pt      = zirc2nb_conduct(temp_pt2)/1000;
conduct_ct      = zircaloy_conduct(temp_ct2)/1000;

% HARDNESS
hard = @ (T) (exp(26.034-(T*(2.639E-2))+((T^2)*(4.3504E-5))-...
                  ((T^3)*(2.5621e-8))))/1000000;

hardness_pt = hard(temp_pt2); %--%
                              %--> Hardness of the softer material
hardness_ct = hard(temp_ct2); %--%

if hardness_pt < hardness_ct;
    hardi = hardness_pt;
else
    hardi = hardness_ct;
end

% HARMONIC MEAN OF CONDUCTIVITIES
conductivity_s = 2/((1/conduct_pt)+(1/conduct_ct));

% PRESURE MICROHARDNESS RATIO
vick_corr = (0.442 * hardi)/(vick_ind + 0.370);
b = 1.62*vick_corr*(((av_roughness*10^6)/av_asp_slope)^vick_ind);
```

```
rat = c_press/b;
xp = 1/(1+(0.071*vick_ind));
ph_ratio = rat^xp;

% ------------------------------------------------------------------------
h_solid = (1.25*((conductivity_s * av_asp_slope)/(av_roughness))*...
            (ph_ratio^0.95));
% ------------------------------------------------------------------------

% GAS CONDUCTANCE ---------------------------------------------------------

%1 CO2 CONDUCTANCE
CO2_conductance = ((9.46e-6)*(((temp_pt2 + temp_ct2)/2))^(1.312))/1000;

%2 MEAN PLANE SEPERATION
Y = 1.184*av_roughness*((-log(3.132*ph_ratio))^0.547);

if isreal(Y)==1 && Y<min_Y
min_Y = Y;
elseif isreal(Y)==0
Y = 1.6426747144E-7;
end

%3 MEAN FREE PATH
mean_free_path = reference_mfp*((temp_pt2+temp_ct2)/(2*ref_temp))*...
                  (ref_press/c_press);

%4 FLUID PARAMETER
Prandtl = 0.03612/(CO2_conductance);
fluid_param = 1.14/Prandtl;

%5 ACCOMODATION PARAMETER
alpha = @ (T) (exp(-0.57*((T-To)/To))*(1.4*Molec_mass_g/...
                  (6.8+(1.4*Molec_mass_g))))+((2.4*mew/((1+mew)^2))*...
                        (1-exp(-0.57*((T-To)/To))));
alpha1 = alpha(temp_pt2);
alpha2 = alpha(temp_ct2);
accomod = (((2-alpha1)/alpha1) + ((2-alpha2)/alpha2));

%6 Gas Parameter
M = accomod * fluid_param * mean_free_path;
h_gas = CO2_conductance/(Y + M);

% ------------------------------------------------------------------------
total_conductance = h_solid + h_gas;
% ------------------------------------------------------------------------

end
```

Plot Generator

```
function plot_it(data,plot_type,j,jay,num_exp)

close all

azim_stress_ct  = data(1:6,:);
azim_stress_pt  = data(7:12,:);
c_press         = data(13:18,:);
diam_ct         = data(19:24,:);
diam_pt         = data(25:30,:);
h_conv          = data(31:36,:);
h_gas           = data(37:42,:);
h_solid         = data(43:48,:);
h_total         = data(49:54,:);
temp_ct         = data(55:60,:);
temp_pt         = data(61:66,:);
strain_rate     = data(67:72,:);
strain_tot      = data(73:78,:);
film_thickness  = data(79:84,:);
time            = data(85,:);

for i = 1:num_exp

figure(1)
subplot(3,2,i);
hold on

if plot_type == 1

plot(time(1,1:j(1,i)-1),azim_stress_pt(i,1:j(1,i)-1),'k')
figure(2)
subplot(3,2,i)
plot(time(1,1:j(1,i)-1),azim_stress_ct(i,1:j(1,i)-1),'k')

elseif plot_type == 2

plot(time(1,jay(i)+1:j(1,i)-1),c_press(i,jay(i)+1:j(1,i)-1),'k');

elseif plot_type == 3

plot(time(1,1:j(1,i)-1),diam_ct(i,1:j(1,i)-1),'k')
plot(time(1,1:j(1,i)-1),diam_pt(i,1:j(1,i)-1),'b')

elseif plot_type == 4

plot(time(1,1:j(1,i)-1),h_conv(i,1:j(1,i)-1),'k')
figure(2)
subplot(3,2,i);
plot(temp_ct(i,1:j(1,i)-1),h_conv(i,1:j(1,i)-1),'k')
```

```
elseif plot_type == 5

plot(time(1,1:j(1,i)-1),h_total(i,1:j(1,i)-1),'k')
plot(time(1,1:j(1,i)-1),h_solid(i,1:j(1,i)-1),'r')
plot(time(1,1:j(1,i)-1),h_gas(i,1:j(1,i)-1),'b')

elseif plot_type == 6

plot(time(1,1:j(1,i)-1),temp_pt(i,1:j(1,i)-1),'k');
plot(time(1,1:j(1,i)-1),temp_ct(i,1:j(1,i)-1),'b')

elseif plot_type == 7

plot(time(1,1:j(1,i)-1),strain_rate(i,1:j(1,i)-1),'k')
figure(2)
subplot(3,2,i)
plot(time(1,1:j(1,i)-1),strain_tot(i,1:j(1,i)-1),'k')

elseif plot_type == 8

plot(time(1,jay(i)+500:j(1,i)-1),...
      film_thickness(i,jay(i)+500:j(1,i)-1),'k')

end

end
```